

UNIVERSIDADE DE SANTIAGO DE COMPOSTELA

FACULTADE DE FÍSICA

Departamento de Electrónica e Computación



**TRANSVERSE DIAGNOSTICS FOR HIGH ENERGY
HADRON COLLIDERS**

María Elena Castro Carballo

Santiago de Compostela

CERN-THESIS-2008-040
19/03/2007



UNIVERSIDADE DE SANTIAGO DE COMPOSTELA

Dr. D. Juan Antonio Garzón Heydt

Profesor titular do Departamento de Física de Partículas da Universidade de Santiago de Compostela

Dr. D. Owain Rhodri Jones

Deputy Group Leader of the "Beam Instrumentation Group" at CERN (*European Organization for Nuclear Research*)

Dr. Ing. D. Fritz Caspers

Senior scientific staff member at CERN

CERTIFICAN:

que a memoria titulada **"TRANSVERSE DIAGNOSTICS FOR HIGH ENERGY HADRON COLLIDERS"** foi realizada por **Dona María Elena Castro Carballo** no **Departamento de Electrónica e Computación da Universidade de Santiago de Compostela** baixo a súa dirección e constitúe o traballo de tese que presenta para acadar o título de Doutor.

Asinado:

Juan Antonio Garzón Heydt

Owain Rhodri Jones

Fritz Caspers

Santiago de Compostela, a de do

Contents

Table of Contents	iv
List of Figures	vii
Agradecimientos	xi
Introduction	1
1 Scientific Context	5
1.1 CERN	5
1.1.1 The historical legacy	6
1.1.2 CERN particle accelerators	7
1.1.3 Experiments at CERN	15
1.2 GENERAL DESCRIPTION OF SYNCHROTRON ACCELERATORS	16
1.2.1 A brief history and review of accelerators	16
1.2.2 The current situation and trends in high energy particle accelerators	19
1.3 INTRODUCTION TO THE MAIN OBJECTIVES OF THE THESIS	20
2 Betatron Tune and Chromaticity Measurements	22
2.1 Q-VALUE OR BETATRON TUNE	22
2.1.1 Tune measurement methods	24
2.2 WHAT IS CHROMATICITY?	29
2.2.1 Chromaticity measurement methods	30
3 Schottky Theory and Measurement Methods	34
3.1 SCHOTTKY SIGNALS	35
3.1.1 The longitudinal Schottky signals of unbunched beam	35
3.1.2 Transverse Schottky signals of unbunched beams	37
3.1.3 The longitudinal Schottky signals of bunched beams	40
3.1.4 The transverse Schottky signals of bunched beams	43
3.2 EXTRACTION OF THE BEAM PARAMETERS FROM THE SCHOTTKY SPECTRA	44
3.2.1 The betatron tune (q_v)	45
3.2.2 The chromaticity (ξ_v)	45
3.2.3 The momentum spread ($\Delta p/p$)	46

3.3	MEASUREMENT METHODS OF SCHOTTKY SIGNALS	46
3.3.1	Monitors for Schottky observation	47
3.3.2	Observation of Schottky signals: spectral analysis	49
4	The SPS 1.8GHz Schottky Monitor	51
4.1	SPS 1.8GHz MONITOR CHARACTERISTICS	51
4.2	THE SPS 1.7GHz ACQUISITION SETUP	54
4.2.1	Data acquisition setup with a spectrum analyzer (SPA)	55
4.2.2	Data acquisition with a FFT analyzer or with an external sound card connected to a laptop	56
4.2.3	Analysis of the data acquired with the sound card	60
5	Results obtained with the SPS 1.8GHz Schottky Monitor	62
5.1	SPS PARAMETERS	62
5.2	EXPECTED PICK-UP RESPONSE	63
5.2.1	S/N calculations	67
5.3	OBSERVED BEAM SPECTRA	70
5.3.1	Transverse spectrum	71
5.3.2	S/N ratio extracted from the transverse Schottky spectrum	72
5.3.3	Extracting the betatron tune (q_v) from the transverse Schottky spectrum	74
5.3.4	Extracting the chromaticity (ξ_v) from the transverse Schottky spectrum	75
5.3.5	Extracting the momentum spread ($\Delta p/p$) from the transverse Schottky spectrum	76
5.3.6	Longitudinal spectrum	77
5.4	TUNE TRACKING: FOURIER TRANSFORM OF BEAM MOTION	77
5.4.1	FFT time evolution of beam motion and sources of frequency distortion	78
5.4.2	Single FFT trace analysis and the effects of frequency mismatches in the data acquisition system	84
5.4.3	Betatron tune lines detected with pilot bunch beam	90
5.5	SPECTRA OBTAINED WITH THE 1.7 GHz SCHOTTKY MONITOR AT RHIC (BNL)	91
5.6	CONCLUSIONS	92
6	Determination of Chromaticity by the Measurement of a Head-Tail Phase Shift	93
6.1	THE HEAD-TAIL PRINCIPLE	93
6.2	THE HEAD-TAIL CHROMATICITY EQUATIONS	95
6.2.1	Single particle dynamics in a bunched beam	95
6.2.2	Chromaticity equation	96
6.3	MEASUREMENT OF THE HEAD-TAIL DEPHASING	99
6.3.1	Stripline coupler	99
6.4	DESCRIPTION OF THE CERN HEAD-TAIL MONITOR SYSTEM	102
7	Orbit Compensation	104
7.1	DESCRIPTION OF DESY BUILT SYSTEM	104
7.2	PROTOTYPE ORBIT CORRECTION TECHNIQUE FOR CERN HEAD-TAIL MEASUREMENTS	106
7.3	BERGOZ MULTIPLEXED BEAM POSITION MONITOR (MX-BPM) BOARD	109

7.3.1	Measurement of the X and Y outputs of the MX-BPM board for different input channel attenuation	110
7.4	ANALOG DEVICES ADuC814 MICROCONVERTER	112
7.5	MICROCONVERTER 'QUICKSTART' DEVELOPMENT SYSTEM	116
7.6	VOLTAGE CONTROLLED ATTENUATORS	117
7.7	ATTENUATION STRATEGY	118
7.8	INTEGRATION OF THE ORBIT COMPENSATION SYSTEM PROTOTYPE FOR THE SPS IN THE FINAL SYSTEM	121
7.9	CONTROL LAW FOR KEEPING THE BEAM CENTERED IN THE PICK-UP	122
7.9.1	Analog PID, basic algorithm and control parameters	123
7.9.2	Mathematical modeling of digital control systems	124
7.9.3	Control algorithm details	127
8	Results with the Orbit Compensation System in the SPS	128
8.1	LHC BEAM TYPE RUNNING IN SPS	128
8.2	EXPERIMENTAL SETTING	129
8.3	CALIBRATION	129
8.3.1	Signals after a RESET in the Quick Start-Plus card	131
8.3.2	Method used to calculate the degree of correction	132
8.4	EXPERIMENTAL RESULTS	135
8.4.1	P control algorithm	135
8.4.2	PI control algorithm	137
8.4.3	Comparison of P and PI control algorithm responses	138
8.5	COMPARISON WITH RESULTS OBTAINED WITHOUT THE ORBIT CORRECTION SYSTEM	140
9	Summary and Conclusions	142
10	Resumo	144
10.1	Introducción	144
10.2	Objetivos	145
10.3	Contido	145
10.4	Resumo dos resultados	148
10.5	Conclusiones	149
	Bibliography	150
	Appendix A	153

List of Figures

1.1	Aerial sight of the location of CERN and its accelerators	5
1.2	Diagram of the CERN accelerator complex (not to scale)	8
1.3	Diagram of the SPS complex	10
1.4	LHC nominal and ultimate proton beam parameters	15
1.5	Possible evolution of the highest energy proton, ion and electron colliders. Project dates are those of completion; in the dashed area they are only tentative	19
2.1	Charged particle orbit in a magnetic field	23
2.2	Time domain representation of transverse oscillation in a bunch of particles	25
2.3	3-D representation of the beam response to a chirp excitation	26
2.4	Schematic diagram of a PLL for continuous tune control	28
2.5	Long time FFT acquisition in the PS	29
2.6	Computer simulation of head-tail motion	33
3.1	Beam current for a single particle	35
3.2	Spectrum for a single particle circulating in the machine	36
3.3	Power spectral density of Schottky lines with increasing n	37
3.4	Time domain representation of a single particle transverse oscillation	37
3.5	Frequency domain representation of a single particle performing transverse oscillation	38
3.6	Time domain representation of the current of a single particle in a bunched beam	41
3.7	Decomposition of each revolution line into synchrotron satellites	41
3.8	Longitudinal Schottky spectrum of a bunched beam for large values of n	42
3.9	Decomposition of each betatron line into synchrotron satellites	43
3.10	Typical transverse spectrum observed in a Schottky monitor	45
3.11	Transverse electrostatic pick-up	48
3.12	Transverse electrostatic pick-up used as Schottky detector	48
3.13	Wall current pick-up	49

3.14 Slot-type pick-up	49
4.1 Schottky pick-up design	52
4.2 Fabricated Schottky pick-up	52
4.3 Schottky pick-up design parameters	53
4.4 Calculated Schottky pick-up frequency response (courtesy of R. Pasquinelly and Ding Sun, FNAL)	53
4.5 Sum and Delta signals obtained from the Schottky pick-up	54
4.6 Experimental setting for measurements with Spectrum Analyzer	56
4.7 Illustration of the filtering and the two down mixing stages	57
4.8 Sound card characteristics vs. FFT analyzer	58
4.9 Illustration of data acquisition for FFT analysis	59
4.10 Appearance of the Matlab GUI for data analysis	60
4.11 FFT computation of sampled signal	61
5.1 25 ns LHC type beam in the SPS	63
5.2 Gaussian fit of the longitudinal impedance of Schottky pick-up	64
5.3 (a)Single bunch in time and frequency domains. (b)Electromagnetic power of a single bunch	65
5.4 (a)Train of 4 bunches of 2.5ns length and spaced by 25 ns (b)Fourier transform of a train of bunches spaced by 25 ns	66
5.5 Longitudinal Schottky pick-up response to a single bunch	67
5.6 Typical SPS beam parameters during data acquisition (9/1/04)	70
5.7 Spectrum of Delta signal from the Schottky detector ion the FFT analyzer	71
5.8 Synchrotron satellites in the revolution line	72
5.9 S/N value in transverse spectrum	73
5.10 Extracting q_v from the transverse Schottky spectrum (II)	75
5.11 (a)Gaussian fit of lower tune sideband (b)Gaussian fit of upper tune sideband	76
5.12 Longitudinal sensitivity of Schottky pick-up	77
5.13 FFT time evolution of delta signal	78
5.14 Down mixing process	80
5.15 Generation of images in the down mixing process	81
5.16 Harmonic distortion in a single tone signal	82
5.17 Intermodulation distortion for a two-tone input signal	83
5.18 Frequency lines identification in the accumulated FFT spectrum	84
5.19 Single FFT trace	85

5.20	Revolution and tune lines	86
5.21	Filtering and 1 st down mixing in SPA	86
5.22	2 nd down mixing and shifting of spectrum to base band	87
5.23	Sampling in sound card	87
5.24	Generation of images in the sound card	87
5.25	Expected spectrum considering all distortion effects	88
5.26	Peaks identification in FFT single trace	88
5.27	Suppression of intermodulation products	89
5.28	Expected spectrum for the suppression of intermodulation products	90
5.29	Transverse spectrum obtained with Schottky monitor at RHIC	91
6.1	(a)Transverse signal in a pick-up after applying a kick to the beam with $\xi \neq 0$ (b)Turn by turn response	94
6.2	Determination of head and tail phase shift in a synchrotron period	95
6.3	Accelerating voltage in an RF cavity as a function of the particle's arrival time	96
6.4	Longitudinal 'phase-space'	98
6.5	(a)Signal supplied by a single strip in a stripline pick-up (b)Sum and Delta signals from a stripline pick-up	100
6.6	Δ signal for different positions and inclinations of a bunch in the stripline pick-up	101
6.7	Layout of the SPS Head-Tail monitor	102
6.8	Straight stripline coupler used for Head-Tail monitor	103
6.9	Straight stripline coupler used for Head-Tail monitor	103
7.1	Hardware setup for the chromaticity measurements at HERA proton ring	105
7.2	Schematic diagram of the orbit compensation system designed at DESY	106
7.3	Layout of the proposed orbit correction system for SPS Head-Tail Monitor	107
7.4	BPM signal processor simplified block diagram	109
7.5	BPM X and Y algorithm for an orthogonal pick-up	110
7.6	Measurements of X and Y outputs in Bergoz board with a variable attenuator	111
7.7	X and Y outputs for different attenuations in the four channels	112
7.8	ADuC814 functional block diagram	113
7.9	Specifications for DAC and ADC channels.	114
7.10	ADuC814 ADC Transfer Function	115
7.11	Quick Start-Plus assembly	117
7.12	Data Sheet, Attenuation vs. Control Voltage in HMC121G8	118
7.13	Attenuation vs. Control Voltage for LHC beam	118

7.14	DC level shifting for inverting amplifiers	119
7.15	General Schematic for signal level adaptation	120
7.16	Final orbit compensation system to be tested in SPS	121
7.17	A simple feedback control loop with PID controller	123
7.18	PID terms and their effect on a control system.	124
7.19	Digital control system with output sampling	125
7.20	Digital control system for attenuation control	125
8.1	25ns LHC beam in SPS	129
8.2	Schematic diagram of the experimental setting for the X path	130
8.3	Expected Sum and Delta signals after a RESET	131
8.4	SUM and DELTA signals after reset with time delay correction	132
8.5	Sum signals coming out from hybrids with 3 dB in attenuators	133
8.6	Expected Sum and Delta signals after 3 dB attenuation	134
8.7	7.2 dB applied to SUM' to get SUM	135
8.8	Behaviour of the control signals for the attenuators	136
8.9	(a)P control: calculation of the correction factor from Σ signals (b)Degree of amplitude reduction in Δ signal	137
8.10	(a)PI control: calculation of the correction factor from Σ signals (b)Degree of amplitude reduction in Δ signal	138
8.11	Comparison between P and PI control algorithms	139
8.12	SPS head-tail monitor acquisition system	140
8.13	Raw scope data for Σ and Δ signals in head-tail monitor	141

Agradecementos

Escribir estes agradecementos supón tomar conciencia de que remata un periodo de grande importancia na miña vida, xa que traballar nesta Tese non só supuxo un importante enriquecemento profesional senón tamén personal.

Toda esta historia, comeza hai uns cinco anos lonxe da casa, no CERN. Alí, en Xenebra, atopei o ambiente e a xente que me motivaron a continuar polo peculiar camiño que desembocou neste traballo.

Os meus primeiros pasos neste mundo dinos a carón de Ken Wyllie, que me axudou a perderlle medo ós laboratorios cheos de cables, como eu soia dicir... A ruleta da fortuna levoume ao grupo de traballo AB/BDI/EM, onde fun tratada como unha colega máis... merci beaucoup pour votre gentillesse, merci Eva Calvo. Gracias ao meu xefe Rhodri Jones por darme infinitos grados de liberdade, a Fritz Caspers pola súa comprensión e bos consellos e ó xenio Tom Kroyer co cal pasei longas noites de tomas de datos.

Teño que agradecer moi especialmente a Juan A. Garzon o apoio que me prestou desde a distancia, confiando cegamente en min e na miña capacidade para sacar adiante este proxecto.

Fago tamén especial mención a Javier Bruguera por facilitarme o camiño e o entendemento coa Universidade.

E para facerme a existencia agradable ali estaban eles... Carmen González, Ignacio León, Alejandro Bastos, Monserrat Zurita, Mónica Moles, Alex García, Rubén Gaspar, Delia Rodríguez, Joaquin Egea, Eva Dafonte, Antonio Delgado, Ángela Salom, Miriam Muñoz, Pascale El-Kallasi, Krzysztof Nienartowicz, Christos Sagianos, Peter Cwetanski, Paul Nilsson, Antonio Jimeno, Antonio Delgado, Nuria Catalán, Ana Guerrero, Sabrina Picazo, Sergio Tena, Jocelyn Tan... necesarios e imprescindibles para levar unha vida mental saludable e equilibrada.

Sen o apoio incondicional da miña familia non tería sido capaz de facer absolutamente nada.

Introduction

The Large Hadron Collider (LHC) is a circular synchrotron accelerator that will explore new Physics at the higher energies ever achieved, aiming to find the Higgs boson. The LHC is being built at CERN and by 2007 it will be ready to produce head-on collisions of protons at a centre-of-mass energy of 14 TeV. The employment of superconducting magnets for achieving high energies, the high luminosity required for physics, the limited dynamic aperture and the large energy stored in the beams will make the machine very challenging to operate, especially during the injection process and the energy ramp. Two particular problems will be a high sensitivity to beam losses and a relatively poor field quality requiring the use of many types of magnetic correction elements. This may lead to the inclusion of certain beam measurements in feedback loops, making special demands on the control system.

The injection and acceleration of the LHC proton beams without particle losses and emittance blow up will require an accurate control of the beam parameters. The value of the betatron tune is about 63 units and needs to be controlled to a level of $\Delta Q = \pm 0.003$. Orbit excursions should be limited to less than 0.5 mm. The linear chromaticity should be limited to some units (nominal value $Q'_{H,V} = 2$). This Thesis will be focused on the improvement of new instrumentation for the measurement of beam parameters that is compatible with LHC high intensity running. In this sense, the importance for the performance of the accelerator of terms such as tune or chromaticity will be pointed out. This work can be considered to be divided into two differentiated parts: the tests performed to a potentially beam diagnostics device and the improvement of the sensitivity of an already existing monitor. However, behind both subjects there is a common objective: the need of implementing new sensitive and non destructive methods for measuring parameters of major importance to keep the beam within the tight tolerances imposed to the superconducting and high energy accelerator LHC.

Chapter 1 will firstly explain what CERN is and which are the characteristics and aims of the LHC project. This will be followed by a brief description of the synchrotron accelerators and the future trends in particle accelerators to introduce the context in which this work has been developed. We will finish with a mention to the importance of beam diagnostic instruments in accelerators and how the results obtained with my Thesis could have contributed to this field.

Chapter 2 will explain the importance of tune and chromaticity for beam diagnostics in particle accelerators. The concept of both parameters will be explained, giving a brief mathematical introduction that will be extended in chapters devoted to them. In addition, I will present some of the current techniques being used for the measurement of tune and chromaticity. Among these techniques there are the ones on which my work relies: *Schottky noise* as non destructive diagnostic tool and chromaticity measurement via *head-tail diphase in a bunch* of particles after the application of a transverse kick.

In Chapter 3, and as an introduction to the results obtained with the Schottky monitor, I will make a whole mathematical development of Schottky theory applied to the beam in a circular accelerator considering the beam as being composed by individual particles each one moving incoherently. The result of this development will allow us to know the kind of signal we would expect to observe in frequency domain. Some examples of Schottky monitors will be overviewed.

Chapter 4 describes the characteristics of the Schottky monitor tested in the SPS and that could be used as a tool for transverse beam diagnostics in future LHC. I will also describe the whole experimental setting that was installed for the data acquisition of the signal generated in the Schottky pick-up. This signal had to be conveniently adapted to the devices used for the acquisition: a conventional spectrum analyzer, a FFT analyzer and a sound card connected to a laptop.

In Chapter 5 I will present the results obtained with the 1.7 GHz Schottky pick-up in the SPS and with LHC beam type. Before showing the results, and knowing the characteristics of the pick-up, I will make a study of the type of response we should observe in a conventional spectrum analyzer, that is, the S/N ratio and the frequency range of the received signal. Following, I will show the experimental results: transverse and longitudinal frequency spectrums, where we tried to observe all of the features that were predicted by Schottky theory. To finish, I will concentrate on the analysis of the data that was acquired with the most efficient acquisition device: the sound card connected to a laptop. Most of the data was acquired using this setup and the analysis showed additional

frequency components not associated to Schottky, for this reason, it was crucial to understand the origin of those frequency lines if we wanted to end up with a clean Schottky spectrum potentially useful for diagnostics. A whole study of the possible sources of noise will be done to the FFT spectrums.

After analyzing the previous Schottky method that was proposed for transverse diagnostics in LHC beam, I will start developing the chromaticity monitor based on transverse signals produced by 'head-tail phase shifts' in a bunch of particles.

In Chapter 6 I will describe a particular effect that happens in a bunch of particles with non-zero chromaticity when a transverse kick is applied to the beam: in half a synchrotron period the particles at the head of the bunch and the ones at the tail interchange their positions. Sampling transverse oscillations in two fixed points of the bunch, one at the head and one at the tail, leads to the observation of a phase difference between these two points with a maximum value in half a synchrotron period. A complete mathematical development of the single particle dynamics in a bunched beam will give us a formula from which it will be possible to extract the value of the relative chromaticity using the head-tail diphas. Also, as an introduction to what can be considered to be the second part of my subject of Thesis, I will explain the way the head-tail phase shifts can be measured and how the sensitivity to the head-tail betatron motion can be improved by taking out the closed orbit offset in the signal.

Chapter 7 will describe a method to improve the sensitivity (S/N) of the Head-Tail monitor installed in the SPS to the head-tail betatron motion in a bunch of particles. This method is an orbit compensation system that will remove, from the transverse signal of the stripline pick-up, the component associated to the displacement of the beam from the center of the coupler. That way the only transverse signal detected will be the one associated to the betatron motion of the head and tail of the bunch after a kick. We will present the proposed system with automatic control implemented as a feedback loop where the input is the position of the beam in the coupler and the output is a control voltage for attenuators connected to the electrodes of the pick-up and that will attenuate the signal for electronically center the beam. I will describe all the devices included the orbit correction system.

In Chapter 8 I will show the results obtained with the implemented orbit compensation system

for one plane and that was tested in the SPS with type LHC beam. I will describe the procedures followed for calibration of the components and the way I will perform the quantization of the degree of improvement in the correction of the orbit and for different control algorithms.

Chapter 9 presents a summary of the results shown in precedent chapters together with the conclusions that can be extracted from them and the improvements to perform in the described instrumentation.

Chapter 1

Scientific Context

1.1 CERN

CERN is the European Organization for Nuclear Research, the world's largest particle physics center. Founded in 1954, the laboratory was one of Europe's first joint ventures, and is an example of international collaboration. From the original 12 signatories of the CERN convention, membership has grown to the present 20 Member States.

The laboratory sits astride the Franco-Swiss border west of Geneva at the foot of the Jura mountains.



Figure 1.1: Aerial sight of the location of CERN and its accelerators

CERN employs some 2500 people including a wide range of skills and trades - physicists, engineers, programmers, technicians, craftsmen, administrators, secretaries, workmen, ... They are essential to design and build CERN's machinery and ensure its smooth operation, to help to prepare, run, analyze and interpret the scientific experiments, and to carry out the myriad of tasks in such a large and special organization. CERN's research programme attracts scientists from the Member States and from further afield - the United States of America, Japan, the Russian Federation, the People's Republic of China, Israel, India, ... Some 6500 scientists, half of the world's particle physicists, use CERN's facilities. They represent 500 universities and over 80 nationalities. CERN's primary function is to provide research facilities and basic support to this community of users.

1.1.1 The historical legacy

The creation of a European Laboratory was recommended at an UNESCO meeting in Florence in 1950. In 1951, a provisional body was created called the "Conseil Européen pour la Recherche Nucleaire" (CERN). This was a council: a body of people. In 1953 the Council, formed by 12 countries, decided to build a central laboratory near Geneva. At that time, pure physics research concentrated on understanding the inside of the atom, hence the word "nuclear", but, very soon, the work at the laboratory went beyond the study of the atomic nucleus, on into higher and higher energy densities. As ratified by the parliaments of the member states, the convention specifies that the laboratory is officially called the "Organisation Européenne pour la Recherche Nucleaire" or "European Organization for Nuclear Research". However, the name of the Council stuck to the organization, which is why it is referred to in the literature as simply "CERN". Scientists here look for effects between the forces of nature that become noticeable only at very high energies. Therefore, from early on, CERN has been a High-Energy Physics institute, or an "HEP" institute. Because this activity is mainly concerned with the study of interactions between particles, CERN is commonly referred to as the "European Laboratory for Particle Physics" ("Laboratoire Européen pour la Physique des Particules") and it is this title that really describes the current work of the laboratory.

From the original 12 signatories of the CERN convention, membership has grown to the present 20 Member States. They are the following: Austria (1959), Belgium(1953), Bulgaria (1999), Czech

Republic (1993), Denmark (1953), Finland (1991), France (1953), Germany (1953), Greece (1953), Hungary (1992), Italy (1953), Netherlands (1953), Norway (1953), Poland (1991), Portugal (1986), Slovak Republic (1993), Spain (1961), Sweden (1953), Switzerland (1953) and the United Kingdom (1953). Yugoslavia was one of the 12 founder members but withdrew in 1961. NOTE: The year in brackets is the accession year of each country. These Member States provide CERN with a vast community of Users (4632 in 2002), mainly physicists from either Universities or Research Institutes and provide pre-determined financial contributions in proportion to their Net National Incomes. CERN facilities are also used by scientists from 217 Institutes and Universities of Non-Member States: Algeria, Argentina, Armenia, Australia, Azerbaijan, Belarus, Brazil, Canada, China, Croatia, Cyprus, Estonia, Georgia, Iceland, India, Iran, Ireland, Israel, Japan, Mexico, Morocco, Pakistan, Peru, Romania, Russia, Serbia, Slovenia, South Africa, South Korea, Taiwan, Turkey, Ukraine, USA.

Reciprocal agreements between the worlds High Energy Physics laboratories allow for free access to experimenters, regardless of their country of origin. However, the physicists and their funding agencies from both Member and Non-Member States are responsible for the financing, construction and operation of the experiments on which they collaborate.

1.1.2 CERN particle accelerators

By accelerating particles to very high energies and smashing them into targets, or into each other, physicists can unravel the forces acting between them. CERN's accelerators are amongst the world's largest and most complex scientific instruments. Accelerators come in two types, linear and circular, and CERN has both. Accelerators use powerful electric fields to push energy into a beam of particles. Magnetic fields are used to keep the beam tightly focused, and in circular machines to steer the particles around the ring. Linear machines push energy into the beam all along the accelerator's length. The longer the machine, the higher the final energy. In circular machines the particles go round and round again, collecting energy with each lap. But the faster the particles are going, the more they try to "skid" off the ring. CERN's newest accelerator, the Large Hadron Collider LHC, has a circumference of 27 and will use strong bending fields to keep the particles on track. With the largest interlinked accelerator complex in the world CERN is unrivalled in providing beams of high energy particles for physicists to use in their experiments.

The CERN accelerator complex

CERN's accelerator complex (see Figure 1.2) includes particle accelerators and colliders and can handle beams of electrons, positrons, protons, antiprotons, and "heavy ions" (the nuclei of atoms, such as oxygen, sulphur, and lead). Each type of particle is produced in a different way, but then passes through a similar succession of acceleration stages, moving from one machine to another. The first steps are usually provided by linear accelerators, followed by larger circular machines. CERN has 10 accelerators altogether, the biggest to date, until it was dismantled, was the Large Electron Positron collider (LEP) which is being superseded by the Large Hadron Collider currently under construction.

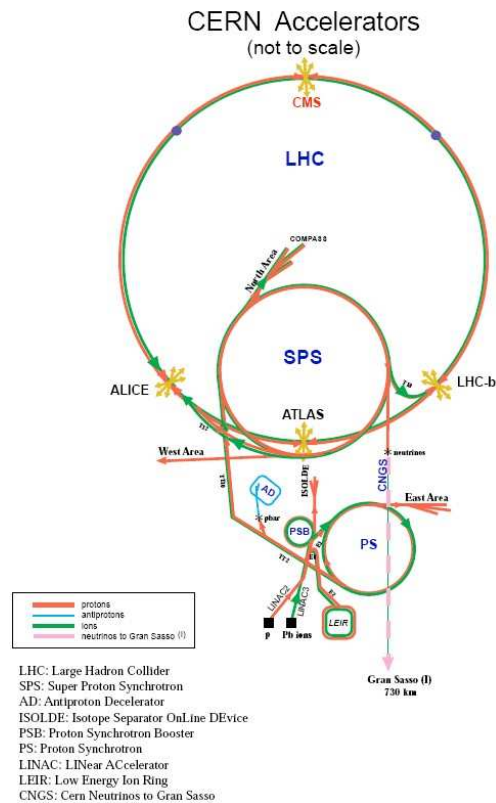


Figure 1.2: Diagram of the CERN accelerator complex (not to scale)

CERN's first operating accelerator, the Synchro-Cyclotron, was built in 1954, in parallel with the Proton Synchrotron (PS). The PS is today the backbone of CERN's particle beam factory, feeding

other accelerators with different types of particles. The 1970s saw the construction of the SPS, at which Nobel-prize winning work was done in the 1980s. The SPS continues to provide beams for experiments and was also the final link in the chain of accelerators providing beams for the 27 kilometer LEP machine. CERN's next big machine, due to start operating in 2007, is the Large Hadron Collider (LHC).

The PS complex

The Proton Synchrotron (PS) is the oldest and most versatile of CERN's accelerators. The PS was commissioned in 1959 and has been running continuously since then. With a diameter of 200 meters and reaching a final energy of 28 GeV, it was for a while the most powerful accelerator in the world. The PS has been modified strongly along the years, adapting it to the ever increasing complexity of CERN's accelerator system. Today the PS complex can accelerate all stable and electrically charged particles (electrons, protons), their antiparticles (positrons, antiprotons), and different kinds of heavy ions (oxygen, sulphur, or even lead). These particles are produced in ion sources: protons are obtained from hydrogen gas using a "duoplasmatron", electrons are extracted from metal surfaces in "electrons guns", and the electron shells of lead atoms are stripped off in "electron synchrotron resonance (ECR)" sources. The first stage of acceleration happens in a linear accelerator (Linac), and each type of particle has its own. This is because of their very different masses - a lead ion is about 200 times heavier than a proton, and almost 400,000 times heavier than an electron. The final energies are 500 MeV for electrons, 50 MeV for protons, and 4.2 MeV/nucleon for lead (Pb) ions. For proton and heavy ion beams there follows a 1.0 GeV "Booster" synchrotron to increase the energy prior to injection into the PS. Electrons are first stored and further accelerated in the "Electron-Positron-Accumulator (EPA)" ring. Anti-electrons (positrons) are produced in collisions of an electron beam with a heavy metal target, and then also stored and accelerated in the EPA. Then all particle beams pass through the PS machine itself. Each acceleration cycle takes 2.4 seconds, and the PS control systems are so versatile that different particle beams can be dealt with on each successive cycle. The beams are then injected into the bigger rings for further acceleration (SPS, in the past into LEP and in the future into LHC). Proton beams from the PS complex are also used for physics experiments (ISOLDE, East Hall) or for the production of antiprotons (Antiproton Decelerator).

The Super Proton Synchrotron (SPS)

The Super Proton Synchrotron is a circular accelerator, 6 km in circumference, buried underground.

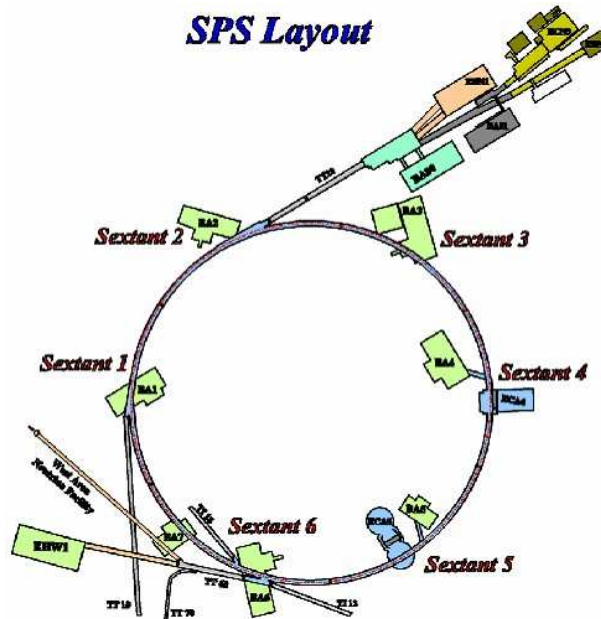


Figure 1.3: Diagram of the SPS complex

It was built originally to accelerate protons - and still does so - but it has also operated as a proton-antiproton collider, a heavy-ion accelerator, and an electron/positron injector for LEP. As a proton-antiproton collider, in the 1980s, it provided CERN with one of its greatest moments - the first observations of the W and Z particles, the carriers of the weak force. The SPS can also accelerate lead ions to an energy of 170 GeV per nucleon, with 208 nucleons in the lead nucleus. At present, this is the highest energy obtained in the world, and it serves the study of the quark-gluon plasma which may have occurred shortly after the big bang.

The Large Electron Positron collider (LEP)

The LEP machine at CERN has been the largest particle collider in the world until it was dismantled. In a ring 27 km in circumference, buried about 100 m underground, bunches of electrons and

positrons (antielectrons) raced round in opposite direction as they were accelerated to almost the speed of the light. When an electron and a positron come close enough, they disappear in an act of mutual destruction to form a burst of energy. Almost immediately, this energy changes back into particles, just as matter must have formed from energy in the early Universe. At four symmetric points around the ring, bunches of particles were focused down to the thickness of a hair and made to collide at the heart of the four LEP experiments. Each bunch contained more than a hundred thousand million particles (10¹¹), but on average only one in about 40,000 collisions between bunches produced the desired effect: a head-on electron-positron collision. For this reason, bunches were made to circulate for hours, each bunch travelling round the ring more than 10,000 times a second. LEP began operation in the summer 1989 and for six years the collision energy of its electrons and positrons was tuned exactly to the value needed to produce the neutral carrier of the weak force, the Z⁰. Since the autumn of 1995, the energy was increased to almost double its earlier value. In the summer of 1996, LEP ran at the exact value needed to produce pairs of the charged carriers of the weak force, the W⁺ and W⁻ particles. Detection of millions of Z⁰s and hundreds of Ws has allowed the LEP experiments to make extremely precise tests of the Standard Model of particles and their interactions.

The Large Hadron Collider (LHC)

In the mid 1980s, a new round of discussion took place with the aim of defining various options for the post-LEP era. There is a general consensus among the world's scientific community that by reaching higher energies we shall probably be able to answer fundamental questions left unanswered by LEP, the most important being the mechanism which gives matter its mass. In December 1994 CERN's governing body, Council, officially approved the construction of CERN's Large Hadron Collider (LHC), a technologically challenging superconducting ring, which will be installing in the existing LEP tunnel, to provide proton-proton collision energies 10 times greater than any previous machine and that will be fed by existing particle sources and pre-accelerators. The LHC will use the most advanced superconducting magnet and accelerator technologies ever employed. LHC experiments are being designed to look for theoretically predicted phenomena. However, they must also be prepared, as far as possible, for surprises. The LHC is a particle accelerator which will probe deeper into matter than ever before, it will collide two beams of protons at an energy of 14 TeV (7 TeV per beam) although beams of lead nuclei will also be accelerated, smashing together with a collision

energy of 1150 TeV. The start-up is planned for 2007.

Why do we need it?

Because our current understanding of the Universe is incomplete. The theory we use, known as the Standard Model, leaves many riddles unsolved. Why do the elementary particles have mass, and why are their masses different? Are the apparently different forces of nature really just manifestations of a single force? Why is there seemingly no antimatter left in the Universe? The question of mass is the most perplexing. It's remarkable that such a familiar concept is so poorly understood. The answer may lie within the Standard Model, in an idea called the Higgs mechanism. According to this, the whole of space is filled with a 'Higgs Field', and by interacting with this field, particles acquire their masses. Particles which interact strongly with the Higgs field are heavy, whilst those which interact weakly are light. The Higgs field has at least one new particle associated with it, the Higgs boson. The LHC will be able to make this particle detectable, if it exists. In relation to the different forces of nature, today, we live in a cold Universe with four apparently distinct forces acting on matter. When the universe was young and much hotter than today, perhaps these forces all behaved as one. Particle physicists hope to find a single theoretical framework to prove this, and have already had some success. Two forces, the electromagnetic force and the weak force were 'unified' into a single theory in the 1970s. This theory was verified in a Nobel prize-winning experiment at CERN a few years later. A very popular idea suggested by the unification of the forces is called supersymmetry, or SUSY for short. SUSY predicts that for each known particle there is a 'supersymmetric' partner. If SUSY is right, then supersymmetric particles should be found at the LHC. Antimatter poses another riddle the LHC will help us to solve. At the Universe's birth, the Big Bang, matter and antimatter are believed to have been created in equal amounts, yet today, we live in a Universe apparently made entirely of matter. So where has all the antimatter gone? It was once thought that antimatter was a perfect 'reflection' of matter - that if you replaced matter with antimatter and looked at the result in a mirror, you would not be able to tell the difference. We now know that the reflection is imperfect, and this could have led to matter-antimatter imbalance. The LHC will be a very good 'antimatter-mirror', allowing us to put the Standard Model through one of its most gruelling tests yet. These are just a few of the questions the LHC should answer.

How it will work?

By using superconductivity. To keep the LHC's beams on track needs stronger magnetic fields than

have ever been used before in a CERN accelerator. Superconductivity makes such fields possible, but a superconducting installation as large as the LHC has never before been built. Intensive R&D with European industry has shown that it can be done. At the end of 1994, an important milestone was reached with the first operation of an entire prototype section of the accelerator. Superconductivity is the ability of certain materials to conduct electricity without resistance or energy loss, usually at very low temperatures. The LHC will operate at about 300 degrees below room temperature, ever colder than outer space. With its 27 km circumference, the accelerator will be the largest superconducting installation in the world. Because the LHC will accelerate two beams moving in opposite directions, it is really two accelerators in one. To keep the machine as compact and economical as possible, the magnets for both are built into a single 2-in-1 housing. The LHC will be built in the same tunnel as CERN's LEP. Proton beams will be prepared by CERN's existing accelerator chain before being injected into the LHC. The beams will be stored at high energy for hours and during this time collisions will take place inside the four main LHC experiments: CMS, ALICE, ATLAS and LHCb.

How will we use it?

By building huge detectors to study what happens when the LHC's beam collide. These detectors will handle as much information as the entire European telecommunications network does today. They will stand up to 20 metres high, as tall as office blocks, and bristle with electronics. At their centres, protons will collide some 800 million times a second. Understanding what happens in these collisions is the key to the LHC's success. Collisions will happen so fast that particles from one collision will still be travelling through the detector when the next collision happens. The need to unravel all this requires new advances in computing and electronics. LHC collisions will produce thousands of particles, and keeping track of them will be a mammoth task. The detectors will supply 20 times more information than CERN's biggest detectors today, producing around 10 million separate pieces of information for each collision. Thousands of physicists and engineers from all over the world are involved with the LHC and its detectors, with industry playing a vital role. Although the LHC is being built for fundamental science, the technologies it demands are already showing a rich seed bed of ideas for the future.

LHC Vital Statistics

- Particles used: Protons and heavy ions (Lead)
- Circumference: 26,659 m
- Injector: SPS
- Injected beam energy: 450 GeV (protons)
- Nominal beam energy in physics: 7 TeV (protons)
- Magnetic field at 7 TeV: 8.33 Tesla
- Operating temperature 1.9 K
- Number of magnets: ~ 9300
- Number of main dipoles: 1232
- Number of quadrupoles: ~ 858
- Number of correcting magnets: ~ 6208
- Number of RF cavities: 8 per beam; Field strength at top energy ≈ 5.5 MV/m
- RF frequency: 400.8 MHz
- Revolution frequency: 11.2455 kHz
- Power consumption: ~ 120 MW
- Gradient of the tunnel: 1.4%
- Difference between highest and lowest points: 122 m

With following proton beam parameters:

			Injection	Collision		
Energy		[GeV]	450	7000		
Luminosity	nominal	[cm ⁻² s ⁻¹]		10 ³⁴	3564 bunch places	
	ultimate			2.5 × 10 ³⁴		
Number of bunches			2808			
Bunch spacing		[ns]	24.95			
N _b intensity per bunch	nominal	[p/b]		1.15 × 10 ¹¹		
	ultimate			1.70 × 10 ¹¹		
Beam current	nominal	[A]		0.58		
	ultimate			0.86		
ε _n (transverse emittance, rms, normalised), nominal & ultimate		[μm]	3.5	3.75		Emittances equal in both planes, small blow-up allowed in LHC
Longitudinal emittance, total		[eVs]	1.0	2.5		Controlled blow-up during accel. has to fit into 400 MHz buckets
Bunch length, total (4σ)		[ns]	1.7	1.0		
Energy spread, total (4σ)		[10 ⁻³]	1.9	0.45		

Figure 1.4: LHC nominal and ultimate proton beam parameters

A detailed description of LHC and the requirements of such an accelerator are reported in the 'LHC Design Report' [5].

1.1.3 Experiments at CERN

Some experiments study what happens when a beam of particles smashes into the atoms of a heavy target. These are called fixed target experiments. These kinds of experiments can collect a large number of interesting collisions, as the density in a heavy target is very high. This is important in searches for very unlikely events or when large number of events are needed. The price to pay is that only a fraction of the incoming energy is spent in creating new particles. At CERN, fixed target experiments use primary beams of protons, and all sorts of secondary beams are used as

pions, muons and neutrinos. Other experiments study the head-on collisions of two beams of particles travelling in opposite directions and are called colliding beam experiments. Here, all the beam energy is available for the creation of new matter, but the number of collisions is smaller. At CERN these types of experiments use electrons against positrons, as it was the case of LEP, and protons against antiprotons as in the SPS. In the future LHC machine, very high energy protons or heavy ions, will collide against each other.

1.2 GENERAL DESCRIPTION OF SYNCHROTRON ACCELERATORS

1.2.1 A brief history and review of accelerators

The origin of particle accelerators sits at the end of 18th century and is the result of the natural progression through atomic physics to nuclear physics and the inevitable need for higher energy and higher intensity 'atomic projectiles' than those provided by natural radioactive sources. In this context, the particle accelerator was conceived to split the atom.

Direct-voltage accelerators

In the early 1920's, Rutherford realized the need for an electrostatic machine supplying many MeV for continuing the research of the nucleus, but at that time, there were not such high voltage sources. The situation changed in 1928 when Gurney and Gamov independently predicted tunnelling and it appeared that an energy of 500 keV might suffice to split the atom. Rutherford encouraged Cockcroft and Walton to start designing a 800 kV particle accelerator. Their source reached 700 kV and in 1932 they split the Lithium atom with 400 keV protons. The limit in these splitting machines was the generator, but improvements in this area means that nowadays energies up to 24.5 MV can be reached with this technique.

Linear accelerator (Linac)

The direct voltage accelerators were limited by the maximum voltage that could be generated in the system and an alternative was needed. In 1924 Ising proposed time varying fields across drift

tubes to accelerate particles. This is known as resonant acceleration and became the underlying principle of all of today's ultra high energy accelerators. In 1928 Wideroe built a linear accelerator by connecting alternate drift tubes to the same terminal of an RF generator. He used a 1 MHz, 25 kV oscillator to make 50 keV potassium ions. The generator frequency is adjusted so that a particle traversing a gap sees an electric field in the direction of its motion and while the particle is inside the drift tube the field reverses so that it is again the direction of motion at the next gap. As the particle gains energy and speed the structure periods must be made longer to maintain synchronism. The underlying principle remains the same but there are variants of the accelerating structure design. The next generation of linear colliders will be in the TeV range with RF frequencies in the GHz range.

The cyclotron

Technologically, the linac was difficult to build and during 1930's it was pushed into the background by a simpler idea conceived by Ernest Lawrence in 1929, the fixed-frequency cyclotron. It makes use of the magnetic force on a moving charge to bend charges into a semicircular path between accelerations by an applied RF electric field. This electric field accelerates particles between the 'D's' of the magnetic field region so called because of their shape. The field is reversed at the cyclotron frequency to accelerate particles back across the gap. By 1939, Lawrence's cyclotron was capable of delivering 20 MeV protons. The cyclotron, however, was limited in energy by relativistic effects and despite the development of the synchrocyclotron, a new idea was still required to reach yet higher energies. This new idea was to be the synchrotron, which will be described later.

The betatron

The betatron basically consists of a circular vacuum tube placed between the two poles of an electromagnet. The accelerated electrons enter tangentially into the tube and describe circular orbits due to the magnetic field. A problem that arises with this accelerator is that as particles are accelerated, the magnetic field needs to be increased to keep a constant orbit.

The betatron was re-invented in 1940 by Kerst following annotations of Wideroe. He reached energy of 300 MeV by 1950.

The synchrotron

By the 1940's three accelerator techniques had been demonstrated: DC acceleration, resonant acceleration and the betatron mechanism. In fact, there were no new ideas for acceleration until the mid 1960's. However, the acceleration mechanism is not sufficient by itself and other equally important developments were needed like bending and focussing mechanisms of the beam.

The cyclotron is limited by relativistic effects, which cause the particles to slow down and lose synchronism with the RF field at high energy. At first glance it would appear that one would only have to reduce the frequency in order to maintain synchronism but the spread in revolution frequency with energy would quickly exploit the natural energy spread in the beam and disperse the particles away from the peak of the RF voltage. In this case, a longitudinal mechanism is needed. This problem was overcome by E. McMillan and independently by V. Veksler who discovered the principle of phase stability in 1944 and invented the synchrotron. Phase stability is general to all RF accelerators except the fixed-frequency cyclotron. The effect is that a bunch of particles, with an energy spread, can be kept bunched throughout the acceleration cycle by simply injecting them at a suitable phase of the RF cycle. In the synchrotron the guide field increases with particle energy to keep the orbit stationary as in the betatron, but acceleration is applied with a RF voltage via a gap or cavity. In 1946 F. Goward and D. Barnes were the first to make a synchrotron work, and in 1947 M. Oliphant, J. Gooden and G. Hyde proposed the first proton synchrotron for 1 GeV in Birmingham, UK.

Up to this time, the only mechanism known for focussing in the transverse plane was called weak or constant gradient focusing. In this case, the guide field decreases slightly with increasing radius and its gradient is constant all around the circumference of the machine. The tolerance of the gradient is severe and sets a limit to the size of such an accelerator. By 1952, E. Courant, M. Livingstone and H. Snyder proposed strong focusing also known as alternating-gradient (AG) focusing. It is directly analogous to a result in geometrical optics: alternating focussing and defocusing lenses leads to a global focussing of a light beam. In an analogous way, for focussing the beam quadrupoles of alternating gradient are used. With all these improvements, the synchrotron quickly overshadowed the synchrocyclotron and betatron in the race for higher energies.

The next step was the storage ring collider. In physics experiments, the useful energy for new particle production is the energy that is liberated in the centre-of-mass of the system. When an accelerator beam is used on a fixed target, only a fraction of the particle's energy appears in the

centre-of-mass, whereas for two equal particles in a head-on collision, all of the particle's energy is available. This fundamental drawback of the fixed-target accelerator becomes more punitive as the energy increases. The storage-ring collider now dominates the high-energy physics field. Single-ring colliders, using particles and antiparticles in the same magnetic channel, were the first type of collider to be exploited at Frascati in the AdA project (1961). The first double-ring proton collider was the CERN ISR, 1972-1983. The use of superconductivity in proton machines has made the very highest energies possible with synchrotrons.

1.2.2 The current situation and trends in high energy particle accelerators

In the present situation, circular colliders dominate the high energy field, with the only exception of the Stanford linear collider (SLC). Up to now, the highest energy collisions were obtained at FNAL with the 1TeV Tevatron collider but it is expected to get 14TeV $p - p$ collisions at LHC.

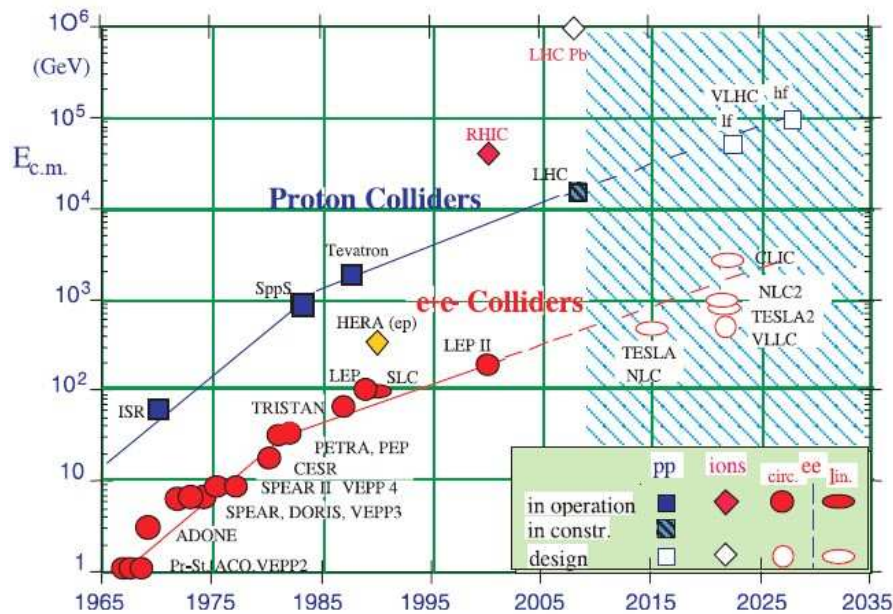


Figure 1.5: Possible evolution of the highest energy proton, ion and electron colliders. Project dates are those of completion; in the dashed area they are only tentative

There is a general consensus in the physics community on the fact that an e^+e^- collider with

a collision energy ~ 1 TeV should be built early enough to provide significant time overlap with the LHC and that solid R&D programs should also be maintained, in preparation for very large Hadron colliders (VLHC) with an energy 100TeV, 3-5 TeV e^+e^- linear colliders, neutrino factories and heavy lepton colliders.

1.3 INTRODUCTION TO THE MAIN OBJECTIVES OF THE THESIS

LHC will require an accurate control of beam parameters imposed by the tight tolerances on their values required for successful LHC operation.

An important challenge in accelerator technology is to preserve beam emittance, the phase space occupied by the beam, and even to reduce it. In the case of LHC, beam measurement techniques should contribute to an emittance blow-up of less than 2%. However, the measurement of transverse beam parameters typically requires either kicking the beam or exciting coherent oscillations and in both cases the emittance of Hadron beams increases, leading to possible beam loss. For this reason it would be desirable to implement high sensitivity/low excitation instrumentation systems.

This Thesis describes the development of suitable instrumentation for beam diagnostics in the LHC, and can be divided in two main parts:

- A first study of the possible future use in the LHC of a Schottky monitor similar to that already used operationally in the Tevatron at FNAL.
- A study of the Signal to Noise (S/N) improvements of the so-called Head-Tail monitor for chromaticity measurements that has been operational in the SPS for a few years.

These two systems could be of interest for LHC for several reasons:

- The Schottky monitor can be used as a non-destructive measurement system of betatron tunes, chromaticity, momentum spread, transverse and longitudinal emittance and the synchrotron frequency, since the detection does not need beam excitation. The drawback of such a technique is the low S/N requiring long integration times and making it difficult for bunch by bunch analysis.

- If the applied excitation could be kept very low, then the head-tail monitor could be considered as quasi-non destructive . It relies on the evolution of the head-tail phase shift in a bunch of particles after a transverse dipole excitation. This technique does not need an accurate knowledge of the fractional part of the betatron tune and, for machines working above transition, is virtually independent of beam energy.

This Thesis presents the results obtained with prototypes of both of these measurement systems using LHC type beam in the SPS.

Chapter 2

Betatron Tune and Chromaticity Measurements

This chapter reviews some of the diagnostic tools used for the measurement of these beam parameters but, before proceeding with the description of the principles, a brief theoretical introduction is needed to clarify the concepts of *betatron tune* and *chromaticity*.

2.1 Q-VALUE OR BETATRON TUNE

A beam of particles enters the machine as a set of trajectories which are centered around the nominal orbit. At any instant, a particle may be displaced horizontally or vertically from the ideal position and this would cause them to leave the vacuum pipe if there were no restoring fields, to make the particle oscillate around the ideal orbit. These restoring fields are supplied by quadrupole magnets embedded in the dipole bending magnets in an alternating pattern in such a way that half of them focus the beam and half defocus the beam. The envelope of these oscillations follows the *betatron function* $\beta(s)$ which has minimums near the defocusing magnet and maximums at the center of the focusing magnets. The particles do not follow the $\beta(s)$ curves but oscillate within them in a form of modified sinusoidal motion whose phase advance is φ . This function $\beta(s)$ appears in the result of the equation for the motion of a particle around the ring [9].

To arrive at the definition of the Q-value, let's start by considering a particle moving around the ring, passing through magnetic fields of bending dipoles and focusing quadrupoles with following coordinate system:

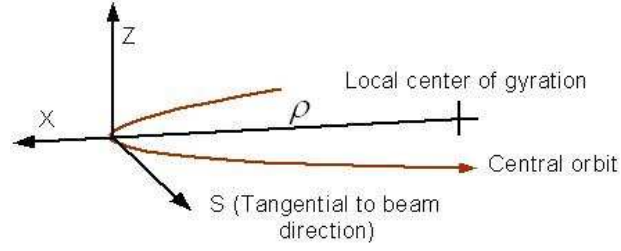


Figure 2.1: Charged particle orbit in a magnetic field

The differential equation for the horizontal plane that describes transverse motion of a particle passing through a short quadrupole is known as Hill's equation:

$$\ddot{x} + \left[\frac{1}{\rho(s)^2} - k(s) \right] x = 0 \quad (2.1.1)$$

where $k(s)$ is the function describing the focusing strength of the quadrupole around the ring.

The most general solution of the Hill's equation is a pseudo-harmonic oscillation:

$$x(s) = \sqrt{\beta(s)} \varepsilon \sin[\phi(s) + \phi_0] \quad (2.1.2)$$

The amplitude and wavelength depend on the coordinate s so that their values depend on the point of the ring circumference, and are both given in terms of the betatron function:

$$\text{amplitude} \propto \sqrt{\beta(s)}; \lambda(s) = 2\pi\beta(s) \quad (2.1.3)$$

By simple differentiation we get:

$$\dot{x} = \sqrt{\beta(s)} \varepsilon \cos[\phi(s) + \phi_0] - \left(\frac{\beta'(s)}{2} \sqrt{\frac{\varepsilon}{\beta(s)}} \sin[\phi(s) + \phi_0] \right) \quad (2.1.4)$$

The set of coordinates (x, \dot{x}) define the *phase space diagram* that has the shape of an ellipse of axis: $\sqrt{\beta(s)} \varepsilon$ and $\sqrt{\varepsilon/\beta(s)}$; and an area of: $\text{Area} = \pi \varepsilon$ ($\varepsilon = \text{emittance}$). ε is the emittance of the beam and is a measure of its area in phase space.

The *Q-value* or *betatron tune* is defined as the number of betatron oscillations per turn, that is, the number of oscillations that a particle describes around the nominal orbit when traveling around the machine, and can be expressed in the following way:

$$Q = \frac{R}{\beta} = \frac{2\pi R}{\lambda} \quad (2.1.5)$$

where β is nothing more than a local wavelength of the oscillations.

Q must not be a simple integer, otherwise the particle will repeat its path in the machine and will see the same field imperfections, leading to a resonant growth and the eventual loss of the particle. This is a dangerous condition which can be avoided by de-tuning the restoring gradients of the quadrupoles. The importance of Q is then that its value determines the stability of the beam.

Since Q must not be an integer, we define it a combination of an integer term and a fractional term:

$$Q = Q_{int} + q \quad (2.1.6)$$

with q the '*fractional part of the betatron tune*', a parameter of major importance in beam diagnostics.

From the definition of betatron tune it is possible to extract the concept of *betatron frequency* (ω_{bet}), whose relation with the revolution frequency (ω_{rev}) is:

$$\omega_{bet} = Q\omega_{rev} \quad (2.1.7)$$

With this definition it is possible to say that a particle in a beam performing betatron oscillations, describes a sinusoidal path around the nominal orbit associated to its energy (E_i), of the form:

$$x_i(t) = x_0 + x_i \cos(q\omega_{rev}t + \phi_i) \quad (2.1.8)$$

where x_0 is the mean position of the particle in the monitor ($x_0 = 0$ if it is centered), x_i is the oscillation amplitude, $q\omega_{rev}$ is the betatron frequency (ω_{bet}) at a fixed location in the ring, and ϕ_i is the initial random phase.

2.1.1 Tune measurement methods

The most common method for tune measurement is the excitation of the beam motion and the observation of the resulting signal in transverse detectors and analysis in the frequency domain. The following gives an overview of some of the common excitation techniques and the advantages of using FFT analysis for tracking the time evolution of the tunes. A new method for tune determination without perturbation of beam motion will be also introduced.

Measurement of Q by kicking [9, 11]

The method is to fire a kicker magnet with a pulse lasting less than one turn and observe the way in which the center of charge of the beam oscillates as it passes through a pick-up on sequential turns.

In order to understand this method, it is convenient to imagine a beam consisting of one short bunch circulating around the accelerator. At a given location in the ring, the beam will produce a periodic train of impulse functions separated in time by T_{rev} . In frequency domain, this periodic waveform is represented by a Fourier series with components at frequency multiples of the revolution frequency:

$$\rho(t) = \sum_n a_n \sin(2\pi n f_{rev} t) \quad (2.1.9)$$

Following the kick, the beam position detector fixed in one point of the ring, will see the line density current modulated by the betatron oscillation $y(t)$:

$$y(t) = y_0 \cos(q 2\pi f_{rev} t) \quad (2.1.10)$$

An oscilloscope connected to the pick-up will give a display of the modulated signal, the product of ρ and y :

$$\rho(t) \cdot y(t) = \frac{1}{2} \sum_n a_n y_0 [\sin 2\pi(n+q)f_{rev} t + \sin 2\pi(n-q)f_{rev} t] \quad (2.1.11)$$

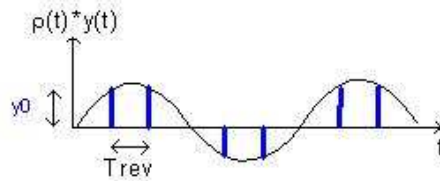


Figure 2.2: Time domain representation of transverse oscillation in a bunch of particles

The pick-up signal consists of bands centered at the frequencies:

$$f_{u,l} = (n \pm q) f_{rev} \quad (2.1.12)$$

If we measure the upper sideband and the lower sideband of the same harmonic we can calculate the non-integer part of Q with the formula:

$$q = n \frac{f_u - f_l}{f_u + f_l} \quad (2.1.13)$$

The difficulty, when frequencies of two peaks are measured, is to know if a frequency corresponds to the upper sideband of harmonic ' $n+1$ ' or to the lower sideband of harmonic ' n '. Some knowledge about the choice of the machine optics is needed.

A drawback of this method is that the tune measurement does not give information about the integer part of Q .

Chirp excitation [12]

The beam is excited with a sine wave whose frequency is increased linearly in time within a certain sweep range. The chirp frequency range is set around the expected betatron tunes and the duration of the chirp is taken depending on the requested time resolution and precision of the tune measurements. The data analysis of the beam motion is done either via sliding window Fourier Transform or via harmonic analysis. Figure 2.3 shows the result of a chirp measurement in the SPS and illustrates nicely the resulting beam oscillations during the excitation. It can be seen that the chirp starts below the beam resonance and crosses it at a certain moment before the chirp stops.

Every 30 ms the beam is excited for 20 ms with a sine wave ranging in frequency from tunes of 0.55 to 0.7. In the amplitude spectrum, the tune is defined via the maximum oscillation amplitude.

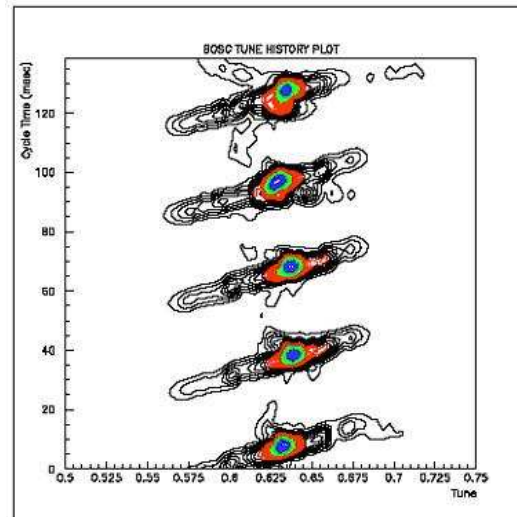


Figure 2.3: 3-D representation of the beam response to a chirp excitation

White noise excitation [12]

In this case, the beam is excited with bursts of white noise. The treatment of the data similar to the one used for chirp excitation as are the obtained results. The important difference is that for a white noise excitation much larger excitation strength is needed because most of the excitation energy is not used to excite the resonance.

Phase Locked Loop Tune Tracker (PLL) [12, 13]

Most tune measurements use the amplitude peak of the beam oscillation as the signal for tune measurements. This is somewhat odd, since the amplitude information with '0-slope' at its maximum suffers much more from noise than the phase information, which has its maximum slope at the tune resonance. Phase Locked Loop circuits make use of the phase slope. The beams are excited with a continuous sine wave. By changing the frequency of the exciting oscillator an analog or digital circuit assures that the phase difference between excitation and beam motion is 90° and this phase can be monitored continually by a PLL circuit. The tune measurement simply consists in the readout of the filtered frequency of the oscillator. In reality the design of such a PLL is more complicated, in particular the lock-in procedure and additional regulation circuits for constant amplitude excitation of the beam oscillation. Since the readout of the oscillator frequency can be made almost continuous a PLL circuit is the ideal tool for tracking the time evolution of the betatron tunes during machine transitions.

The signal flow diagram of a phase locked loop is shown in Figure 2.4. The phase detector compares the frequency of the beam motion with the frequency of a local oscillator. The phase detector output voltage is a measure of the frequency difference of its two inputs. After low pass filtering and amplification, this signal is used to adjust the frequency of the local oscillator (VCO), such that the oscillator 'locks' to the frequency of the input beam signal. The oscillator frequency serves as the betatron tune signal which is displayed or processed by the accelerator control system. .

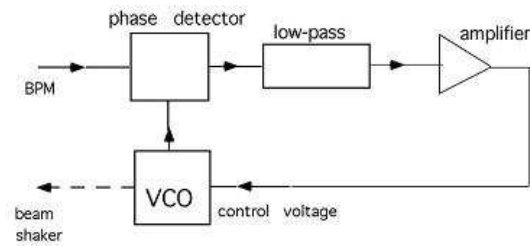


Figure 2.4: Schematic diagram of a PLL for continuous tune control

Measuring Tune from Schottky noise

All the techniques reported so far measured the *coherent betatron* tune, i.e., the oscillation frequency of the beam centroid. It is also possible to measure the *incoherent betatron tune*, that is, the oscillation frequency of individual particles in the beam by extracting information from the statistical noise signal detected by a transverse pick-up and displayed by a spectrum analyzer. This signal is called the *Schottky signal* and comes from the statistical fluctuations of the finite number of particles in the beam.

The way of measuring the tune, and the formulae used, are the same for the Schottky and the kicking methods. The advantage of the Schottky method is that it does not require the beam to be excited. Schottky theory will be discussed in detail in Chapter 3.

Data analysis: Fast Fourier Transform (FFT) of beam motion [12]

The tune value can be extracted using the amplitude or power density spectrum in frequency domain calculated from samples of the oscillation. With this method, the betatron tunes are determined as the frequency with the highest amplitude peak. The frequency resolution Δf is inversely proportional to the number of oscillation samples (N_{samp}). One can write: $\Delta f = 2/N_{samp}$. So if for example, one needs a tune resolution of 10^{-3} , at least 2000 samples have to be acquired. A modern computer can perform the time frequency transform FFT of 2048 samples in about 1 msec. If there is enough external excitation from other sources (ground motion, power supply ripple) or the beam is slightly unstable the method also gives useful information without specific beam excitation.

The time evolution of the tunes can be measured by accumulating many spectra and presenting them in a mountain range display. Figure 2.5 ⁽¹⁾ illustrates the accumulated magnitude spectra acquired with the 3D-BBQ system (Direct Diode Detection (3D) Base-Band Q) under develop at CERN [10]. The data was acquired on 2004 in the PS and on an AD cycle:

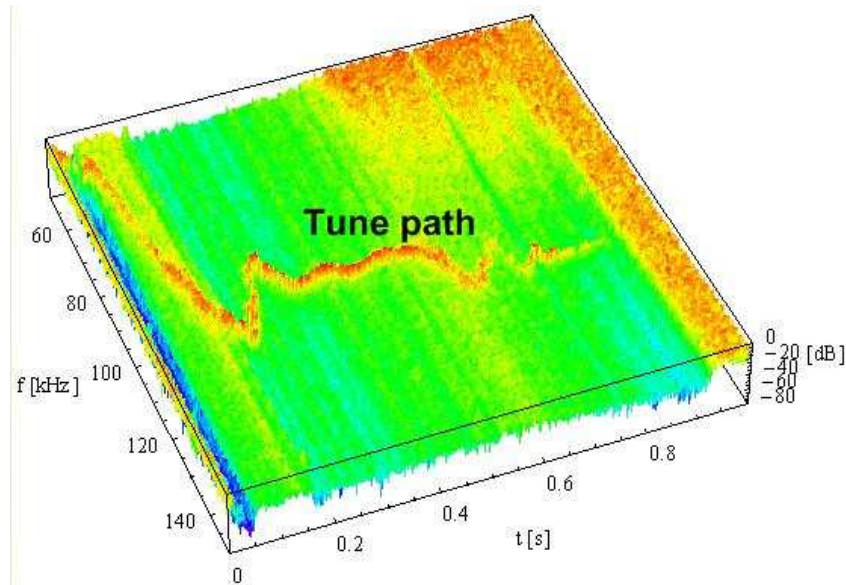


Figure 2.5: Long time FFT acquisition in the PS

Such a tool is indispensable for machine set-up and the study of many dynamic processes.

2.2 WHAT IS CHROMATICITY?

In the design of storage rings there are many similarities with the geometry of optics. In analogy to chromatic aberrations in optics, in particle accelerators a parameter called *chromaticity* is introduced. In optics, rays of different wavelength find a different refraction index in a lens and therefore experience a different focal length. Similarly, in a storage ring, particles of different momentum see a different focusing strength in the quadrupoles ($k_i = eg/p_i$) and, as a consequence, they have different betatron oscillation frequency [14].

The chromaticity is defined as the variation of the betatron tune Q with the relative momentum

¹Courtesy of Marek Gasior (CERN)

deviation $\Delta p/p$:

$$Q' = \frac{\Delta Q}{\Delta p/p} \quad (2.2.1)$$

Sometimes the *relative chromaticity* ξ is used:

$$\xi = \frac{Q'}{Q} = \frac{\Delta Q}{Q} \cdot \frac{p}{\Delta p} \quad (2.2.2)$$

The chromaticity has an important influence on the beam dynamics for two main reasons:

- First, a momentum spread $\Delta p/p$ is always present in a particle beam; therefore the chromaticity produces a tune spread in the beam: $\Delta Q = Q' \cdot \Delta p/p$. The wider this spread, the more chance there is of the particle hitting a resonance and being lost.
- Second, in the case of bunched beams, chromaticity produces a transverse instability called '*head-tail effect*'. The wake field produced by the leading part of a bunch (the head) excites an oscillation of the trailing part (the tail) of the same bunch. This can lead to instability of the bunch breaking it up and causing beam loss.

2.2.1 Chromaticity measurement methods

Measurement of tune during frequency modulation of the RF system [11, 15]

The standard procedure for measuring the machine chromaticity is based on frequency modulations of the radio frequency (RF) system. A change in the RF frequency moves the central orbit of the machine and this leads to a variation in the average beam momentum or energy. The energy and orbit variations change the tune proportionally to the total machine chromaticity. By measuring the tune for various RF frequencies it is possible to get the value of the chromaticity from the formula:

$$\frac{\Delta Q}{Q} = \xi \frac{1}{\left(\frac{1}{\gamma^2 - \alpha_p}\right)} \frac{\Delta f_{RF}}{f_{RF}} \quad (2.2.3)$$

where α_p is known as the *momentum compaction factor*.

The above procedure tends to be slow (measurement rate lower than 0.1 Hz) and, due to the change in energy and orbit, it perturbs the normal machine operation. Because of the limited momentum acceptance of the LHC this procedure may not be compatible with the nominal LHC operation.

Chromaticity measurement via RF phase modulation and continuous tune tracking

This method is still under development but it would allow the measurement of the machine chromaticity via RF phase modulation and continuous tune tracking [15]. The RF phase modulation also changes beam energy and orbit but it can be done at much higher frequencies than a classical RF frequency variation and thus, allows chromaticity measurements with a time resolution below the second.

The first measurements in the CERN SPS without tune tracking showed that a RF phase modulation can be used to generate an energy modulation of $\Delta p/p_0 = 10^{-4}$ at 600 Hz to 800 Hz without generating particle losses or longitudinal emittance growth. The first results show that the resulting transverse tune modulation is proportional to the machine chromaticity. The next steps for validating the proposed method include a continuous tune measurement with a PLL.

Width of tune resonance [12]

The momentum spread of the beam results in a width of the betatron lines that comes from decoherence due to the chromaticity when the bunch is kicked. Hence, the measurement of the width of the resonance could be used as a measure of the chromaticity ξ . But there are other effects contributing to the line width (radiation damping, transverse feedbacks) so that one only normally looks for variations in the width in order to deduce chromaticity changes. But in particular during acceleration this analysis is quite complicated as the momentum spread changes during the measurement and it would require a knowledge of how the momentum spread in the beam changed with energy.

Amplitude of synchrotron sidebands [12]

The chromaticity introduces amplitude modulation at the synchrotron frequency. This leads to sidebands on the tune. The amplitude ratio of the betatron lines to their synchrotron sidebands contains information about the chromaticity of the machine. However, this method can suffer from resonant behavior not linked to chromaticity. In addition, in proton machines the measurements are quite difficult since the synchrotron tune is low and the signals of the sidebands are often hidden in the spectral leakage of the main betatron tune peak.

Measuring chromaticity from the Schottky noise

From Schottky noise it is possible to obtain information about the chromaticity by analyzing the width of the betatron tune sidebands that appear at both sides of the revolution lines in the characteristic transverse spectrum of a bunched beam and using the formula:

$$\xi = \frac{\eta}{Q} \cdot \left[n \cdot \frac{\Delta f_u - \Delta f_l}{\Delta f_u + \Delta f_l} - q \right] \quad (2.2.4)$$

This method will be addressed in detail in Chapter 3.

Phase of Head and Tail betatron oscillations [12]

The so-called 'Head-Tail' chromaticity measurement method allows the chromaticity to be calculated from several hundred turns of data after a transverse kick. The measurement relies on the periodic de-phasing and re-phasing that occurs between the head and tail of a single bunch for non-zero chromaticity. By measuring turn-by-turn position data from two longitudinal positions in a bunch it is possible to extract the relative de-phasing of the head and tail, and so to determine the chromaticity.

The observable, linked to chromaticity is the phase difference between the head and tail oscillations. By the exciting kick, this phase difference is initially forced to zero, evolving to a maximum after half a synchrotron period. Figure 2.6 shows a computer simulation of the head and tail motion for non zero chromaticity. The vertical axis is time (in [ns] along the longitudinal bunch profile), the horizontal axis is the revolution number after the kick stimulus and the amplitude of the betatron oscillations is encoded in gray scale.

The chromaticity can be expressed as follows:

$$\xi = \frac{-\eta \Delta \Psi(n)}{Q_0 \omega_{rev} \Delta \tau [\cos(2\pi n Q_s - 1)]} \quad (2.2.5)$$

where $\eta = 1/\gamma^2 - \alpha_p$ is the slip factor; Q_s is the synchrotron tune, ω_{rev} is the nominal angular revolution frequency; $\Delta \Psi(n)$ is the head-tail phase difference; $\Delta \tau$ is the time between the head and the tail and Q_0 is the nominal betatron tune. Practically the fractional part of the betatron tune can be ignored as Q_0 in equation 2.2.5 is the total tune of the machine where the integer part dominates.

The advantages of this method are that: it allows a single point measurement since there is no need of varying the RF frequency; it is a fast tool, a chromaticity measurement can be made during

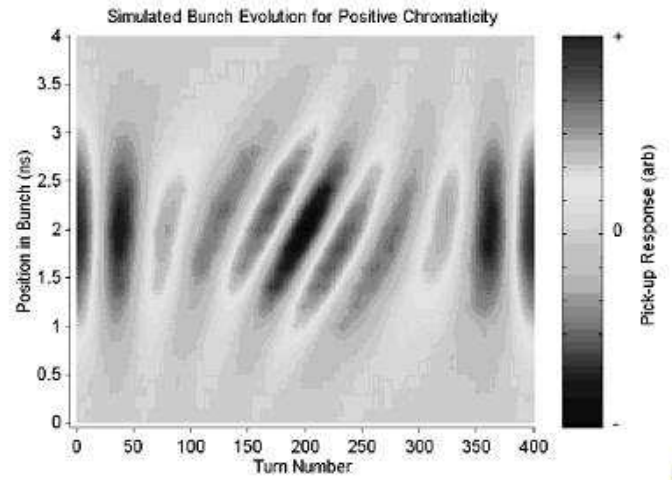


Figure 2.6: Computer simulation of head-tail motion

one synchrotron period (about 15-50 ms in the case of LHC) and it is not limited by the speed the RF frequency can be cycled ; in addition, it can allow for other parasitic measurements, i.e., 2^{nd} order chromaticity, transverse instabilities and maybe impedance.

A detailed explanation of this method and a complete analytical study will be developed in Chapter 6.

Chapter 3

Schottky Theory and Measurement Methods

In 1918 W. Schottky published a paper in which he described his observations on the electron current obtained when electrons were emitted from a thermionic cathode and attracted towards an anode. He found that the current measured contained a noise component due to the random emission process from the cathode. The Schottky formula simply reflects the fact that the anode current is composed of individual electrons randomly emitted by the cathode. Very similarly, the beam current in a particle accelerator exhibits the random component which comes from the large, but finite, number of particles in the beam [16].

In fact, the original noise measured by Schottky was white noise that is, it had spectral components at all frequencies in equal amounts. The Schottky noise observed in a particle beam has the same statistical properties but is, in general, composed of an infinite number of bands of noise which approach white noise only at high frequencies.

The analysis of "Schottky noise" signals is a very powerful tool to study accelerator behavior, allowing machine parameters such as betatron tune, chromaticity, momentum spread and emittance to be calculated without requiring additional beam excitation.

In the following sections, formulae describing the Schottky phenomenon are derived and measurement methods of Schottky signals in a beam will be described.

3.1 SCHOTTKY SIGNALS

To find out the information we can extract from these signals and to understand their properties better, a few formulae will be derived.

For Schottky signals, as well as taking into account the plane of beam motion (transverse or longitudinal), it is also convenient to consider the beam as either bunched or unbunched according to whether the radio-frequency (RF) system is on or off respectively. At first sight it might seem that the action of the RF system in constraining particles to remain within the bucket would remove the randomness which gives the Schottky signals. It is true that some degrees of freedom have been lost, but the large number of particles in the bucket, having different synchrotron frequencies according to their particular orbits, is nevertheless randomly spread in this bucket and noise signals related to those ones that can be seen in the unbunched case can be detected. Unbunched signals are the easiest to deal with and will be treated first.

3.1.1 The longitudinal Schottky signals of unbunched beam

For a single particle circulating in a machine (charge e , revolution period $T_{rev} = 1/f_{rev}$), the average beam current is:

$$i_i = \frac{e\omega_{rev}}{2\pi} \quad (3.1.1)$$

At a given location in the ring, this particle will produce a periodic train of impulse functions separated in time by T_{rev} :

$$i_i(t) = \sum_{n=0}^{\infty} i_i \delta(t - nT_{rev}) = \frac{e\omega_{rev}}{2\pi} \sum_{n=0}^{\infty} \delta(t - nT_{rev}) \quad (3.1.2)$$

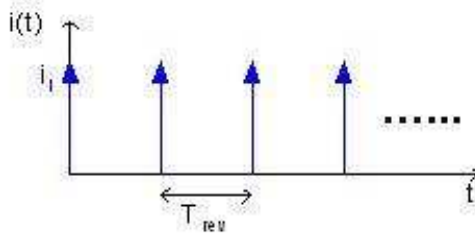


Figure 3.1: Beam current for a single particle

In frequency domain, this periodic waveform is represented by a line spectrum, the distance between lines being ω_{rev} .

$$I_i(\omega) = e\omega_{rev} \sum_{n=0}^{\infty} \delta(\omega - n\omega_{rev}) \quad (3.1.3)$$

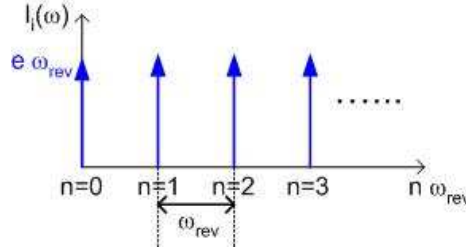


Figure 3.2: Spectrum for a single particle circulating in the machine

For N particles, randomly distributed in azimuth along the ring circumference (debunched beam case) and having slightly different ω_{rev} , each line at frequency $n f_{rev}$ which is infinitely narrow in the case of a single particle, will be replaced by a band of frequencies (Schottky band) whose width is given by:

$$\Delta f = n \Delta f_i = n f_{rev} \eta \frac{\Delta p}{p} \quad (3.1.4)$$

with Δf_i being the spread in the particle's revolution frequencies resulting from the relative momentum spread $\Delta p/p$; η the 'slip factor', $\eta = (1/\gamma_t^2 - 1/\gamma^2)$; and f_{rev} the average revolution frequency.

When averaging equation 3.1.3 over N particles, only the DC term remains ($i_{DC} = N e f_{rev}$) and the r.m.s. current per band is given by the sum:

$$\langle i^2 \rangle = \left\langle (2e f_{rev})^2 \left[\sum_N \cos(\cos n \omega_{rev} t) \right]^2 \right\rangle = (2e f_{rev})^2 \sum_N \langle \cos^2(n \omega_{rev} t) \rangle = 2e^2 f_{rev}^2 N \quad (3.1.5)$$

$$i_{rms} = \sqrt{\langle i^2 \rangle} = 2e f_{rev} \sqrt{\frac{N}{2}} \quad (3.1.6)$$

The r.m.s. current per band (Schottky current) is independent of n (harmonic number) and proportional to the square root of the number of particles N .

The total power in the n^{th} band is therefore independent of n , i.e., constant, but the width of each band increases with the harmonic number, therefore, the amplitude of each band will decrease correspondingly. At the same time, the increase in width with n eventually leads to frequency

spreads larger than the spacing between the lines, f_{rev} , causing the lines to overlap and leading to a spectrum that looks more like white noise.

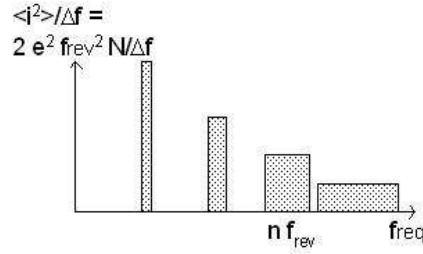


Figure 3.3: Power spectral density of Schottky lines with increasing n

3.1.2 Transverse Schottky signals of unbunched beams

Again we consider a single particle but in this case it performs betatron oscillations and is being observed with a pick-up which is sensitive to transverse motion. At any point of the machine, this particle will produce a train of impulse functions modulated by the betatron frequency.

The beam current, $i_i(t)$, must be replaced by the dipole moment $d_i(t) = a_i(t) \cdot i_i(t)$, where $a_i(t)$ is the transverse displacement. The i_{th} particle executes a sinusoidal betatron oscillation, of amplitude a_i , which can be written as:

$$a_i(t) = a_0 + a_i \cos(q\omega_{rev}t + \phi_i) \tag{3.1.7}$$

where a_0 is the mean position of the beam in the monitor, a_i is the oscillation amplitude, $q\omega_{rev}$ is the betatron frequency (ω_{bet}) at a fixed location in the ring and ϕ_i is the initial random phase.

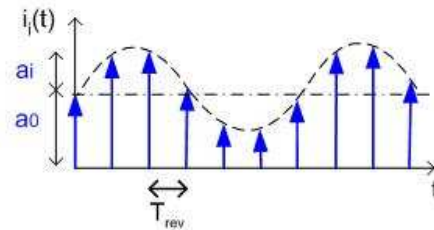


Figure 3.4: Time domain representation of a single particle transverse oscillation

In time domain it can be written as:

$$\begin{aligned}
 d_i(t) &= [a_0 + a_i \cos(q\omega_{rev}t)] \cdot \left[e f_{rev} + 2e f_{rev} \sum_{n=0}^{\infty} \cos(n\omega_{rev}t) \right] \\
 &= a_0 e f_{rev} + a_0 2e f_{rev} \sum_{n=0}^{\infty} \cos(n\omega_{rev}t) + \\
 &\quad a_i e f_{rev} \left[\cos(q\omega_{rev}t) + \sum_{n=0}^{\infty} \cos\{(n-q)\omega_{rev}t\} + \sum_{n=0}^{\infty} \cos\{(n+q)\omega_{rev}t\} \right] \quad (3.1.8)
 \end{aligned}$$

This more complicated expression only says that two sidebands are added to each revolution frequency line $n f_{rev}$, one at frequency $n f_{rev} + f_{bet}$ and another one at frequency $n f_{rev} - f_{bet}$. The spectrum is now a series of lines placed at revolution harmonics ($n f_{rev}$) and two betatron sidebands per revolution line at frequencies $(n-q) f_{rev}$ and $(n+q) f_{rev}$. With a beam centered in the pick-up, the harmonics of f_{rev} will not be present.

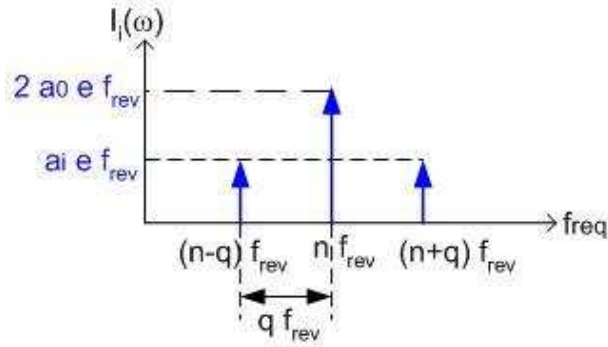


Figure 3.5: Frequency domain representation of a single particle performing transverse oscillation

Following the argument used with the longitudinal lines, the effect of having particles with different energies leads to a spread in revolution frequency. There is, however, a second effect in the transverse plane, due to the passage through the quadrupoles of these particles with different energies. This leads directly to a change in focusing strength that the particle experiences and hence to a change in its tune or q . The change in q is related to the difference in momentum by the chromaticity ξ .

The two effects are:

$$\frac{\Delta f}{f_{rev}} = \eta \cdot n \frac{\Delta p}{p}$$

$$\frac{\Delta q}{Q} = \xi \frac{\Delta p}{p} \quad (3.1.9)$$

The sum of both effects gives the line width for the lower and upper sidebands:

$$\Delta f_{u,l} = f_{rev} \frac{\Delta p}{p} [(n \pm q)\eta \pm Q\xi] \quad (3.1.10)$$

For N particles in the beam randomly distributed in azimuth and in betatron phase, the averaging of equation 3.1.8 gives:

$$\langle d^2 \rangle = \langle a_i^2 \rangle = e^2 f_{rev}^2 \frac{N}{2} \quad (3.1.11)$$

$$d_{rms} = e f_{rev} a_{rms} \sqrt{\frac{N}{2}} \quad (3.1.12)$$

Again, the total power per Schottky band $\langle d^2 \rangle$ is independent of the harmonic n , and is proportional to the number of particles in the beam and to the square of the average betatron amplitude a_i .

According to the signs of the chromaticity and the slip factor, either the upper or the lower sideband will be wider. The same argument as used for the longitudinal lines shows that the total power in the two sidebands, regardless of n , is the same. Therefore the amplitude of the broader line will be smaller than that of the narrower one.

By measuring the frequency of two sidebands $f_l = (n - q)f_{rev}$ and $f_u = (n + q)f_{rev}$, the average q value may be found:

$$q = n \frac{f_u - f_l}{f_u + f_l} \quad (3.1.13)$$

What is measured here is the incoherent q value. This is in contrast to the method where the entire beam is kicked and the coherent signals are observed which results in the measurement of coherent tune.

The comparison between equations 3.1.6 and 3.1.12 gives a direct measure of the *r.m.s* beam size:

$$a_{rms} = 2 \frac{d_{rms}}{i_{rms}} \quad (3.1.14)$$

This equation can be used to directly measure the transverse beam emittance but requires a well calibrated electronics chain to measure d_{rms} and a calibrated beam current monitor to measure i_{rms} .

Machines such as the SPS normally work with the RF on to hold the particles within a small percentage of the circumference of the machine. Under these conditions it is not evident that arguments about randomness are valid. Certain signals that are seen at the output of the Schottky detector are in fact very different and show properties due to coherence of the bunch, i.e. that the particles are in certain ways forced to act together. However, the large number of particles within the bunch shows a random distribution and this leads to noise-like signals as before.

3.1.3 The longitudinal Schottky signals of bunched beams

Returning once more to the circular accelerator with one particle moving around and being observed by a longitudinal monitor, this time with the addition of an RF cavity. The RF frequency is at some harmonic of the particle revolution frequency so that a particle that happens to pass through a given value will see the same cavity voltage on every passage. This particle is called *synchronous particle*. A particle that does not sit exactly at this stable point will be periodically accelerated and decelerated so that its position relative to the stable particle oscillates back and forth at the synchrotron frequency f_s .

In the bunched beam case, every individual particle executes synchrotron oscillations around the synchronous particle at the frequency f_s . The time of passage of the particle at the detector is modulated according to:

$$\tau_i(t) = \hat{\tau}_i \sin(\Omega_s t + \varphi_i) \quad (3.1.15)$$

being $\hat{\tau}_i(t)$ is the time difference with respect to the synchronous particle (frequency f_0), $\hat{\tau}_i$ is the amplitude of the synchrotron oscillation and φ_i is the starting phase. In time domain, the beam current is represented in Figure 3.6, as a series of delta pulses, with a modulated time of passage.

Taking the original equation for unbunched longitudinal motion and modifying it with the above synchrotron, we get:

$$i_i(t) = e f_{rev} + 2e f_{rev} \operatorname{Re} \left\{ \sum_{n=1}^{\infty} e^{jn\omega_{rev}} [t + \hat{\tau}_i \sin(\Omega_s t + \varphi_i)] \right\} \quad (3.1.16)$$

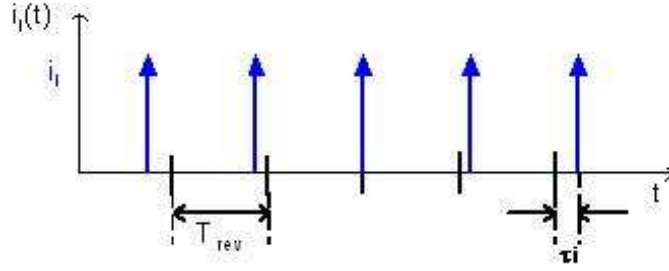


Figure 3.6: Time domain representation of the current of a single particle in a bunched beam

Using the relation:

$$e^{j(z \sin \Theta)} = \sum_{p=-\infty}^{+\infty} J_p(z) e^{jp\Theta} \quad (3.1.17)$$

where J_p is the Bessel function of order p , one can expand the n^{th} harmonic in equation 3.1.16 one obtains:

$$i_n = 2ef_{rev} \text{Re} \left\{ \sum_{p=-\infty}^{+\infty} J_p(n\omega_{rev}\hat{\tau}_i) \exp j(n\omega_{rev}t + p\Omega_s t + p\varphi_i) \right\} \quad (3.1.18)$$

Then, the beam current is:

$$i_i(t) = ef_{rev} + 2ef_{rev} \sum_{n=1}^{\infty} \sum_{p=-\infty}^{+\infty} J_p(n\omega_{rev}\hat{\tau}_i) \cos j(n\omega_{rev}t + p\Omega_s t + p\varphi_i) \quad (3.1.19)$$

Each revolution frequency line nf_{rev} now splits into an infinite number of synchrotron satellites, spaced by $\Omega_s/2\pi$, the amplitudes of which are proportional to the Bessel functions of argument $n\omega_0\hat{\tau}_i$.

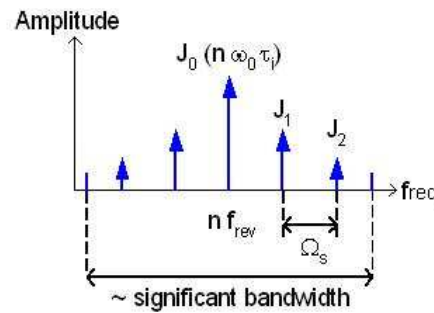


Figure 3.7: Decomposition of each revolution line into synchrotron satellites

Knowing the frequency of the particular harmonic $n f_{rev}$ and the amplitude of the oscillation in the bucket, the tables of Bessel functions give the amplitude of the different lines $p=1, p=2$, etc. Nothing limits the maximum value that p can have but in practice all the lines with significant amplitude are within the range $df = 2n f_{rev} \hat{\tau}_i \Omega_s$.

The spread in the instantaneous revolution frequency of the i^{th} particle due to the synchrotron oscillation is simply:

$$2\Delta\omega = 2\Omega_s n \omega_{rev} \hat{\tau}_i \quad (3.1.20)$$

Consequently, for large values of n , the *significant bandwidth* around line n is the same as that of many particles in an unbunched beam having the same $\Delta\omega_i$ and therefore the same $\Delta p/p$. In practice, such spectra are observed on a spectrum analyzer when the interfrequency filter bandwidth is set larger than the synchrotron frequency. For a given n , the central line ($p=0$) shows the same

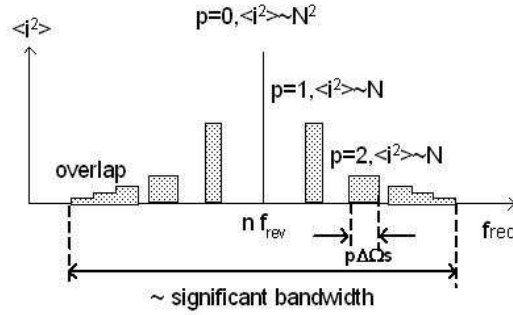


Figure 3.8: Longitudinal Schottky spectrum of a bunched beam for large values of n

phase factor ($\exp jn\omega_{rev}t$) for all particles. This line is therefore proportional to N and not to \sqrt{N} and is simply the macroscopic RF current of the bunch. On the contrary, the synchrotron satellites ($p \neq 0$) add r.m.s wise because of the random phase factor $\exp(jn\omega_{rev}t + p\Omega_s t + p\varphi_i)$.

Each line is infinitely narrow if the synchrotron oscillation is the same for all particles and if the machine has no imperfections. However, magnet and RF fluctuations broaden in practice each individual line. In addition, a spread in synchrotron frequency within the bunch $\Delta\omega_s$ transforms each satellite ($p \neq 0$) into a band of width $p\Delta\Omega_s$. For large values of n , overlap between successive synchrotron satellites ($p\Delta\Omega_s > \Omega_s$) can occur within the significant width of the Schottky band of order n .

In practice, the width of the central line will not be infinitely thin. Any imperfections in the RF oscillator or in the magnetic dipole field which modify the orbit length will change f_{rev} , and this will show up as an increase in the line width.

3.1.4 The transverse Schottky signals of bunched beams

Here we have to combine the amplitude modulation (betatron oscillation) and the time modulation (synchrotron oscillation) to obtain:

$$d_i(t) = [a_0 + a_i \cos(q\omega_{rev}t + \phi_i)] \cdot \left[e f_{rev} + 2e f_{rev} \operatorname{Re} \left\{ \sum_{n=1}^{\infty} \exp jn\omega_{rev}[t + \hat{\tau}_i \sin(\Omega_s t + \varphi_i)] \right\} \right] \quad (3.1.21)$$

It is not difficult to deduce how the frequency spectrum that this equation represents will look like on a spectrum analyzer. Starting with lines at f_{rev} , the amplitude modulation will split each line into two betatron lines at frequencies $(n - q)f_{rev}$ and $(n + q)f_{rev}$. The phase modulation will further subdivide these lines into sets of synchrotron lines spaced by f_s .

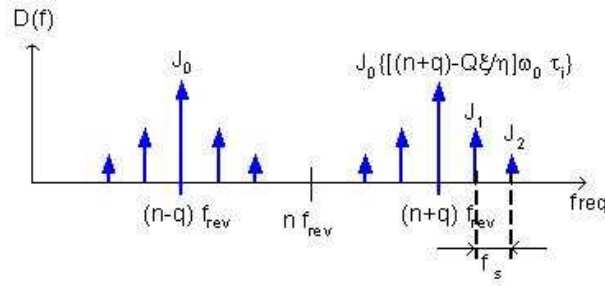


Figure 3.9: Decomposition of each betatron line into synchrotron satellites

Assuming the exact centering of the beam ($a_0 = 0$) in the monitor, no revolution lines are observed and an expression can be derived for the amplitude of a particular line of a single particle:

$$d_{i,n}(t) = e f_{rev} a_i \operatorname{Re} \left\{ \sum_{p=-\infty}^{+\infty} J_p[(n \pm q)\omega_{rev} \hat{\tau}_i] \exp j[(n \pm q)\omega_{rev} + p\Omega_s t + p\varphi_i + \phi_i] \right\} \quad (3.1.22)$$

If precaution is not taken to very accurately center the beam, then the f_{rev} signal will reappear, as in the bunched longitudinal signal, and will hide the other lines.

For a non-zero chromaticity, the argument of the Bessel function should be replaced by: $J_p[(n \pm q) - Q\xi/\eta]\omega_{rev} \hat{\tau}_i$. In this case, the relative amplitudes of the synchrotron satellites also depend

on chromaticity. In particular, for the chromatic frequency $\omega\xi = Q\omega_0\xi/\eta$, only the term J_0 is significant: all the energy of the Schottky band is concentrated in the central line.

For many particles, we should average over the two random variables ϕ_i and φ_i . Unlike the longitudinal case, the central lines ($p=0$) add r.m.s. wise due to the random betatron phase factor ϕ_i .

The width of the central line is determined by RF and magnetic field fluctuations, but also by transverse non-linearities (tune spread due to octupole fields, beam-beam or space charge forces). In addition, the synchrotron satellites are broadened by the spread in synchrotron frequencies within the bunch.

The total power per band for a given n is:

$$\langle d_n \rangle^2 = e^2 f_{rev}^2 \langle a_i^2 \rangle \frac{N}{2} \sum_p J_p^2[(n \pm q)\omega_{rev}\hat{\tau}_i] \quad (3.1.23)$$

With the identity $\sum_{p=-\infty}^{+\infty} J_p^2(x) = 1$, one obtains:

$$\langle d_n \rangle^2 = e^2 f_{rev}^2 \langle a_i^2 \rangle \frac{N}{2} \quad (3.1.24)$$

The total power per band is the same as in the coasting beam case, for the same total number of particles and the same transverse oscillation amplitude.

3.2 EXTRACTION OF THE BEAM PARAMETERS FROM THE SCHOTTKY SPECTRA

The analysis of the spectra obtained with a Schottky monitor is a method for easily extracting the beam parameters without perturbing the beam, as traditional methods do.

For deriving the expressions that are used to calculate the *tune*, the *chromaticity* and the *momentum spread*, let's consider first the typical transverse Schottky spectrum observed in a Schottky pick-up for unbunched beam (or bunched beam without synchrotron frequency resolution) that is illustrated in Figure 3.10.

In the picture there are the upper and lower tune sidebands centered around the harmonic nf_{rev} and that arise as a consequence of the betatron motion. Since there is a spread in the energy of the particles, the frequency lines become frequency bands.

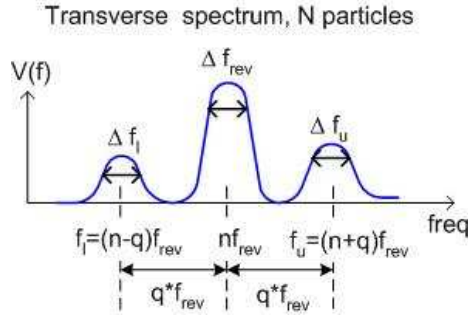


Figure 3.10: Typical transverse spectrum observed in a Schottky monitor

3.2.1 The betatron tune (q_v)

As it was derived in Section 3.1.2, the upper and lower tune sidebands sit at frequencies:

$$\text{Upper sideband } f_u = (n + q)f_{rev}$$

$$\text{Lower sideband } f_l = (n - q)f_{rev}$$

By addition and subtraction of both expressions one obtains:

$$f_u + f_l = 2q_v f_{rev}$$

$$\text{and } f_u - f_l = 2n f_{rev}$$

that leads to the following equation:

$$q_v = \frac{f_u - f_l}{2 \cdot f_{rev}} \quad (3.2.1)$$

3.2.2 The chromaticity (ξ_v)

The spread in the energy of the particles leads to a spread in the revolution frequency and in the betatron tune of the particles. As a consequence, the frequency lines in the Schottky spectrum become frequency bands of width:

$$\text{Upper sideband } \Delta f_u = f_{rev} \frac{\Delta p}{p} [(n + q)\eta + Q\xi]$$

$$\text{Lower sideband } \Delta f_l = f_{rev} \frac{\Delta p}{p} [(n - q)\eta - Q\xi]$$

The addition and subtraction of both expressions gives:

$$\Delta f_u + \Delta f_l = f_0 \frac{\Delta p}{p} 2n\eta$$

$$\text{and } \Delta f_u - \Delta f_l = f_0 \frac{\Delta p}{p} (2q_v\eta + 2Q\xi)$$

Dividing both equations one finally gets the value of chromaticity given by:

$$\xi_v = \frac{\eta}{Q_V} \left[n \cdot \frac{\Delta f_u - \Delta f_l}{\Delta f_u + \Delta f_l} - q_v \right] \quad (3.2.2)$$

3.2.3 The momentum spread ($\Delta p/p$)

As in the previous case, the momentum spread can be easily obtained from the addition of the widths of the upper and lower tune sidebads ($\Delta f_u + \Delta f_l$). The resulting equations is:

$$\frac{\Delta p}{p} = \frac{\Delta f_u + \Delta f_l}{f_{rev} \cdot 2 \cdot n \cdot \eta} \quad (3.2.3)$$

3.3 MEASUREMENT METHODS OF SCHOTTKY SIGNALS

Accelerator instrumentation is used to observe the particle beam as it travels in the machine. Monitors such as the *beam current transformer* (BCT), the *beam position monitor* (BPM), or the *longitudinal wideband monitor*, are designed to look at the global properties of the particle beam behaving as a modulated electric current. The *Schottky monitor* couples to the electromagnetic fields of the beam in exactly the same way as the more familiar monitors cited, but is designed, with its associated electronics, to look deeper in the beam, into its microstructure, using properties of the beam that come from the fact that the beam is not a continuous electric current but a vast number of individual particles acting only approximately together [17].

Let's consider a beam that has been accelerated to top energy and left coasting (unbunched particles distributed all along the machine). This beam is composed of a very large number N of particles that give a current of Nef_{rev} on the BCT as they rotate in the machine at the revolution frequency f_{rev} . In the beam, the particles will probably not be uniformly distributed around the circumference. A snapshot of the beam at a given instant with sufficient resolution to see individual particles would show that, although the number of particles per unit length is on average always the same for any sample, there are small variations in this value. In fact, the distribution of particles is entirely random. The exact number of particles in a given slice of beam cannot be predicted. When working with a large number of randomly distributed objects such as in this case, the properties can only be described in statistical terms. It may not be possible to predict exactly how many particles

will be found at a given place in the machine, but something can be said about the probability of how many particles there will be, about the mean values of currents, which we know from the BCT, about the probable deviations from these mean values and the distribution about the mean.

In practice this means that in a monitor, superimposed to a D.C. signal (beam current in a scope, mean radial position on a radial beam position monitor...) there will be a noisy signal giving random variations caused by the individual particles. Usually great effort is made to eliminate noise and obtain nice clean signals however it is likely that this noise contains more detailed information about beam properties.

It is with this purpose that Schottky monitors are used. The BCTs and the BPMs can also give this information but are not optimized for the purpose. The Schottky monitors are specially designed to observe the extremely small signals existing on the beam due to this random distribution of particles.

3.3.1 Monitors for Schottky observation

Because of the relative weakness of Schottky signals, one important requirement for the detectors is very high sensitivity. A second problem frequently encountered is the contamination of the Schottky signal by the much stronger coherent signal produced by the bunched beam. One way to overcome this problem is to make the detector resonant at a frequency above the '*single-bunch cutoff frequency*'.

Different types of electromagnetic devices can be used as beam detectors: resistive-gap pick-up, electrostatic pick-up, wall-current pick-up, slot-type pick-up... and some of them can be adapted to act as Schottky signals detectors. This section reviews some of the most common monitors used for Schottky detection.

The transverse electrostatic pick-up [16, 18]

An electrostatic pick-up is a capacitive structure like the one in Figure 3.11.

Electrostatic theory shows that the difference in voltage between the two plates is a linear function of the beam displacement. These couplers are mostly used for closed orbit measurements and sometimes horizontal and vertical pick-ups are combined in a single unit. They can be made resonant and be tuned to act as a Schottky monitor if a coil is connected to the electrode.

The mechanical configuration can be modeled by an electric circuit as depicted in Figure 3.12 where C_p is the coupling capacitance between the two electrode plates, C_g is the capacitance between

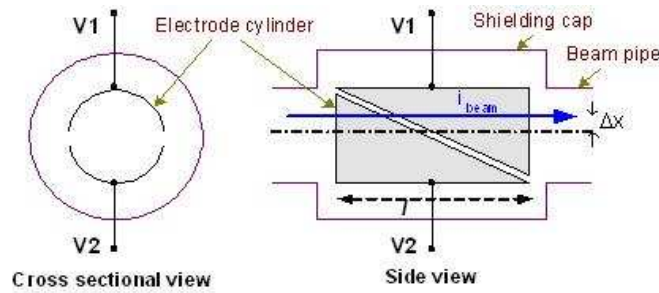


Figure 3.11: Transverse electrostatic pick-up

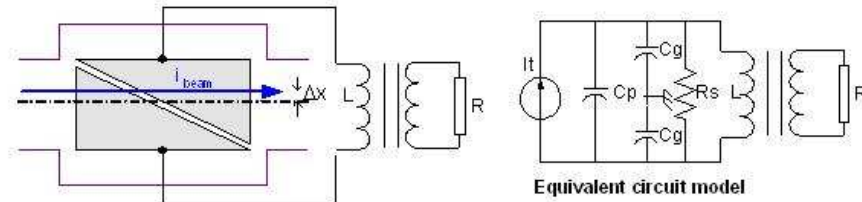


Figure 3.12: Transverse electrostatic pick-up used as Schottky detector

the electrodes and the beam pipe, and R_s is resistance associated with the inductor L .

This technique has been used in the Fermilab Recycler Ring as a Schottky detector. The pick-up was tuned to resonate at 7.59 MHz for tracking betatron sidebands.

The wall current pick-up [19]

Consider a circular vacuum chamber with a proton beam passing along the axis. For a relativistic proton beam, the image charge in the walls is an accurate representation of the charge distribution in the beam. If the vacuum chamber is cut around the circumference and a resistance inserted across the gap formed, then a voltage proportional to the beam current is developed and can be measured. In deriving an equivalent circuit for this pickup it is supposed that there will be a closed chamber around the gap for shielding the gap from external fields and for providing a vacuum seal.

As in the derivation of the equivalent circuit for electrostatic pickups, the beam is taken as an infinite current source, C represents the capacitance across the gap, R the measuring resistance and Z the impedance of the box measured at the gap. As $Z \rightarrow \infty$ this becomes a low pass network, C providing the high frequency cut off. Again, this detector can be implemented as a resonant

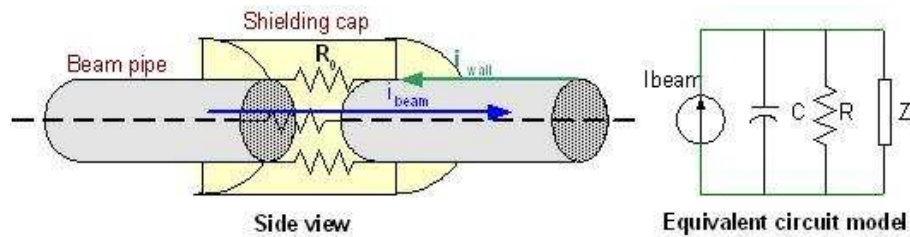


Figure 3.13: Wall current pick-up

configuration and used as a Schottky detector.

A Schottky pick-up like this one was used in the SPS to get information about the momentum distribution of protons in the beam, operating at frequencies between 500 and 1500 MHz.

Slot-type pick-ups [20]

At high frequencies (typically > 1 GHz), slot-type pick-ups become interesting. The field from the particles couples to the transmission line behind the slots. If the latter are shorter than $\lambda/2$, the coupling is weak and the contributions from each slot may all be added together, provided the velocity along the line is equal to the particle velocity.

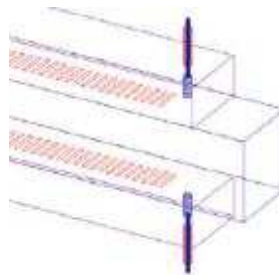


Figure 3.14: Slot-type pick-up

3.3.2 Observation of Schottky signals: spectral analysis

The measurement of the power spectral density of the Schottky signals gives the particle distribution in either momentum or betatron tune. Therefore, spectral analysis is the natural technique for observing Schottky signals [16].

The easiest way to observe Schottky spectra is by means of a *spectrum analyzer*. It works on the principle of a '*super-heterodyne receiver*' to convert higher frequencies to measurable quantities. However, one problem with this instrument is that the measurement is slow since the received frequency spectrum is scanned through a given frequency span Δf_s with a given resolution Δf_r .

The frequency span of interest is of the order of the revolution frequency. The signals are essentially noise signals and it is necessary to average them to get a good estimate of the most probable value. If there are changes in the beam or machine parameters then it is convenient to be able to follow them as quickly as possible while maintaining sufficient resolution to see the details. These factors all lead to the use of the Fast Fourier Transform (FFT) to evaluate in real time the signal spectrum.

FFT spectrum analyzers typically have bandwidths of 100 kHz (i.e. half the sampling frequency), have averaging and windowing possibilities together with data manipulation facilities. In the FFT technique, the signal is being continuously sampled and digitized at a frequency F_s . The time record obtained this way is transformed into the frequency domain by a built-in processor that computes the Fourier transform. Each digital word is stored in a memory of M locations: the duration of the signal sample to be analyzed is then $T = M/F_s$. The frequency content of the sampled signal extends only up to $F_s/2$ (Nyquist theorem) and the resolution of the frequency analysis is of the order of $1/T$. Depending on the choice of the signal processing 'window', the resolution varies a little: $1/T$ for the rectangular window; $1.4/T$ for the 'Hamming' window, better optimized for noise signals.

The Schottky band to be analyzed will normally be much higher than the operating frequency of the FFT analyzer ($\sim 100kHz$) and must be translated to low frequency prior to analysis. This requires a careful prefiltering to reject the unwanted image frequencies. The signal processing chain has, as its task, the amplification of the signal without the introduction of noise and the frequency change from the operating frequency of the monitor to the range of frequency of the analyzer.

Chapter 4

The SPS 1.8GHz Schottky Monitor

A Schottky detector for high-frequency signals in the LHC has been designed in the framework of the US-LARP collaboration.

Preliminary tests were performed on a 1.8GHz waveguide Schottky detector system installed in the SPS accelerator and that was built following the design of those in the Fermilab Tevatron and Recycler accelerators. The waveguide detector is designed to measure the transverse and longitudinal Schottky signals of the accelerator at a frequency high enough to avoid, in principle, coherent beam signals that could overlap the incoherent Schottky bands. In the Recycler this pickup is used to provide the signal for stochastic cooling, while in the Tevatron it is used for the non-destructive measurement of beam emittance and tune. This chapter describes the characteristics of such a monitor together with the electronics employed in data acquisition in the SPS.

4.1 SPS 1.8GHz MONITOR CHARACTERISTICS

The '*slow wave slotted waveguide Schottky pickup*' that was installed in the SPS consists of a rectangular beam pipe with two waveguides on either side [21]. The wall between waveguide and beam pipe is made of slotted thin aluminium foil for coupling the signal into the waveguide as illustrated in Figure 4.1.

The image current that flows along the walls of the beam pipe due to a charged particle beam traveling in the center of the pick-up, excites electromagnetic waves in the slots which in turn excite traveling waveguide modes in the side waveguides of the beampipe. This kind of detector is bi-directional and is used in FNAL to provide both proton and antiproton signals. The design goal of

these Schottky pickups is to achieve high impedance at the frequency of operation with a bandwidth of 100MHz.

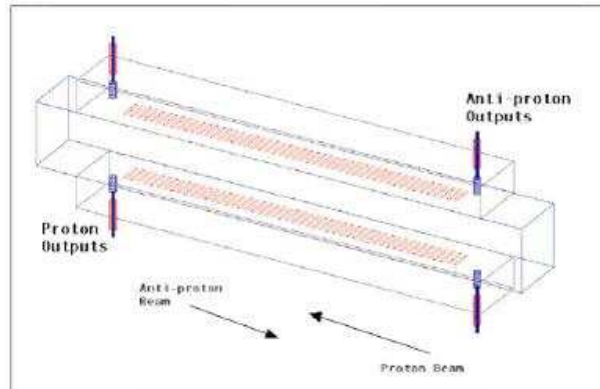


Figure 4.1: Schottky pick-up design

Figure 4.2 shows the Schottky pickup fabricated for installation in the SPS.



Figure 4.2: Fabricated Schottky pick-up

The basic design parameters of the pick-up are listed in table below.

Slot length	Slot width	Spacing	Number of slots	Waveguide width	Waveguide height	Beam pipe width	Beam pipe height
62.20mm	2.03mm	2.03mm	216	109.22mm	54.61mm	109.22mm	75mm

Figure 4.3: Schottky pick-up design parameters

Shown in Figure 4.4 is the transfer impedance of the pick-up (plot of square root of impedance versus frequency). The SUM and DELTA (difference) mode impedances are calculated as [23]:

$$\begin{aligned} Z_{\Sigma} &= (g-1) \frac{N_f S_{therm}}{e I_{dc}} \\ Z_{\Delta} &= (g-1) \frac{N_f S_{therm}}{2e I_{dc} \left(\frac{\sigma}{d}\right)^2} \end{aligned} \quad (4.1.1)$$

where N_f is the noise figure of the pre-amplifying chain, S_{therm} is the power spectral density of white thermal noise, I_{dc} is the beam current, σ is the r.m.s. size of the beam, d is the transverse size of the beam pipe and g is a ratio of power per revolution band when there is beam in the machine to when there is o beam.

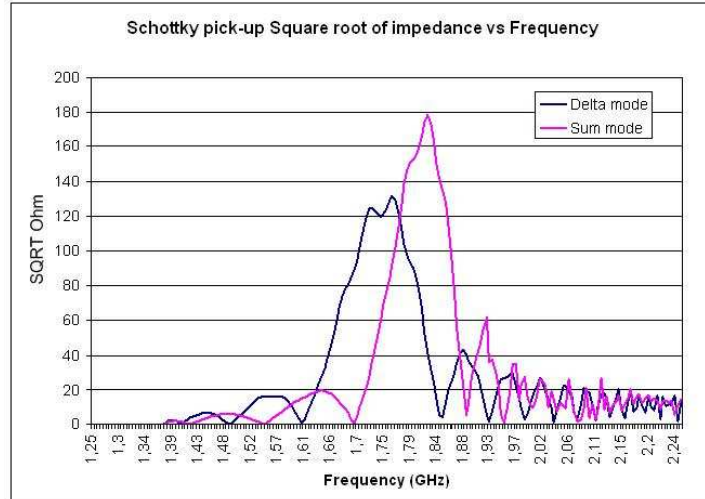


Figure 4.4: Calculated Schottky pick-up frequency response (courtesy of R. Pasquinelly and Ding Sun, FNAL)

The frequency of peak impedance is 1.765 GHz for DELTA mode ($Z_{\Delta} = 16900\Omega$) and 1.82 GHz for SUM mode ($Z_{\Sigma} = 31684\Omega$).

The Schottky PU at CERN has been used as a vertical detector and was tuned for an operating frequency of 1.8 GHz. At this frequency, the transverse impedance is approximately equal to $Z_{\Delta} \sim 7320\Omega$ and there is still longitudinal sensitivity, this could be a problem because the sum mode signals might not be completely suppressed causing a corruption of the transverse Schottky spectra used for diagnostics.

4.2 THE SPS 1.7GHz ACQUISITION SETUP

The Schottky pick-up and all the data acquisition setup were installed and tested in the SPS.

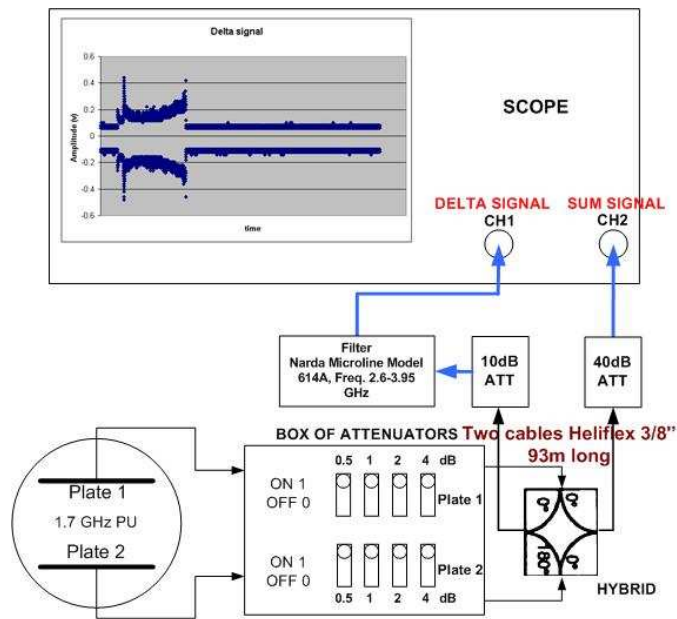


Figure 4.5: Sum and Delta signals obtained from the Schottky pick-up

As illustrated in Figure 4.5, each of the plates was first connected in the tunnel to a set of mechanical attenuators, that could be controlled from the surface, in such a way that attenuation for each channel could be varied in steps of different values, between 0 and 7.5dB. The objective of the attenuators was to minimize the longitudinal signal (common-mode lines) in the transverse

spectrum by trying to electrically center the beam in the pick-up and that way avoid that the revolution lines could hide the betatron lines.

The signals coming out from the pick-up plates were combined in a 180° hybrid giving the so-called *Delta* (Δ) and *Sum* (Σ) signals. The *Sum signal* is an indicator of the longitudinal sensitivity of the detector whilst the *Delta signal* was used to get the transverse Schottky spectrum.

The Delta signal was fed into a narrowband filter (3MHz BW) installed in tunnel and centered at 1.803GHz. Taking into account the attenuation of the cables that carried the signals to the surface (~ 12 dB at 1.8GHz), the Sum signal provided $\approx 100V_{peak-peak}$ and the Delta signal $\approx 10V_{peak-peak}$.

The measurements were performed using a spectrum analyzer, a FFT analyzer and an external sound card connected to a laptop running a Matlab interface. The different data acquisition configurations depending on the measurement device will be described in detail in following subsections.

4.2.1 Data acquisition setup with a spectrum analyzer (SPA)

As was said in previous chapter, measurements with a spectrum analyzer are slow. For this reason it was only used for basic frequency checks (PU longitudinal frequency response, comparison of spectrums with those ones obtained via FFT analyzer to see coherence of results, measurement of S/N ratio, ...).

The experimental setting for data acquisition with this device is schematically depicted in Figure 4.6. In this example, the Delta signal for transverse scans is directly measured in the SPA after being filtered in a passive 1.8GHz BPF and preamplified in a low noise preamplifier.

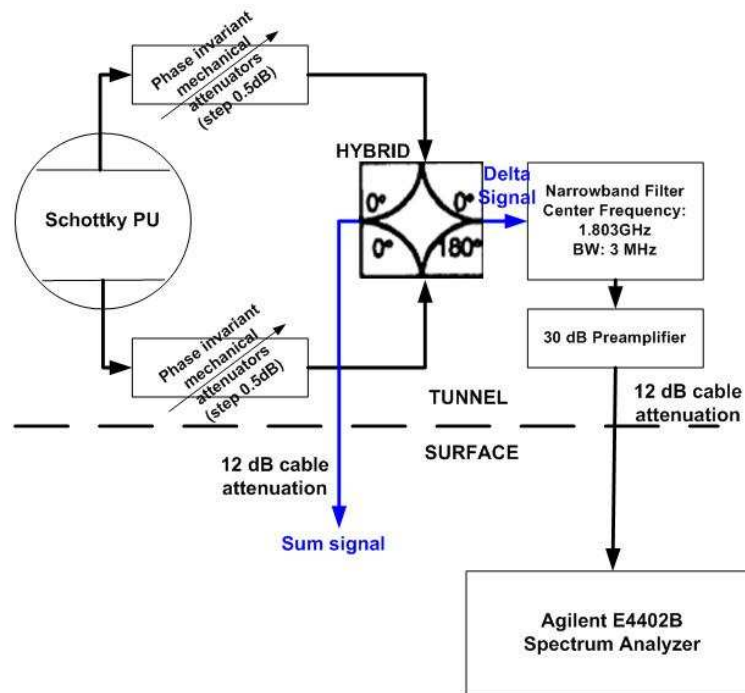


Figure 4.6: Experimental setting for measurements with Spectrum Analyzer

4.2.2 Data acquisition with a FFT analyzer or with an external sound card connected to a laptop

The real signal analysis was initially done using a conventional *FFT analyzer* (SR785 Dynamic Signal Analyzer). With a sample frequency of 262.1kHz, the frequency range of the device ranges from 195.3mHz to 102kHz and, since Schottky signals were expected to appear at frequencies around 1.8 GHz, the whole spectrum needed to be shifted to that interval. To do that, a further filtering and two down mixing stages were employed.

Filtering and first down mixing in the SPA

The Delta signal coming out from the tunnel is preamplified and applied to the RF input of the HP 8566B spectrum analyzer that performs the filtering and first downmixing stage. For the filtering, the center frequency was set to 1.8 GHz and the chosen resolution bandwidth was 30 kHz, the lowest available on the instrument. Then, the Delta signal was mixed with the signal generated by an internal oscillator in the SPA 8566B. This LO signal is placed 21.4MHz below the center

frequency so that after filtering the Delta signal, the whole spectrum is moved to 21.4 MHz. The IF output of SPA 8566B is now the RF input to the next mixing stage.

Second down mixing stage

This was performed in a conventional RF mixer. The RF input was supplied by the IF output of the SPA after the first down mixing, and the LO signal was supplied by a conventional signal generator. The frequencies chosen for the LO were around 21.45-21.46 MHz, so that the final signals were well centered on 50-60 kHz.

Figure 4.7 illustrates the whole process of filtering and down mixing of the response of a PU whose maximum value is shifted with respect to the center frequency of the BP filter in the SPA.

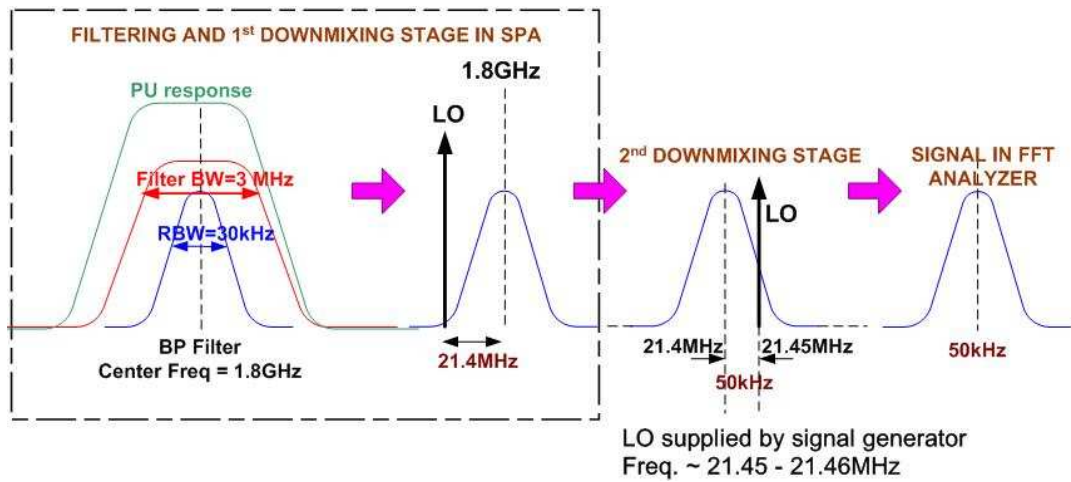


Figure 4.7: Illustration of the filtering and the two down mixing stages

A new data acquisition system with a *sound card* was used later instead of the FFT analyzer. The drawback of the FFT analyzer was the limitations for data processing. The storage of data was done in an internal memory of limited space meaning that only a few seconds of beam could be tracked. Retrieval of the data was a very slow process and the device remained un operational for several minutes. A means to solve this problem was to use an USB external sound card (Sound Blaster Audigy2 NX, 24bit, 96kS/s) for sampling the signal. It was connected to a laptop where a Matlab interface program was running for data storage, for visualization of the pick-up signal and for performing the FFT. However, the sampling frequency of 96 kHz gave a frequency range goes

from 20Hz to 48 kHz and in the second down mixing, the LO frequency had to be changed to 21.41 MHz in order to get the signal centered at around 10 kHz.

The sound card allowed the acquisition of large amounts of data and an online visualization of the FFT time evolution for the tracking of the lines of interest in the resulting frequency spectra.

Table of Figure 4.8 lists the main differences between the data acquisition with the FFT analyzer and with the sound card.

	SOUND CARD	FFT ANALYZER
SAMPLING FREQ.	96 kHz	262.1kHz
FREQ. RANGE	~20Hz-48kHz	~0Hz-102kHz
DATA STORAGE	Fast storage of big amounts of data, limited by laptop memory.	Data storage limited by internal FFT buffers. Data transfer for analysis is a slow process & device remains un operational.
LO FREQ.	~21.41MHz	~21.45-21.46MHz
SIGNAL DOWN MIXED TO FREQUENCY	~10 kHz	~50-60 kHz

Figure 4.8: Sound card characteristics vs. FFT analyzer

Figure 4.9 shows the whole experimental setting for data acquisition with both FFT analyzer and sound card.

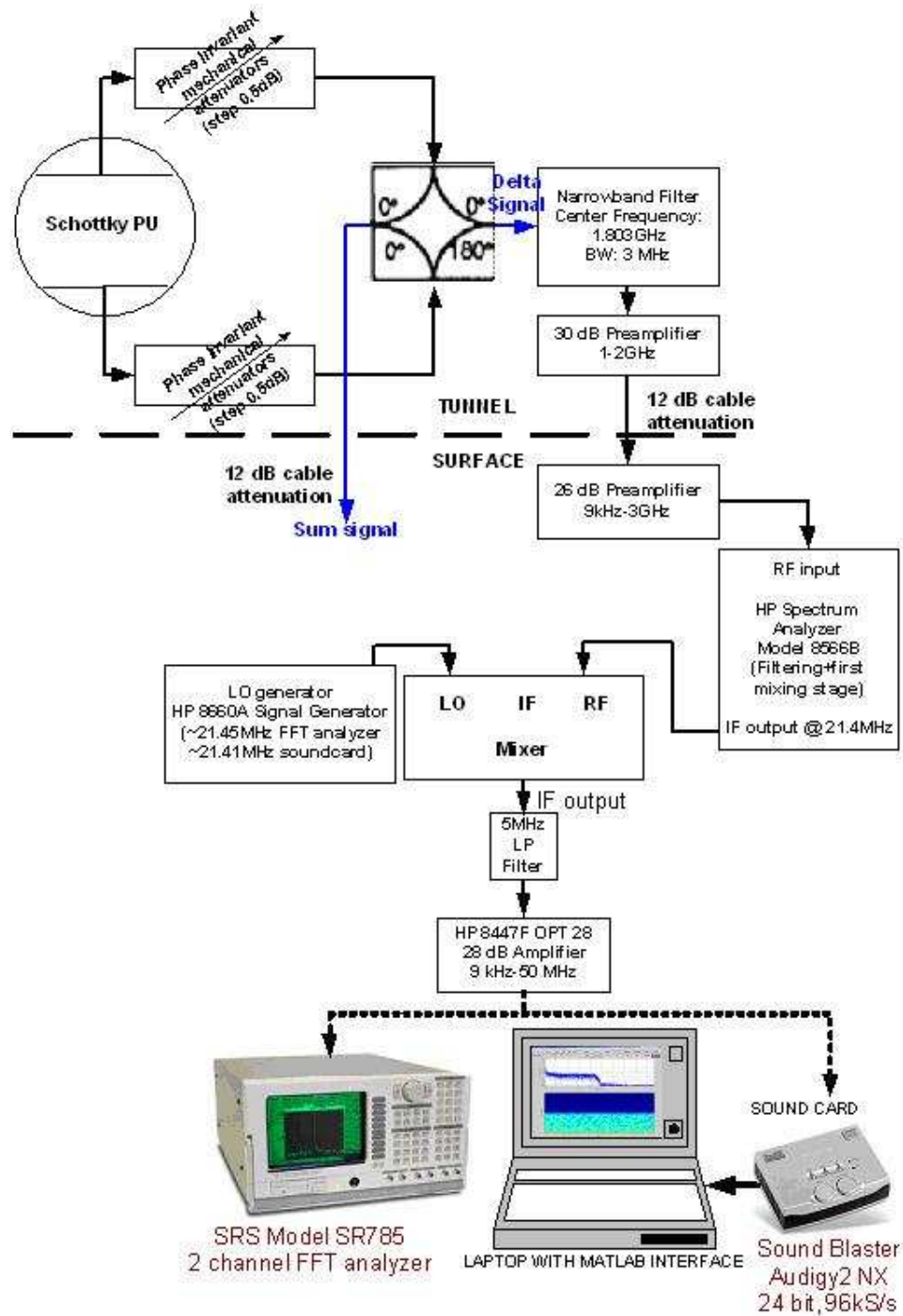


Figure 4.9: Illustration of data acquisition for FFT analysis

4.2.3 Analysis of the data acquired with the sound card

The program running in the laptop for data acquisition stored data in a '.wav' format. The offline data analysis was done using a Matlab GUI (Graphical User Interface) shown in Figure 4.10.

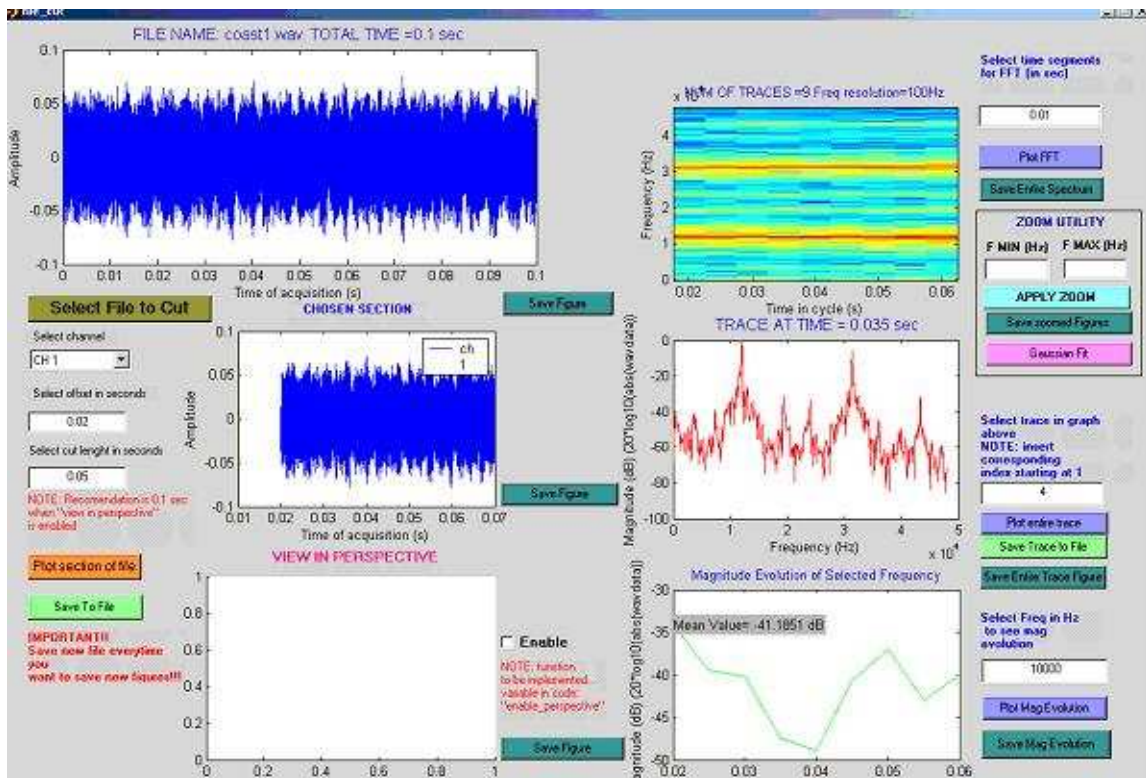


Figure 4.10: Appearance of the Matlab GUI for data analysis

The tool allowed the fragmentation of long data records into small time slices in order to make FFT analysis in a reasonable fast way. Furthermore it allowed the visualization of the FFT time evolution of a single FFT trace, and the magnitude evolution of a selected frequency.

The FFT was calculated applying a Hanning window to overlapping segments of data, illustrated in Figure 4.11.

It was possible to select the number of points per FFT trace in order to get different frequency resolutions (Δf):

$$\Delta f = \frac{1}{\Delta t} = \frac{f_s}{N} \quad (4.2.1)$$

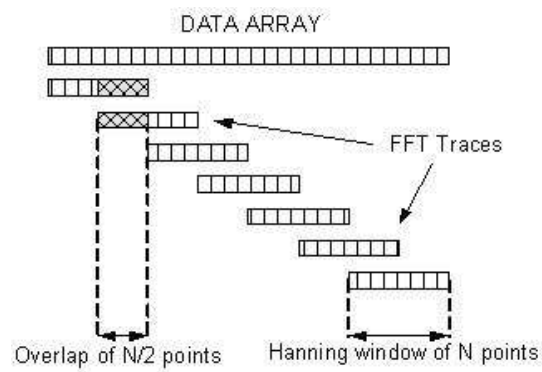


Figure 4.11: FFT computation of sampled signal

where Δt is the time slice of recorded data chosen for the Hanning window; f_s is the sampling frequency (96 kS/sec) and N is the number of points contained in Δt .

Chapter 5

Results obtained with the SPS 1.8GHz Schottky Monitor

In this chapter I will present the results of the measurements performed with the Schottky pick-up in the SPS during several runs as well as the conclusions derived from the observed signals after a detailed analysis. A lot of data were recorded for different types of beam in the SPS, however, only those results corresponding to LHC beam type will be shown (40MHz beam pattern: batches with 72 bunches of protons spaced by 25 ns). Due to this, an introductory section about SPS parameters is needed for a better understanding of the beam characteristics.

A first study of the expected results was also done, i.e. a calculation of the expected frequency response of the pick-up to bunched beam and the signal to noise level of the signal that should be observed in the output of the detector.

5.1 SPS PARAMETERS

The SPS will be the final pre-injector for the LHC, accelerating 26 GeV/c protons from the PS to 450 GeV/c before extraction to the LHC.

The majority of 2004 machine development beam time was dedicated to LHC test beams and, although data acquisition with the Schottky monitor was performed using other beam types, I was mostly interested in results obtained with the 40 MHz LHC type beam whose structure is depicted in Figure 5.1.

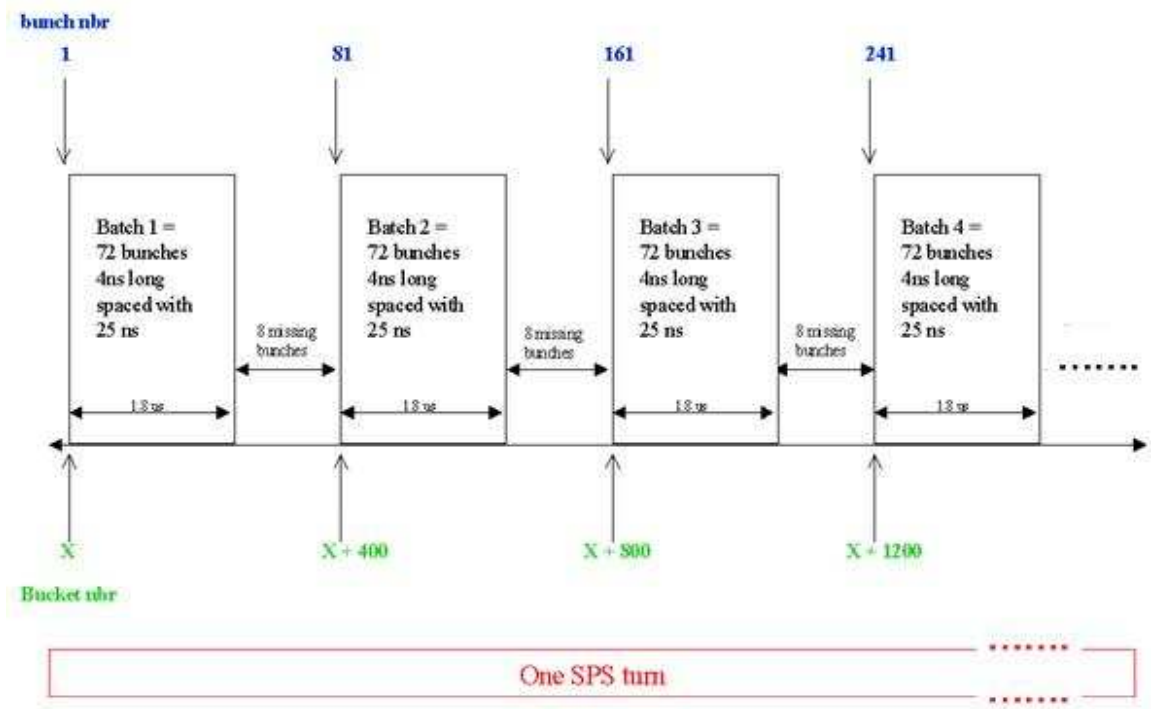


Figure 5.1: 25 ns LHC type beam in the SPS

5.2 EXPECTED PICK-UP RESPONSE

In this section a first estimation is made of the longitudinal frequency response that should be obtained with the Schottky monitor to LHC beam type. This is an exercise of great help for the better understanding of the final results observed with real beam.

The longitudinal power spectrum in the pick-up is calculated as the product of the longitudinal transfer impedance and the frequency response of the beam, according to the formula below [25]:

$$PU_{response}(f)|_{beam} \propto Z_{\Sigma}(f) \cdot I_{beam}(f) \quad (5.2.1)$$

The SUM mode (longitudinal) impedance was already given in Chapter 4 and has a peak value of 31684Ω at 1.82GHz. It was fitted to a Gaussian function, (5.2) giving following result:

$$Z_{\Sigma}(f)[\Omega] = 2.936 \cdot 10^4 \cdot \exp \left[\frac{-(f - 1.812 \cdot 10^9)^2}{(4.577 \cdot 10^7)^2} \right] \quad (5.2.2)$$

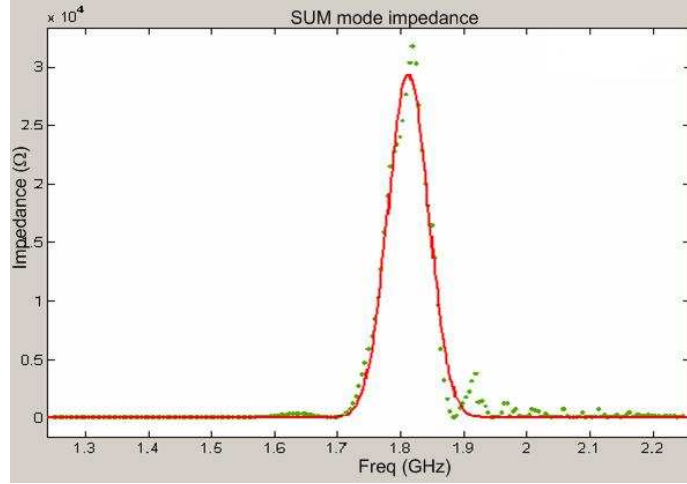


Figure 5.2: Gaussian fit of the longitudinal impedance of Schottky pick-up

The LHC beam is composed of bunches of particles spaced by 25 ns. This means that the time distribution of this train of bunches can be calculated as the convolution of the field for a single bunch with a series of Dirac pulses spaced by 25 ns. More in detail, the most common representation of a bunch of particles is a Gaussian distribution, hence, a bunch of N_b particles of charge e moving around the accelerator will produce, at a fixed point of the machine, a signal of the form [25]:

$$i_{bunch}(t) = \frac{dQ(t)}{dt} = \frac{N_b e}{\sqrt{2\pi}\sigma_t} \cdot \exp\left(-\frac{t^2}{2\sigma_t^2}\right) \quad (5.2.3)$$

where σ_t is a quarter of the length of the bunch, and N_b is the number of particles per bunch.

The Fourier transform is given by another Gaussian of width $1/\sigma_t$:

$$I_{bunch}(f) = N_b e \cdot \exp(-2\pi^2 f^2 \sigma_t^2) \quad (5.2.4)$$

The electromagnetic power induced by a single bunch on the beam pipe is proportional to the squared modulus of the Fourier transform $|I_{bunch}(f)|^2$.

$$P_{bunch}(f) \propto |I_{bunch}(f)|^2 \propto \exp(-4\pi^2 f^2 \sigma_t^2) \quad (5.2.5)$$

Both signals are plotted in Figure 5.3 for the typical bunch used in the measurements, with a length of 2.5 ns ($4\sigma_t$ of Gaussian $\Rightarrow \sigma_t = 0.625$ ns) and $N_b = 1.3 \cdot 10^{11}$.

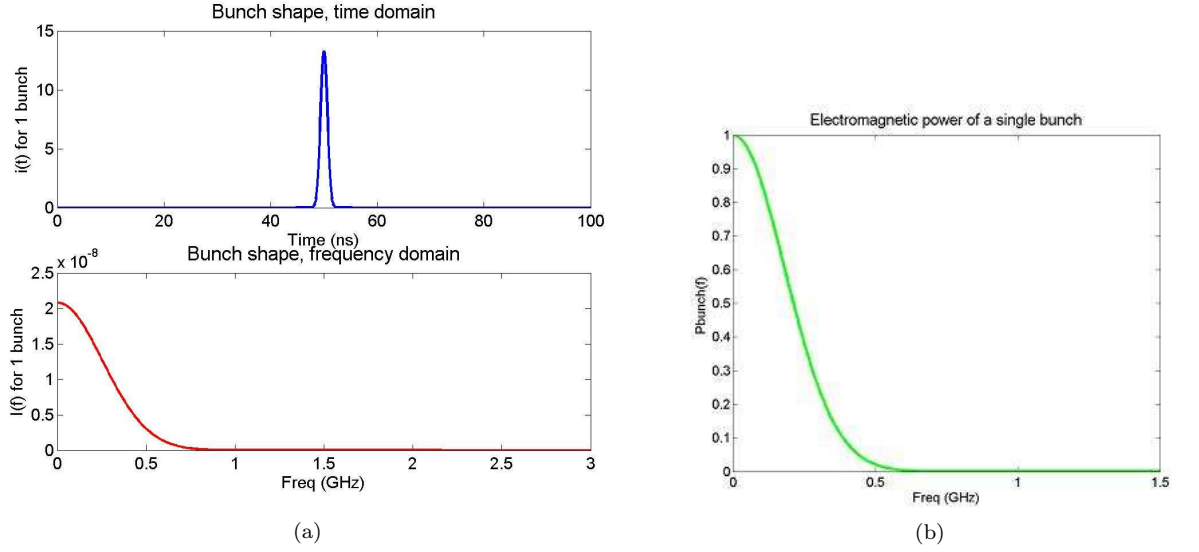


Figure 5.3: (a) Single bunch in time and frequency domains. (b) Electromagnetic power of a single bunch

If we consider a set of bunches which all have the same Gaussian charge distribution, the time distribution of this train can be written as the convolution of the field for one single bunch with a train of Dirac pulses spaced by the separation in time between bunches ($T_{bunch-bunch}$), in this case it is 25 ns:

$$\begin{aligned}
 i_{train}(t) &= i_{bunch}(t) \otimes \sum_{n=-\infty}^{+\infty} \delta(t - nT_{bunch-bunch}) = A \exp \left[\frac{-(t - T_{bunch-bunch})^2}{2\sigma_t^2} \right] + \dots \\
 &\dots + A \exp \left[\frac{-(t - N \cdot T_{bunch-bunch})^2}{2\sigma_t^2} \right] + \dots
 \end{aligned} \tag{5.2.6}$$

with $A = \frac{N_b e}{\sqrt{2\pi}\sigma_t}$. This is illustrated in Figure 5.4 (a).

By calculating the Fourier transform of the previous expression, one gets a set of spectral lines spaced by $f_{bunch-bunch} = 1/T_{bunch-bunch}$ (40MHz in our case), and with an envelope equal to the Fourier transform of one of the bunches:

$$\begin{aligned}
 I_{train}(f) &= I_{bunch}(f) \sum_{n=-\infty}^{+\infty} \exp(-j2\pi f n T_{bunch-bunch}) = \\
 &= I_{bunch}(f) \sum_{n=-\infty}^{+\infty} \sqrt{2\pi} \delta(f - n/T_{bunch-bunch})
 \end{aligned} \tag{5.2.7}$$

Therefore, the power spectrum of a train of electron bunches is proportional to $|I_{train}(f)|^2$ and

can be derived from the following equation:

$$P_{train}(f) \propto \exp(-4\pi^2 f^2 \sigma_t^2) \cdot \left[\left(\sum_{n=1}^{N_b} \cos(2\pi f n T_{bunch-bunch}) \right)^2 + \left(\sum_{n=1}^{N_b} \sin(2\pi f n T_{bunch-bunch}) \right)^2 \right] \quad (5.2.8)$$

It is composed by spectral lines spaced by 40MHz and enveloped by the spectrum of a single bunch with the same rms length as the individual bunches in the train.

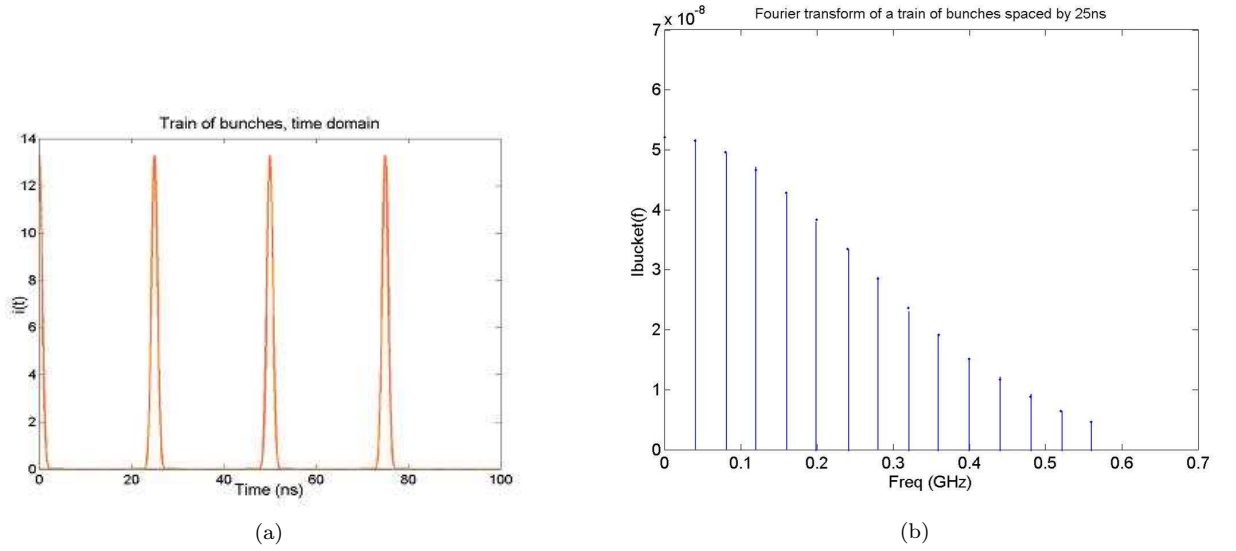


Figure 5.4: (a) Train of 4 bunches of 2.5ns length and spaced by 25 ns (b) Fourier transform of a train of bunches spaced by 25 ns

If, for simplicity, we consider only one bunch then, the response of the pick-up will be:

$$PU_{response}(f)|_{1bunch} \propto Z(f) \cdot I_{bunch}(f) \quad (5.2.9)$$

This result can be clearly analyzed by having a look to Figure 5.5. In this figure it can be seen that the maximum response of the Schottky pick-up to a bunch or a train of bunches of 2.5ns length is around 1.8 GHz. This is what we will expect to see with real LHC beam, a maximum of the measured signal at a frequency around 1.8 GHz.

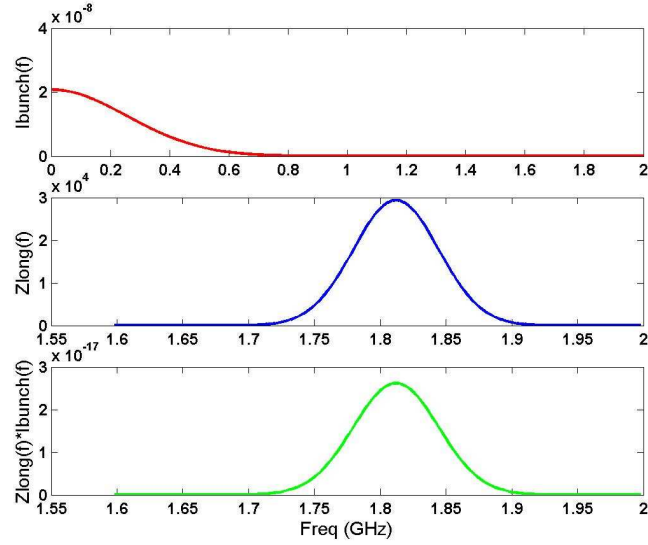


Figure 5.5: Longitudinal Schottky pick-up response to a single bunch

In case we had a bunched beam with bunches every 25 ns, we would observe lines spaced by 40 MHz and enveloped by a Gaussian, corresponding to the response of the pick-up to a single bunch of width the same as the width of all bunches in the bucket:

$$PU_{response}(f)|_{train} \propto Z(f) \cdot I_{train}(f) = Z(f) \cdot I_{bunch} \sum_{n=-\infty}^{+\infty} \sqrt{2\pi} \delta(f - n/T_{bunch-bunch}) \quad (5.2.10)$$

5.2.1 S/N calculations

The calculation of the *signal to noise ratio* (S/N) will give an idea about the level of the signal being delivered by the Schottky monitor considering all the elements involved in the data acquisition.

The definition of the S/N over a Schottky band is given by expression:

$$S/N(dBm) = 10 \cdot \log \left[\frac{P_{beam}}{P_{noise}} \right] \quad (5.2.11)$$

In the Schottky pick-up, the sources of noise are the thermal noise ($P_{th} = kT$) and the noise introduced by the signal processing chain at the output of the monitor (N_f). Then, the power associated to the total noise is given by:

$$P_{noise} = P_{th} \cdot N_f \quad (5.2.12)$$

For the calculation of the power associated to the beam (P_{beam}), we need to introduce the definition of the **Sensitivity** of the monitor, that is different depending on the considered plane [17].

Longitudinal sensitivity:

$$S_L[\Omega] = \frac{V_{beam}}{i_{beam}} \quad (5.2.13)$$

where V_{beam} is the voltage at the output of the monitor measured in R_0 and i_{beam} is the *rms* beam current per Schottky band (i_{rms}).

Transverse sensitivity:

$$S_T[\Omega/m] = \frac{V_{beam}}{D} \quad (5.2.14)$$

where D is the dipole moment equal to: $D = i_{beam}dx$, being dx the position of the beam in the monitor measured from the electrical center.

a) S/N ratio in the longitudinal plane

Knowing that $S/N(dBm) = 10 \cdot \log [P_{beam}/P_{noise}]$ and that $P_{noise} = P_{th} \cdot N_f$, we need to get the value of P_{beam} . For that purpose we use the longitudinal sensitivity S_L :

$$S_L[\Omega] = V_{beam}/i_{rms}$$

$$V_{beam}[V] = i_{rms}S_L$$

$$i_{rms}[A] = 2ef_{rev}\sqrt{N/2}$$

$$P_{beam}[W] = V_{beam}^2/R_0 = (i_{rms}S_L)^2/R_0$$

The power output per Hz is calculated over the *full width* of the Schottky band (Δf) that is equal to four times the *rms* width of a single longitudinal Schottky line: $\Delta f = 4 \cdot df = 4 \cdot n f_{rev} \eta dp/p$. This way we correct the area of the Gaussian when fitting the observed Schottky line due to the existence of a noise floor [22]. This results in:

$$P_{beam}[W/Hz] = \frac{(i_{rms}S_L)^2}{R_0} \frac{1}{\Delta f} = \frac{S_L^2}{R_0} \frac{(2ef_{rev}\sqrt{N/2})^2}{\Delta f} = \frac{S_L^2}{R_0} \frac{2e^2 f_{rev}^2 N}{\Delta f} \quad (5.2.15)$$

And the S/R is:

$$S/R_L[dBm] = 10 \cdot \log \left[\frac{P_{beam}}{P_{th} \cdot N_f} \right] = 10 \cdot \log \left[\frac{2e^2 N f_{rev}^2 S_L^2}{kT} \frac{1}{R_0} \frac{1}{\Delta f} \frac{1}{N_f} \right] \quad (5.2.16)$$

The longitudinal sensitivity, S_L , of the monitor can be replaced by the longitudinal impedance of the monitor (Z_Σ), a parameter which is calculated by Fermilab for the LHC Schottky pick-up structure and is defined as follows [22]:

$$Z_\Sigma = \frac{S_L^2}{2R_0} \quad (5.2.17)$$

Replacing in the previous S/R_L expression, one gets the final expression for S/N:

$$S/R_L[dBm] = 10 \cdot \log \left[\frac{e^2 N f_{rev}^2 Z_\Sigma}{kT} \frac{1}{df} \frac{1}{N_f} \right] \quad (5.2.18)$$

b) S/N ratio in the transverse plane

In this case, in order to get the value of P_{beam} we use the transverse sensitivity S_T :

$$S_T[\Omega] = V_{beam}/D$$

$$V_{beam}[V] = D \cdot S_T$$

$$P_{beam}[W] = V_{beam}^2/R_0 = (D \cdot S_T)^2/R_0$$

where D is the dipole moment and is equal to the beam current multiplied by the transverse displacement of the beam or the *rms* amplitude of the transverse oscillation (a_{rms}):

$$D = i_{rms} \cdot a_{rms} = a_{rms} e f_{rev} \sqrt{\frac{N}{2}} \quad (5.2.19)$$

a_{rms} is related to the beam emittance (ε) as: $a_{rms} = \sqrt{\varepsilon\beta/2}$, with β the twiss beta function at the location of the monitor. Hence the power output per Hz in a Schottky frequency band calculated over the *full width* ($\Delta f = 4 \cdot df$) is:

$$P_{beam}[W/Hz] = \frac{(DS_T)^2}{R_0} \frac{1}{\Delta f} = \frac{S_T^2}{R_0} \frac{e^2 f_{rev}^2 a_{rms}^2 N}{2\Delta f} \quad (5.2.20)$$

And the S/N is:

$$S/R_T[dBm] = 10 \cdot \log \left[\frac{P_{beam}}{P_{th} \cdot N_f} \right] = 10 \log \left[\frac{e^2 N f_{rev}^2 a_{rms}^2 S_T^2}{2kT} \frac{1}{R_0} \frac{1}{\Delta f} \frac{1}{N_f} \right] \quad (5.2.21)$$

Here again, the sensitivity can be defined in terms of the Fermilab delta mode transfer impedance Z_Δ :

$$Z_\Delta = \frac{d \cdot S_T^2}{4R_0} \quad (5.2.22)$$

with d being the beam pipe diameter at the location of the detector. Replacing it in the previous S/N_T expression, one gets:

$$S/R_T[dBm] = 10 \cdot \log \left[\frac{e^2 N f_{rev}^2 a_{rms}^2 Z_\Delta}{kT} \frac{1}{d^2 2df} \frac{1}{N_f} \right] \quad (5.2.23)$$

The width of the two transverse Schottky bands at the n^{th} harmonic is given as: $df_{u,l} = f_{rev} \frac{dp}{p} [(n \pm q)\eta \pm Q_v \xi]$, where q designates the fractional tune, Q_v the full integer tune, ξ the chromaticity, dp/p the momentum spread and η the momentum compaction factor.

5.3 OBSERVED BEAM SPECTRA

Data was acquired during several separate SPS runs, all of them with bunched beam in coast regime to make long data recording and tracking of tune evolution possible. Energy at coast regime was 26GeV with 40MHz LHC beam pattern (72 bunches spaced by 25ns). Some of the parameters of the beam appear in the Table of Figure 5.6.

	UNITS	SPS
Coast beam Energy	GeV	26
Momentum	GeV/c	26
Machine circumference	m	6911.560387
Revolution Frequency	kHz	43.347
Betatron Tune, Q_H		26.13
Betatron Tune, Q_V		26.19
Intensity per bunch		$1.3 \cdot 10^{11}$
Number of bunches		72
Number of batches		Up to 2
Bunch Spacing	ns	25
Bunch Length	ns	2.5
Normalized r.m.s vertical emittance (ϵ_v)	μm	$\sim 3.5 - 3.6$
$\Delta p/p$ (r.m.s.)		1×10^{-3}
Transverse Beam Size (σ)	mm	1.8
RF Frequency	MHz	200
SPS γ_{tr}		23.4

Figure 5.6: Typical SPS beam parameters during data acquisition (9/1/04)

An important parameter is the *fractional part of the vertical betatron tune* (q_v) which will be used as a reference for comparison for the values of tune obtained with the Schottky method, and the real tune values given by the control room.

Measurements were performed in both *Delta* and *Sum* signal paths to obtain the transverse and longitudinal spectrums respectively. In the following subsections these spectra and a detailed explanation of the information that can be extract from them will be presented. The final spectra are not pure Schottky spectra but contain other frequency components like the coherent lines even though the system is well above the coherent spectrum, and frequency lines resulting from distortions

present during the data acquisition whose origin can be known by considering all possible sources of noise.

5.3.1 Transverse spectrum

The transverse spectra were obtained from the *Delta* signal of the Schottky pick-up. An example of a typical *transverse spectrum* measured with the FFT analyzer for LHC bunched beam is shown in Figure 5.7 and it has all the characteristic lines that were predicted by Schottky Theory (Chapter 3).

The two large peaks are *revolution lines* or *common-mode lines*. They repeat at integer multiples of the SPS revolution frequency (43.347 kHz at 26GeV) and their presence is due to the fact that the beam is not well centered in the detector. If we carefully look at one revolution line, we see that each peak is in fact a compound peak: a narrow one due to the residual coherent signal at 1.8GHz and a broad one that is the longitudinal incoherent Schottky signal. The two peaks appearing on the right and on the left of the revolution lines are the betatron signals or the '*upper and lower tune sidebands*'.

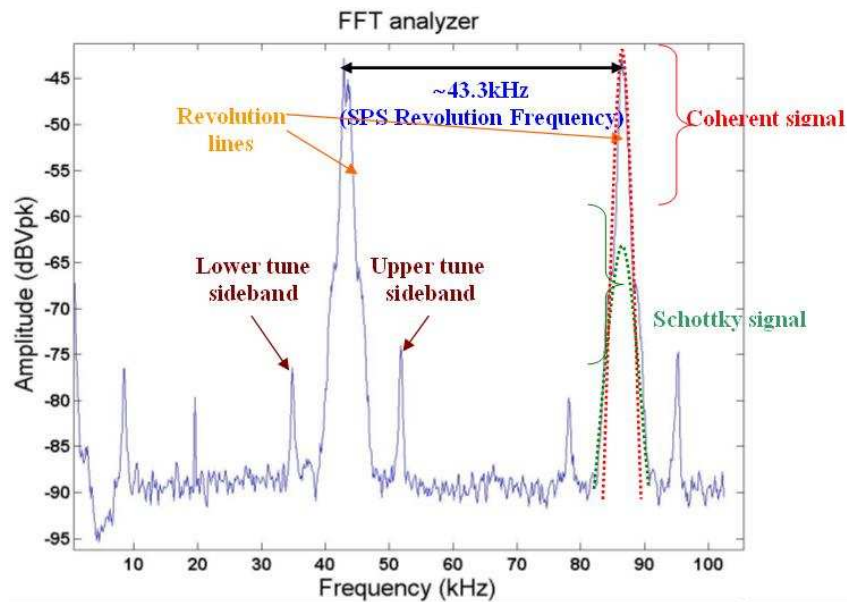


Figure 5.7: Spectrum of *Delta* signal from the Schottky detector ion the FFT analyzer

A zoom on the frequency lines of the previous figure is in Figure 5.8 and it shows the expected spectrum for a bunched beam clearly showing the *synchrotron satellites* spaced by the synchrotron frequency of ~ 280 Hz.

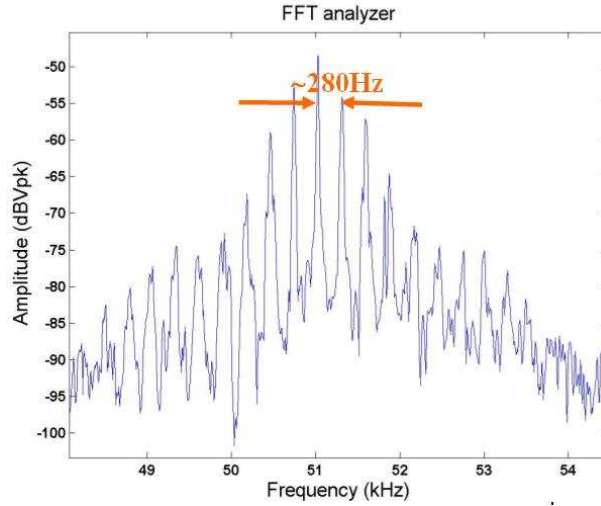


Figure 5.8: Synchrotron satellites in the revolution line

5.3.2 S/N ratio extracted from the transverse Schottky spectrum

In Section 5.2.1 it was mentioned that the S/N ratio for the transverse plane in a Schottky pick-up can be calculated with the formula:

$$S/R_T[dBm] = 10 \cdot \log \left[\frac{e^2 N f_{rev}^2 a_{rms}^2}{kT} \frac{Z_{\Delta}}{d^2 2df} \frac{1}{N_f} \right]$$

All these values are known for our particular case:

- e = charge unit ($e = 1.60210^{-19}C$)
- N = number of particles per bunch \times number of bunches ($1.3 \cdot 10^{11} \times 72 = 9.36 \cdot 10^{12}$)
- $f_{rev} = 43.347kHz$ at 26GeV
- Z_{Δ} = transverse mode impedance ($Z_{\Delta} \approx 7320 \Omega$ at 1.8 GHz)
- N_f = noise figure of signal processing chain ($N_f = 3.2$ (5dB))

- $S_{th} = kT$ = power spectral density of white thermal noise at 300K ($S_{th} = 4.1410^{-21}$ W/Hz)
- d = beam pipe height ($d=75\text{mm}$)
- a_{rms} = transverse beam size ($a_{rms} = \sqrt{\varepsilon\beta_v/2} = 1.8\text{mm}$)
- df = width of a Schottky sideband. In we consider the lower tune sideband and neglect the value of the chromaticity ($\xi \simeq 0$), we get: $df_l = f_{rev} \frac{\Delta p}{p} [(n - q)\eta] = 43347 \cdot 1 \cdot 10^{-3} [(41594 - 0.19)5.24 \cdot 10^{-4}] = 944.6\text{Hz}$

By substitution in the formula, the result is:

$$S/R_T[\text{dBm}] = 10 \cdot \log \left[\frac{(1.60210^{-19})^2 \cdot 9.36 \cdot 10^{12} \cdot (43347)^2 \cdot (1.8 \cdot 10^{-3})^2 \cdot 7320}{4.1410^{-21} \cdot (75 \cdot 10^{-3})^2 \cdot 2 \cdot 942.6 \cdot 3.2} \right] = 18.8\text{dBm}$$

To see if the calculated S/N is in agreement with real results, we extract the S/N from a transverse spectrum measured with a SPA. In the spectrum analyzer we used a span of 50 kHz, 400 points, 50 Hz of resolution, and a center frequency of 1802988500 Hz. The horizontal scale in Figure 5.9 was obtained by subtracting the central frequency.

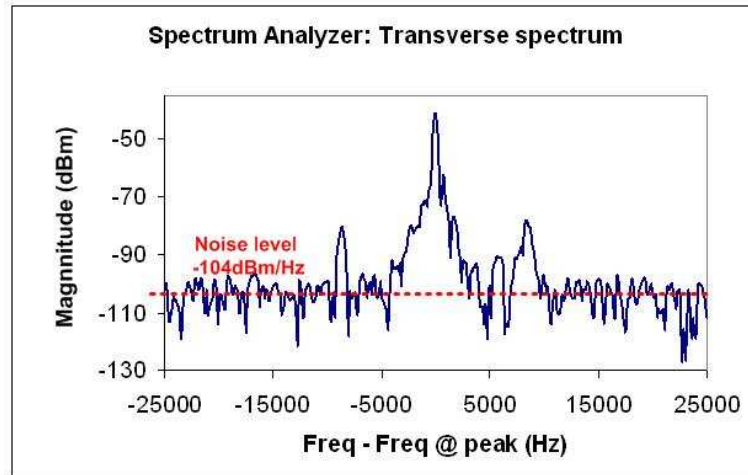


Figure 5.9: S/N value in transverse spectrum

For the noise, we take an average of the power in the region between the beam distribution (e.g., between -25000 Hz and -10500 Hz) and get a value of ~ -104 dBm/Hz. For the signal power,

we consider only the betatron lines because the large peak corresponds to a revolution line whose presence is only due to the fact that the beam is not centered in the detector and hence, a transverse Schottky spectrum for centered beam would only show the betatron satellites [27]. The total power is calculated by integration of the power in a region including a tune sideband. This area depends on the height and width of the peak that might be different for upper and lower tune sidebands, however, the power in the two sidebands should be the same. The total power we get is -90 dBm/Hz. The signal to noise ratio is then:

$$S/N_T = 10 \log \left[\frac{P_{signal}}{P_{noise}} \right] = 10 \log \left[\frac{1 \cdot 10^{-9} mW/Hz}{3.98 \cdot 10^{-11} mW/Hz} \right] = 14dB$$

With these considerations we get a dynamic range of 14dB.

The calculated and the real results differ in almost 5dB but, as a first approximation, the formula 5.2.23 derived for the S/N_T can be used to calculate the level of the signal we are expected to observe with a Schottky monitor in the transverse plane.

5.3.3 Extracting the betatron tune (q_v) from the transverse Schottky spectrum

In Section 3.2.1 it was mentioned that the transverse betatron tune value in a Schottky pick-up can be calculated with the formula:

$$q_v = \frac{f_u - f_l}{2 \cdot f_{rev}}$$

If we consider the transverse spectrum acquired on 1/9/04 that appears on Figure 5.10 and measure the frequencies of the upper and lower tune sidebands at the peak values of the bands ($f_u = 51840Hz$, $f_l = 34816Hz$), considering the nominal revolution frequency $f_{rev} = 43.347kHz$ (with centered beam revolution harmonics should disappear from Schottky spectrums) and applying previous formula 5.3.1 we obtain:

$$q_v = \frac{51840 - 34816}{2 \cdot 43347} = 0.196$$

This compares well with the nominal vertical betatron tune at the time of data acquisition given by control room on 1/9/04 that was $q_v = 0.19$.

Most of the values for the tunes calculated from FFT spectra or SPA spectra and using previous method were almost identical to the real values given by the operators in the control room. This

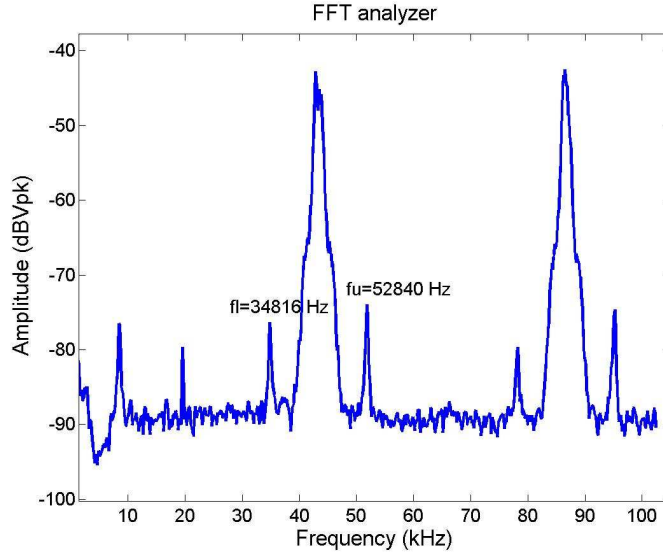


Figure 5.10: Extracting q_v from the transverse Schottky spectrum (II)

leads us to conclude that Schottky signals could be employed as a way to calculate the betatron tune in a non-perturbing way.

5.3.4 Extracting the chromaticity (ξ_v) from the transverse Schottky spectrum

The chromaticity can be extracted from the width of the betatron sidebands using formulas 3.2.2 in Chapter 3

$$\xi_v = \frac{\eta}{Q_V} \left[n \cdot \frac{\Delta f_u - \Delta f_l}{\Delta f_u + \Delta f_l} - q_v \right]$$

where the values in our case are:

- Slip factor: $\eta = \frac{1}{\gamma_{tr}^2} - \frac{1}{\gamma^2} = \frac{1}{(23.4)^2} - \frac{1}{(27.72)^2} = 5.24 \cdot 10^{-4}$, $\gamma_{tr} = 23.4$ for SPS and $\gamma = 27.72$ for protons at 26GeV
- Betatron tune: $Q_V=26.19$
- Fractional part of vertical betatron tune: $q_v=0.19$
- Harmonic number: $n=1802988500\text{Hz}/43347\text{Hz}=41594$

- The width of the tune sidebands Δf_u and Δf_l can be calculated by fitting the peaks to Gaussians. Using data in Figure 5.9 one gets:

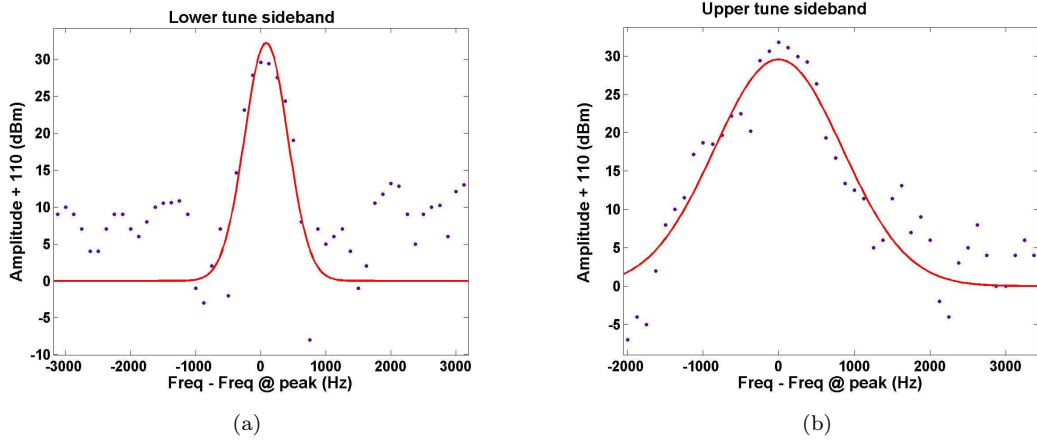


Figure 5.11: (a) Gaussian fit of lower tune sideband (b) Gaussian fit of upper tune sideband

$$\Delta f_l = 2 \times \sigma = 665.1 \text{ Hz} \text{ and } \Delta f_u = 2 \times \sigma = 1692.81 \text{ Hz}$$

This leads to a value for the relative chromaticity of:

$$\xi_v = \frac{5.24^{-4}}{26.19} \left[41594 \cdot \frac{1692.81 - 665.1}{1692.81 + 665.1} - 0.19 \right] = +0.36$$

and the chromaticity is then:

$$Q' = \xi_v \times Q_V = 0.36 \times 26.19 \simeq 8$$

5.3.5 Extracting the momentum spread ($\Delta p/p$) from the transverse Schottky spectrum

Again, with the formula 3.2.3 in Chapter 3 we calculate the momentum spread and get the result below:

$$\frac{\Delta p}{p} = \frac{\Delta f_u + \Delta f_l}{f_{rev} \cdot 2 \cdot n \cdot \eta} = \frac{1692.81 + 665.1}{43347 \cdot 2 \cdot 41594 \cdot 5.24^{-4}} = 1.2^{-3}$$

a value similar to the nominal momentum spread for SPS beam that is around 1.0^{-3} (see Table in Figure 5.6).

5.3.6 Longitudinal spectrum

The longitudinal sensitivity of the detector can be measured using the *Sum* signal coming out from the hybrid.

The observed response in the SPS with a spectrum analyzer shows the bunched structure of the beam (bunches spaced by 25ns) with lines spaced by 40MHz.

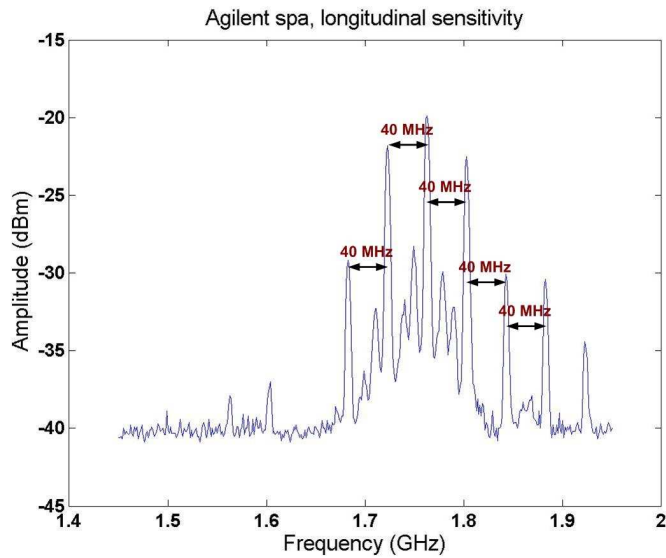


Figure 5.12: Longitudinal sensitivity of Schottky pick-up

The maximum response of the pick-up is at around 1.76 GHz. It has been shifted down from the designed operating frequency for the SUM mode of 1.813 GHz (see Figure 4.4) due to the convolution of the frequency spectrum for our particular beam $I(f)$ with the pick-up impedance $Z(f)$.

5.4 TUNE TRACKING: FOURIER TRANSFORM OF BEAM MOTION

Once it was possible to detect the betatron tune lines in the transverse spectrum, the FFT of long time data records of the *Delta* signal was used for tracking the evolution of the betatron frequency. These acquisitions were done with the external sound card connected to the laptop and

the observed spectrums showed additional lines which were introduced by nonlinearities of devices and the imperfect frequency locking of instruments in the down mixing chain.

In this section some examples of frequency spectra obtained for transverse signals will be shown and the origin of the extra frequency lines observed in long time FFT records and single FFT traces are analyzed.

5.4.1 FFT time evolution of beam motion and sources of frequency distortion

A typical accumulated FFT spectrum during a whole SPS cycle is shown in Figure 5.13.

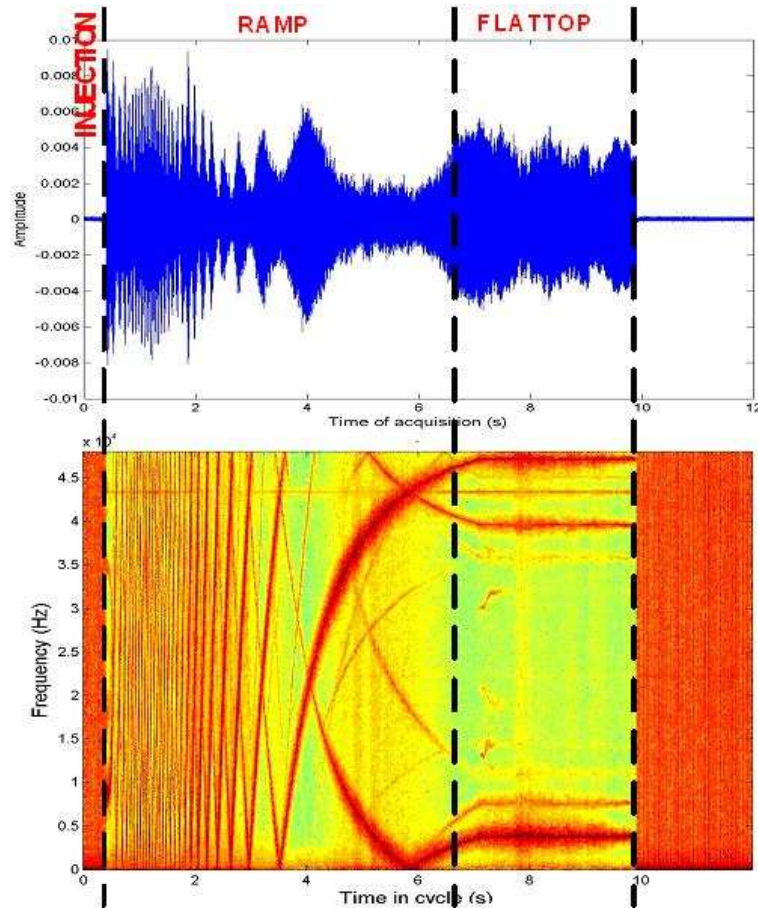


Figure 5.13: FFT time evolution of delta signal

The presence of ramping frequency lines at the beginning of the acceleration stage before the stabilization of the revolution frequency is due to the fact that the LO frequency was not RF synchronous so that while the energy was increasing many revolution lines were swept through the narrow bandwidth of the final filter. This is not optimized for measurement but has the advantage that is easy to distinguish between fixed and moving lines and images.

Our interest is the Schottky spectrum, with the revolution and the tune lines as main identifiers, but FFT spectrum shows additional unwanted frequency lines. Hence a criteria is needed to identify the important lines. After a careful study of all possible sources of noise and distortion, the criteria for identification of frequency lines are:

- The revolution lines are those ones with maximum amplitude, and the distance between them is 43.3 kHz, the SPS revolution frequency.
- If tune is not changing during the ramp, the distance between the tune lines and the revolution lines always stays the same.
- Lines with negative slope (decreasing frequency) are images of negative frequencies resulting from the down mixing process. Lines with positive slope (increasing frequency) are real signals because in the SPS the revolution frequency increases during acceleration.
- The rest of lines appear because of intermodulation and harmonic distortion due to the non linear behaviour of all the devices the Schottky signal passes through, such as the amplifiers, mixers and spectrum analyzers.

In the following, we will try to provide a thorough analysis of the origin of the noisy signals and the reason why they appear in the FFT spectrum. With the explanations that will be given, Figure 5.13 will be finally well understood.

Images resulting from the down mixing process

The down mixing process is schematically depicted in Figure 5.14.

RF mixers convert RF power at one frequency into power at another frequency to make signal processing easier and more efficient. The frequency that has to be shifted is applied at the RF input and the fixed frequency (from a local oscillator, LO) is applied to the RF mixer LO port. By simple

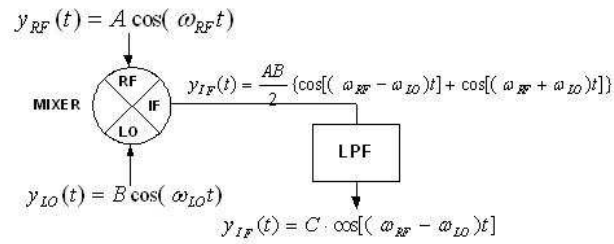


Figure 5.14: Down mixing process

multiplication of both signals one gets two outputs at the mixer’s Intermediate Frequency (IF) port. For a given RF signal, an ideal mixer would produce only two IF outputs: one at the frequency sum of the RF and LO, and another at the frequency difference between the RF and LO. Filtering can be used to select the desired IF output and reject the unwanted one. In this application a low pass filter was used to eliminate the high frequency component.

In the data acquisition system two down mixing stages are used with a 5MHz Low Pass filter after the second RF mixer. The output from the second down mixing was directly sampled by the sound card that detected signals with ”negative frequencies” which arise when the LO frequency is higher than the RF frequency. This effect could clearly be seen in long FFT records as lines with negative slope.

Some tests were performed to reach to such a conclusion. In one test an RF signal which was changed linearly from 21.32 MHz to 21.48 MHz was downmixed with a LO signal of 21.4 MHz. The result showed that ”negative” IF signals are detected by the sound card and after FFT computation, they appeared as lines with negative slope. The test is schematically described in Figure 5.15

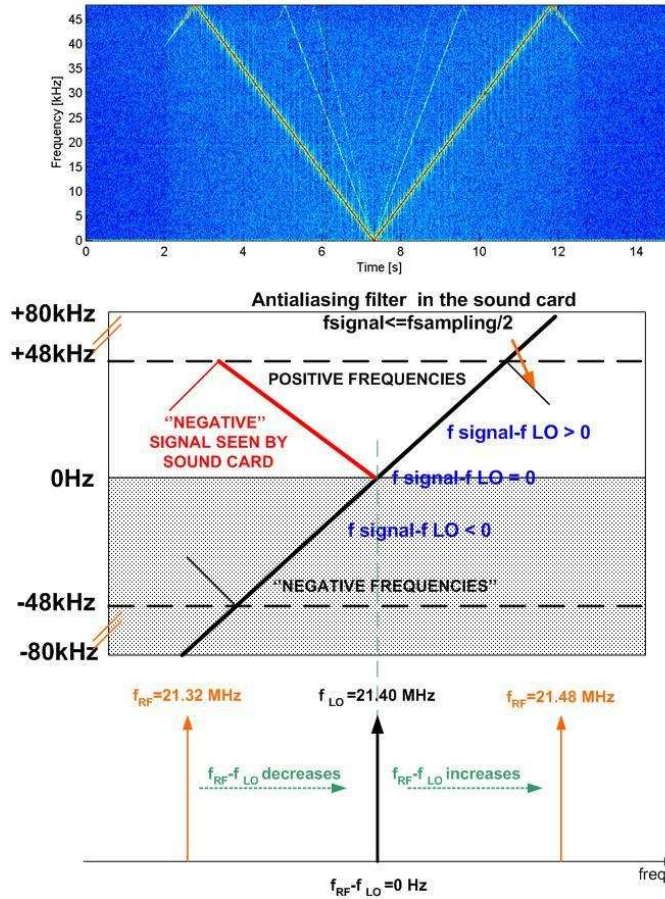


Figure 5.15: Generation of images in the down mixing process

Harmonic distortion

Many of the circuits that are used in electronic systems are considered to be linear. This means that for a sinusoidal input, the output will also be sinusoidal with perhaps a different amplitude and phase. In the frequency domain, we expect to see at the output the same frequency that was at the input and only that frequency. Any other frequencies that are generated due to the input signal are considered as distortion.

Most of the distortion mechanisms measured with spectrum analyzers are of a low level. That is, the devices producing the distortion are mostly linear and have only a slight non-linear behavior

which can be modeled with a power series:

$$V_{out} = k_0 + k_1 V_{in} + k_2 V_{in}^2 + k_3 V_{in}^3 + \dots \quad (5.4.1)$$

For a single tone input $V_{in} = A \cos \omega t$, and considering effects up to third, the distortion model gives:

$$V_{out} = k_0 + k_2 A^2 / 2 + (k_1 A + k_3 A^3 / 4) \cos \omega t + (k_2 A^2 / 2) \cos 2\omega t + (k_3 A^3 / 4) \cos 3\omega t \quad (5.4.2)$$

This leaves us with an output voltage containing a DC component, the fundamental frequency, and its second and third harmonics.

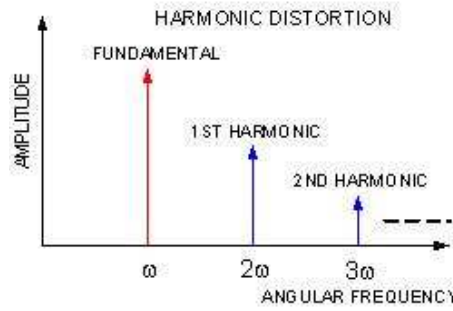


Figure 5.16: Harmonic distortion in a single tone signal

Intermodulation distortion

This appears when several signals are present at the input of a non linear device. Considering previous distortion model for the device and a two-tone input $V_{in} = A_1 \cos \omega_1 t + A_2 \cos \omega_2 t$, the frequencies present in the output satisfy the following criteria:

$$\omega_{nm} = |n\omega_1 \pm m\omega_2| \quad (5.4.3)$$

where n and m are positive integers such that $n + m \leq \text{order of distortion model}$. For a third-order distortion, we would expect to have signals at the frequencies shown in Figure 5.17.

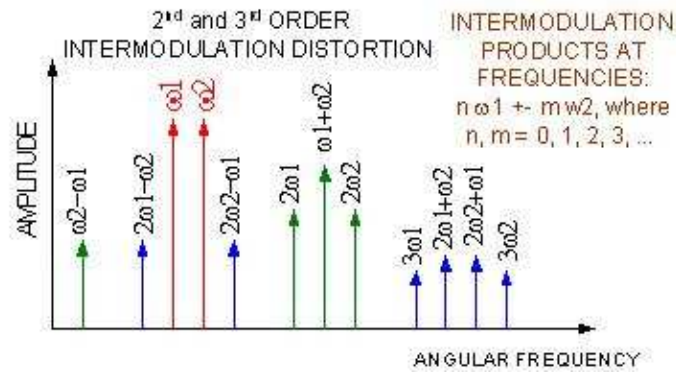


Figure 5.17: Intermodulation distortion for a two-tone input signal

Identification of frequency lines in long acquisition FFT spectra

Once all possible sources of frequency distortion have been analyzed, we will try to reveal the origin of all the frequency lines appearing in spectra of Figure 5.13. At the moment of data acquisition the value of the fractional part of the betatron tune was around $q_v = 0.76$.

It is fairly easy to identify the two highest peaks as revolution lines, which at flattop sit at 3.8 kHz and 47.1 kHz as revolution lines. The difference of this gives the expected SPS revolution frequency of 43.3 kHz. Since $q_v \simeq 0.757$, one would expect to have betatron tune lines at a distance $d = 0.757 \times 43.3 \approx 32.7kHz$ from these revolution lines. These frequency components are seen as the lower and upper sidebands in Figure 5.18. The rest of lines are due to intermodulation and harmonic distortion.

The next step was to find a method to clean up the spectra.

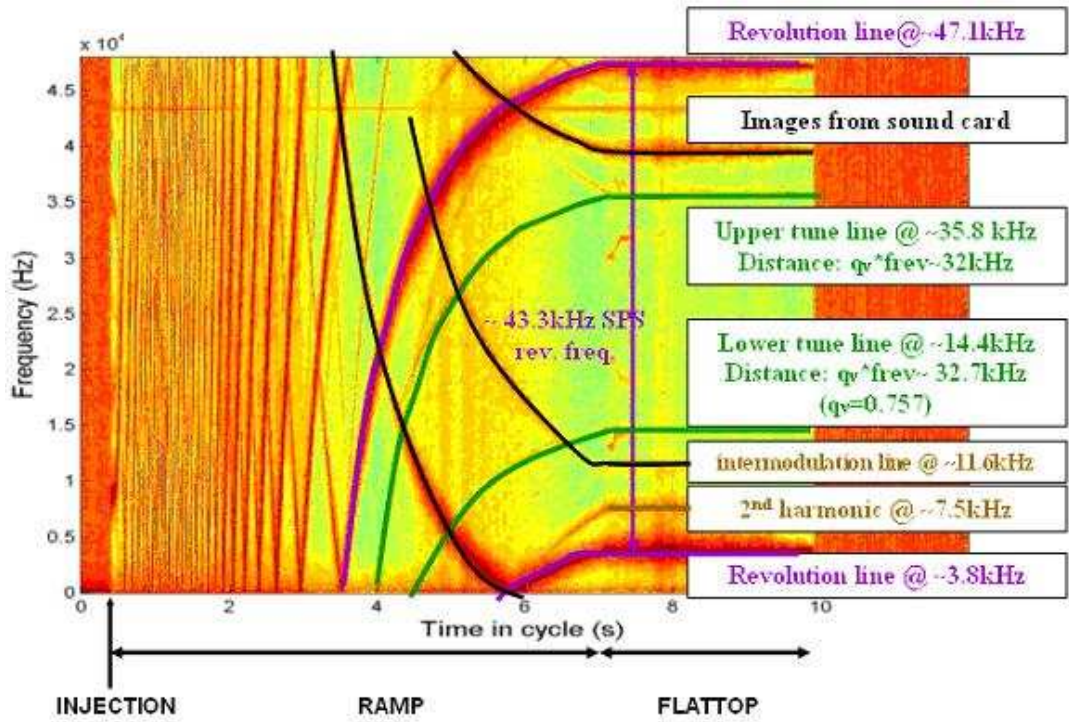


Figure 5.18: Frequency lines identification in the accumulated FFT spectrum

5.4.2 Single FFT trace analysis and the effects of frequency mismatches in the data acquisition system

The data used for this analysis was obtained with coasting beam. The energy at coast was 26GeV with a 40MHz LHC beam pattern (72 bunches spaced by 25ns) and fractional part of the vertical betatron tune, $q_v=0.175$.

The device settings for the two down mixing stages were:

- HP 8566B SPA: Center Frequency: 1.803 GHz, RBW: 30 kHz.
- LO Frequency in 2nd down mixing: 21.40MHz.

And the obtained spectrum was:

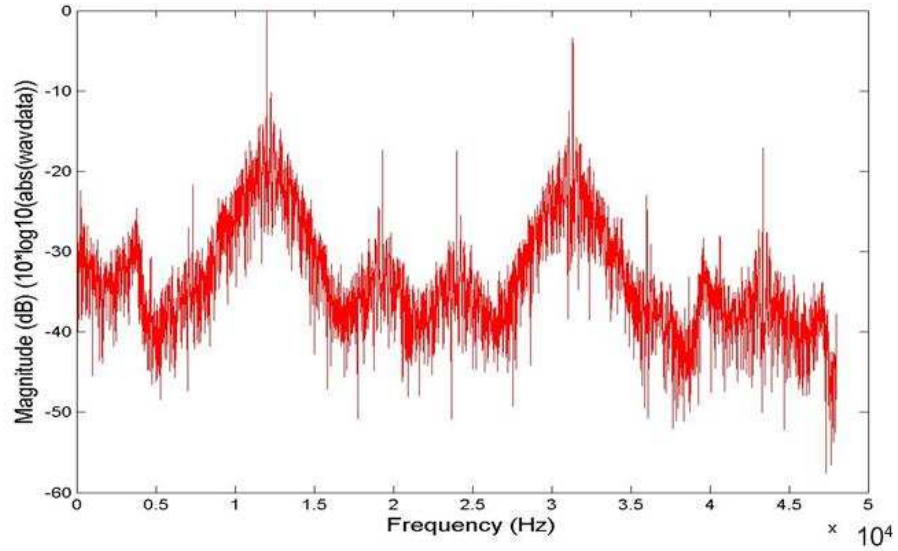


Figure 5.19: Single FFT trace

At first sight one would say that the two highest peaks should correspond to revolution lines and the two smaller peaks appearing in between should be the betatron tune peaks. However, the distance between main peaks is around 19 kHz, far from the 43 kHz corresponding to the SPS revolution frequency. This leads us to analyze spectrum in a more detailed way.

As a starting point, we would expect to have a pure Schottky spectrum consisting of revolution lines spaced by ~ 43 kHz, each one with betatron sidebands at a distance of $43 \text{ kHz} \times 0.175 = 7.5$ kHz (for explanation purposes we will consider 7 kHz), as can be seen below:

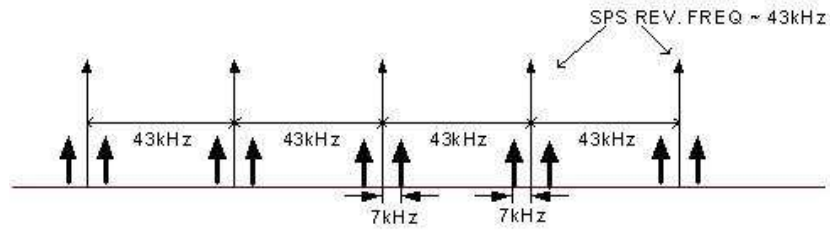


Figure 5.20: Revolution and tune lines

With the help of a spectrum analyzer we observed a revolution harmonic at 1802988500 Hz before entering in the SPA for the first down mixing. Since the center frequency in the SPA was set to 1.803 GHz, there is a difference of ~ 12 kHz between this line and the center frequency of the BP filter in the SPA. After first down mixing, the whole spectrum is shifted to 21.4 MHz. This is illustrated in Figure 5.21.

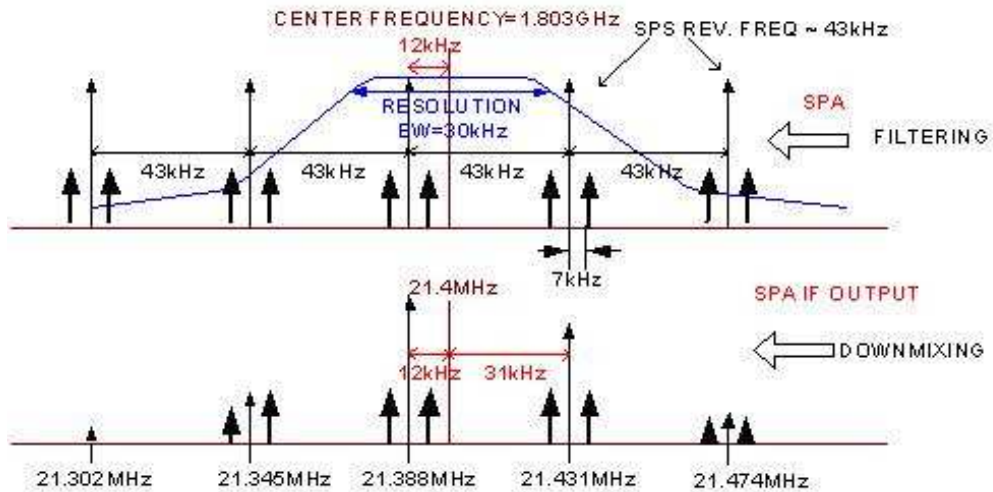


Figure 5.21: Filtering and 1st down mixing in SPA

Next, in the second down mixing, the LO frequency was set to 21.4 MHz and the spectrum was

moved to base band.

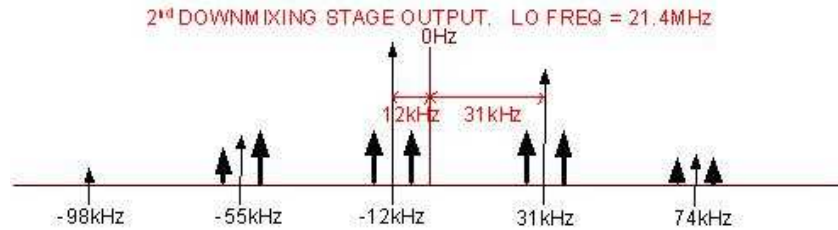


Figure 5.22: 2nd down mixing and shifting of spectrum to base band

After being sampled in the sound card, the spectrum repeats every 96 kHz.



Figure 5.23: Sampling in sound card

But, as we pointed out in Section 5.4.1, the sound card will detect those "negative frequencies" created in the down mixing processes, leading to the generation of images.

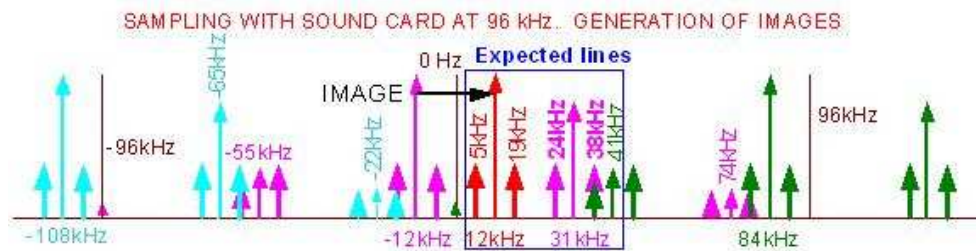


Figure 5.24: Generation of images in the sound card

If now we consider the intermodulation products resulting from the two highest peaks (12kHz and 31kHz) in the frequency range of interest (from 0 Hz to 48 kHz), we expect to have peaks at

frequencies: ~ 7 kHz, ~ 19 kHz, ~ 24 kHz, ~ 36 kHz and ~ 43 kHz (see Figure 5.25).

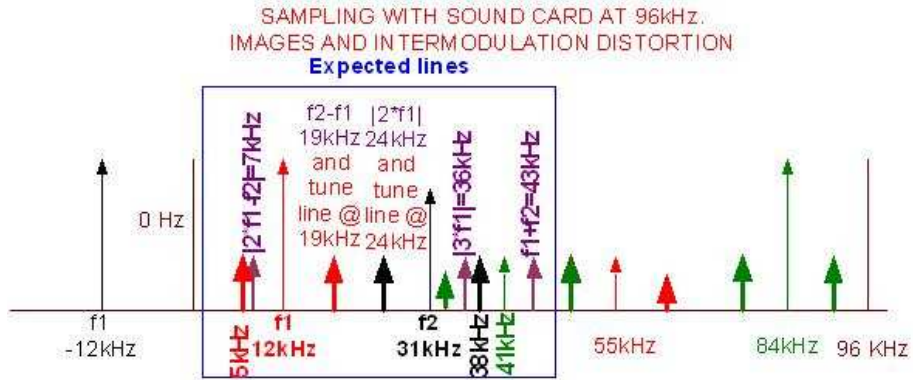


Figure 5.25: Expected spectrum considering all distortion effects

Once we have included all possible distortion effects in frequency domain, we can proceed to identify all the peaks in the single FFT trace of Figure 5.19.

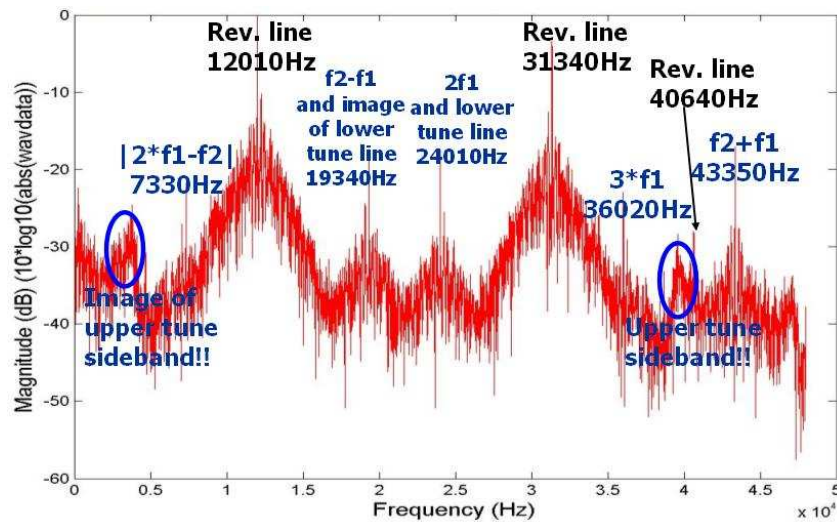


Figure 5.26: Peaks identification in FFT single trace

So, finally nearly all of the lines appearing in the FFT spectra are understood. They are due to harmonic distortion, intermodulation distortion, sampling in the sound card and offsets in the settings of the devices. This mess of lines makes difficult to observe a clean Schottky spectrum since

tune lines may be buried under any of these distortion products.

A way to minimize the generation of images is to set the center frequency in the SPA at exactly the same frequency as the pick-up response; however, slight differences may be unavoidable. This was tried setting the center frequency in the SPA to 1802988500 Hz, exactly the same frequency measured for the measurement of maximum pick-up response. After a detailed analysis it was discovered that there was an offset of 500 Hz due to the fact that the two spectrum analyzers were not phase locked.

A single FFT trace obtained this time is in Figure 5.27.

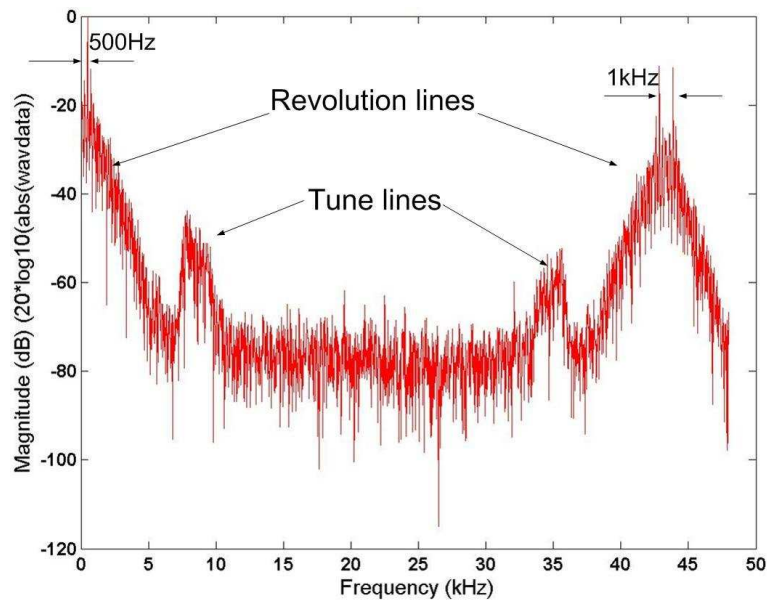


Figure 5.27: *Suppression of intermodulation products*

The previous spectrum shows the overlap of two traces being one the image of the other and shifted by 1 kHz.

This way, the real tune sidebands are almost overlapped by images of negative signals. However, the obtained spectrum is notably cleaner than previous one since intermodulation products are shifted out of the sound card frequency range (0 Hz-48 kHz). The drawback is that this method destroys the Schottky measurement effect because it completely mixes upper and lower sidebands so chromaticity or emittance can not be measured.

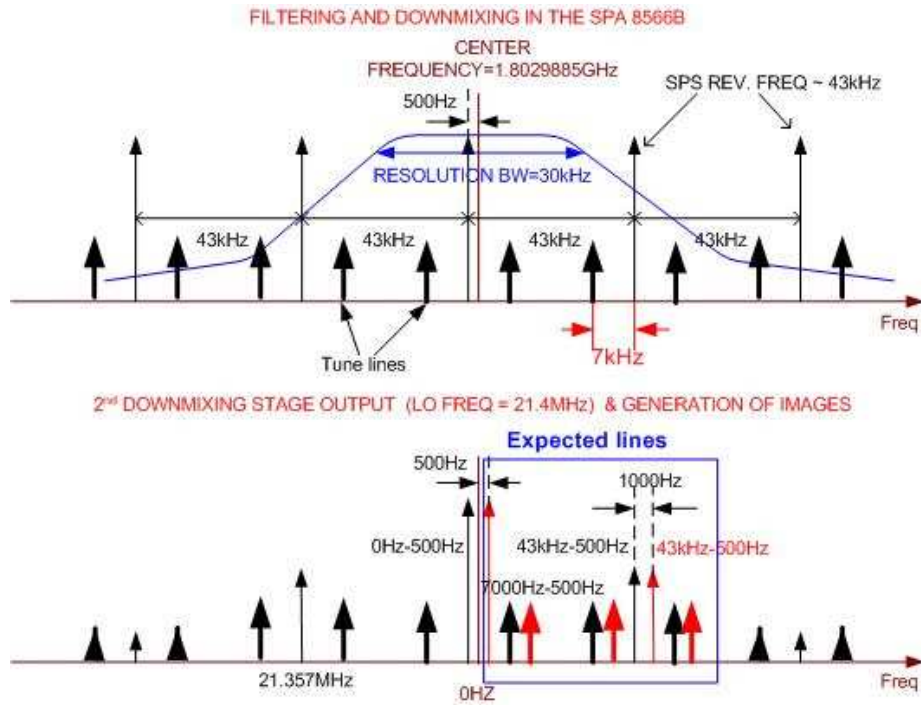


Figure 5.28: Expected spectrum for the suppression of intermodulation products

5.4.3 Betatron tune lines detected with pilot bunch beam

When the beam fills only a small fraction of the machine circumference, the pick-up will detect noise for most of the time. In particular, for the pilot beam, the noise level may become comparable to, or even bigger than the Schottky transverse sidebands. With a priori knowledge of the betatron value we tried to detect the tune lines for a beam with a single LHC pilot bunch with a very low intensity of only $5 \cdot 10^9$ protons. The result was the observation of a faint trace. However, we do not claim that this tune is exclusively incoherent. Anyway, the fact of detecting the frequency tune line originated by a single pilot bunch, reflects the high sensitivity of the Schottky pick-up. The effective noise level could be decreased by gating, where the input signal is switched on only for a relatively short time during the passage of the beam.

5.5 SPECTRA OBTAINED WITH THE 1.7 GHz SCHOTTKY MONITOR AT RHIC (BNL)

The same Schottky monitor tested in the SPS was moved to BNL and installed at RHIC on 2005. Preliminary results in this machine show the presence of coherence in both, the longitudinal and transverse spectra due to a low value of chromaticity. Figure 5.29 ¹ shows a transverse Schottky spectra where coherent signal appears as tiny peaks emerging from the revolution and tune lines. The same coherent lines were present in the spectra acquired in the SPS (see Section 5.3).

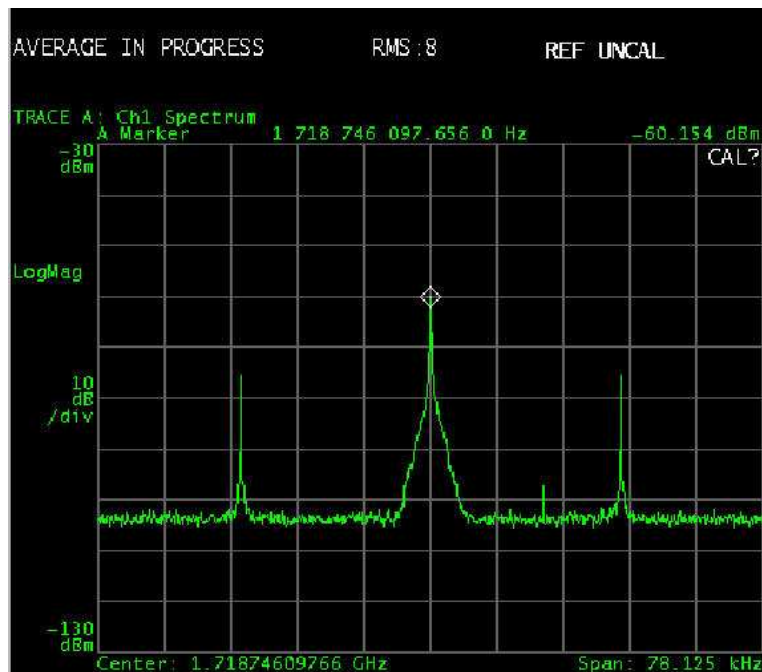


Figure 5.29: Transverse spectrum obtained with Schottky monitor at RHIC

The spectra was acquired with low intensity beam ($\sim 5 \cdot 10^9$) which indicates that these traveling wave pick-ups could be useful at low intensity commissioning, at least to look at coherent injection oscillations and as instability monitors. The 1.7GHz Schottky pick-up system in BNL gives the same spectra as the 2GHz resonant cavity pick-ups installed at RHIC but it is 5-10dB poorer in S/N. Despite we lose sensitivity we gain the possibility of single bunch detection with the traveling

¹Courtesy of Peter Cameron (BNL)

wave pick-up.

5.6 CONCLUSIONS

The 1.8GHz Schottky pick-up was successfully installed in the SPS in 2004. The response of such a pick-up agrees with the one predicted by the theory and the values obtained for the betatron tune, the chromaticity and the momentum spread are approximately equal to the real ones. All the spurious lines that appear as a consequence of the downmixing chain, and that is needed for the data acquisition and on-line analysis, are well understood.

The lessons learned in the SPS with these preliminary tests are valuable for the construction of an LHC system which will be based on the same type of monitor and that will use a similar downmixing chain.

Chapter 6

Determination of Chromaticity by the Measurement of a Head-Tail Phase Shift

A set of methods for chromaticity measurement were overviewed in Chapter 2. As mentioned, the most common method for extracting the chromaticity in a circular machine is to measure the betatron tune as a function of the beam energy and then to calculate the chromaticity from the resulting gradient. This method does not allow instantaneous measurements, for instance during energy ramping. For that reason, in preparation for LHC a new approach has been developed by which transverse oscillations are excited with a single kick and the chromaticity is calculated from the phase difference of the individually sampled head and tail motions of a single bunch. Using this method, the chromaticity can be calculated using the data from only one synchrotron period (about 15-50 ms in the case of the LHC).

This chapter describes the principle and theory behind this technique.

6.1 THE HEAD-TAIL PRINCIPLE

In Chapter 2, the *relative chromaticity* was defined as the variation of the betatron tune Q with the relative momentum deviation $\Delta p/p$:

$$\xi = \frac{Q'}{Q} = \frac{\Delta Q}{Q} \cdot \frac{p}{\Delta p} \quad (6.1.1)$$

In the case of bunched beams, the chromaticity produces a transverse instability called '*Head-Tail effect*': the wake field produced by the leading part of a bunch (the *head*) excites an oscillation of the trailing part (the *tail*) of the same bunch. In half a synchrotron period the head and the tail of the bunch interchange their positions, the bunch of particles oscillates and this oscillation may cause instability and beam loss.

The method of extraction of chromaticity using the Head-Tail technique consists in applying a transverse kick to the bunch and observing the resulting betatron motion . Following the time evolution of any two positions within the bunch, a phase-difference is obtained from which the chromaticity can be calculated. The betatron motion is detected using the transverse difference signal (Δ) supplied by an electromagnetic pick-up. To illustrate this, Figure 6.1 (a) ¹ shows the typical shape of the Δ signal obtained with such a pick-up after applying a transverse kick to a bunch with non-zero chromaticity. The '*inclination*' of the bunch with respect to the plates of the pick-up will change turn after turn leading to the results for consecutive turns illustrated in Figure 6.1 (b).

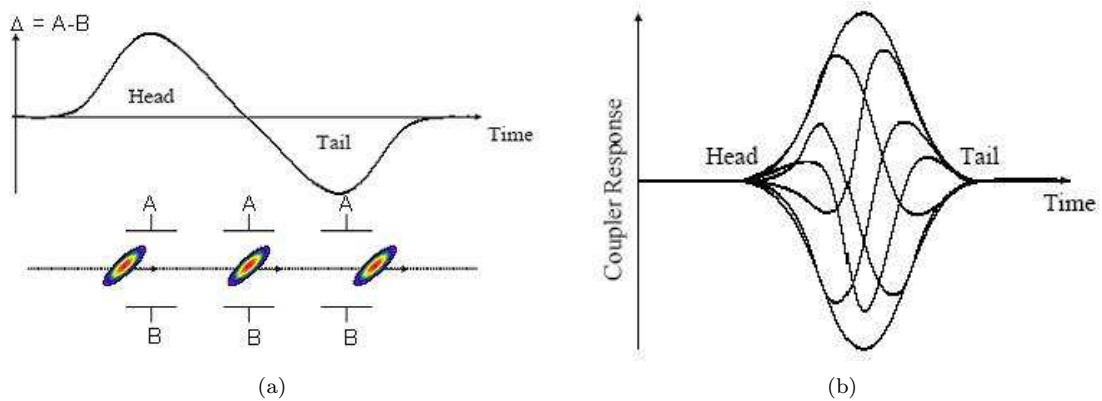


Figure 6.1: (a) Transverse signal in a pick-up after applying a kick to the beam with $\xi \neq 0$ (b) Turn by turn response

Sampling one point near the head and another point near the tail of the bunch would permit the extraction of the phase difference between them, giving a measure of chromaticity. This is clearly illustrated in Figure 6.2. Figure 6.2 (a) shows the result of sampling amplitudes in two points at the head and the tail in a whole synchrotron period and lower plot shows the phase difference. We

¹Pictures from R. Jones (CERN)

should note that, the maximum phase shift is obtained after half a synchrotron period.

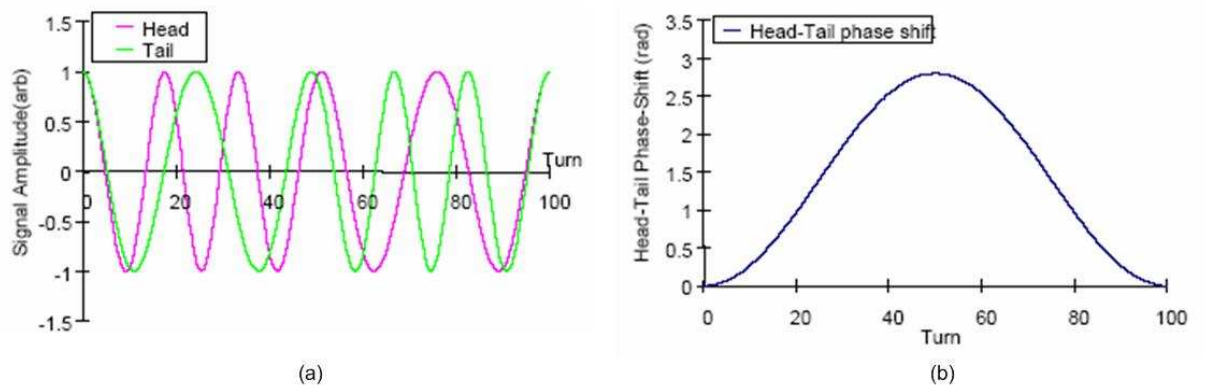


Figure 6.2: Determination of head and tail phase shift in a synchrotron period

6.2 THE HEAD-TAIL CHROMATICITY EQUATIONS

6.2.1 Single particle dynamics in a bunched beam

A single particle traveling around the machine in a bunched beam performs longitudinal *synchrotron oscillations* with respect to the synchronous particle of the bunch and, at the same time, it undergoes transverse *betatron oscillations*. The combination of both phenomena leads to the equation of the position of the particle within a bunch.

Synchrotron oscillations

Figure 6.3 shows the accelerating voltage or the energy gain in an RF cavity as a function of the time of arrival of a particle [30].

The RF frequency is at some harmonic of the revolution frequency so that a particle that arrives on every turn at the correct time (and hence phase with respect to the RF voltage) will subsequently see the same accelerating voltage on every passage. This particle is called the synchronous particle, and its energy is the nominal energy of the design orbit, E_0 . At energies below transition, a particle with a higher energy will travel faster than the synchronous particle. It can be seen in the figure that such a particle will receive less energy at the cavity, which therefore compensates for the energy

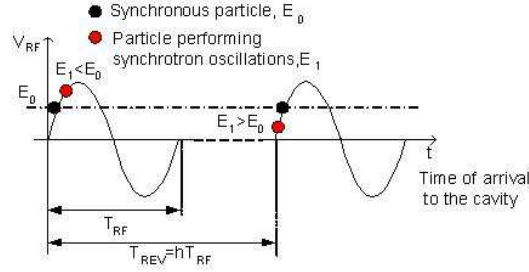


Figure 6.3: Accelerating voltage in an RF cavity as a function of the particle's arrival time

deviation. Similarly, a lower energy particle will arrive later at the cavity and will have a higher energy gain. This describes the usual stable oscillations in energy and time that occur about the synchronous point. A particle that does not sit exactly at the stable point will be periodically accelerated and decelerated so that its position relative to the stable particle oscillates back and forth at the synchrotron frequency ω_s .

Betatron oscillations

Particles moving in a circular accelerator, perform a transverse oscillation of frequency $\omega_{bet} = Q \cdot \omega_{rev}$ due to the action of the focusing and defocusing quadrupoles. The number of betatron oscillations per turn, given by the Q value, must not be a simple integer, otherwise the particle will repeat its path in the machine and will see the same field imperfections, leading to a resonant growth and a hit of the particle with the vacuum pipe. The betatron frequency, or tune, is therefore composed of an integer value and a non integer part, the latter being the most important for machine operation.

6.2.2 Chromaticity equation

The *longitudinal motion* of a particle, i , within a bunch can be described in terms of the synchrotron frequency, ω_s and it can be expressed as [31]:

$$\tau_i(t) = \hat{\tau}_i \cos(\omega_s t + \varphi_i) \quad (6.2.1)$$

where $\tau_i(t)$ is the time difference with respect to the synchronous particle considered as the center of the bunch, $\hat{\tau}_i$ is the amplitude of the synchrotron oscillation, ω_s is the angular synchrotron frequency and φ_i is the starting longitudinal phase of the particle.

During this longitudinal motion, the particle also undergoes sinusoidal *transverse motion*, which can be described by the change in the betatron phase, $\Theta(t)$, along the synchrotron orbit. The i_{th} particle then executes a sinusoidal betatron oscillation, of amplitude A , which can be written as:

$$y_i(t) = A \cdot \cos[\Theta(t)] \quad (6.2.2)$$

The betatron phase can be obtained from the rate of change:

$$\dot{\Theta}(t) = Q \cdot \omega_{rev} = (Q_0 + \Delta Q) \cdot (\omega_0 + \Delta\omega) \Rightarrow \Theta(t) = \int (Q_0 + \Delta Q) \cdot (\omega_0 + \Delta\omega) dt \quad (6.2.3)$$

where Q_0 is the nominal transverse tune, ΔQ is the change in tune due to the momentum spread, ω_0 is the nominal angular revolution frequency and $\Delta\omega$ is the change in frequency due to the momentum spread.

Given the expressions: $\frac{\Delta\omega}{\omega_0} = -\eta \frac{\Delta p}{p}$, $\frac{\Delta Q}{Q_0} = \xi \frac{\Delta p}{p}$ and $\dot{\tau} = -\frac{\Delta T}{T_0} = \frac{\Delta\omega}{\omega_0}$

One obtains ΔQ and $\Delta\omega$ as a function of known parameters: $\Delta Q = -\frac{\xi}{\eta} \cdot Q_0 \cdot \dot{\tau}$ and $\Delta\omega = \omega_0 \cdot \tau$

Which on substitution into equation 6.2.3 gives:

$$\dot{\Theta}(t) = \left(Q_0 - \frac{\xi}{\eta} Q_0 \dot{\tau} \right) \cdot (\omega_0 + \omega_0 \dot{\tau}) = Q_0 \omega_0 \left(1 - \frac{\xi}{\eta} \dot{\tau} \right) (1 + \dot{\tau}) \approx Q_0 \omega_0 \left(1 + \dot{\tau} \left(1 - \frac{\xi}{\eta} \right) \right) \quad (6.2.4)$$

By integration of 6.2.4: $\Theta(t) = Q_0 \omega_0 (t + \tau) - \omega_\xi + \Theta_0$ where $\omega_\xi = Q_0 \omega_0 \frac{\xi}{\eta}$ is known as the *chromatic frequency*. Since τ is usually much smaller than t , it is possible to write:

$$\Theta(t) = Q_0 \omega_0 t - \omega_\xi \hat{\tau} \cos(\omega_s t + \varphi_i) + \Theta_0 \quad (6.2.5)$$

being Θ_0 is the initial betatron phase of the particle.

If we assume that the displacement due to the kick is much larger than the betatron oscillations performed by the particles in the unperturbed bunch, then the initial betatron phase can be set such that all the particles have the same initial position in the transverse plane; i.e. at $t=0$ a particle with a longitudinal position described by $\hat{\tau}_i$ and Θ_i will have an initial betatron phase given by:

$$\Theta_0 = \omega_\xi \hat{\tau}_i \cos(\varphi_i) \quad (6.2.6)$$

And the position of a particle in the bunch, y_i , at any time is:

$$y_i(t) = A \cdot \cos[Q_0 \omega_0 t - \omega_\xi \hat{\tau}_i \cos(\Omega_s t + \varphi_i) + \omega_\xi \hat{\tau}_i \cos(\varphi_i)] \quad (6.2.7)$$

Extracting the chromaticity by considering the head-tail evolution

Consider a system where the particles are distributed along a single synchrotron orbit, and where the particle position is measured as a function of time at the tail of the bunch.

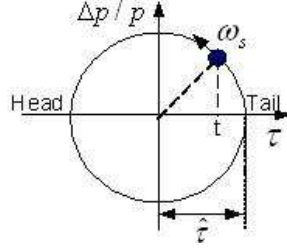


Figure 6.4: Longitudinal 'phase-space'

The initial synchrotron phase, φ_i , of the particle at the tail after a given time t , is given by $\varphi_i = -\omega_s \cdot t$, and therefore the corresponding initial betatron phase, Θ_0 , can be written as $\Theta_0 = \omega_\xi \hat{\tau}_i \cos(-\omega_s t)$. The transverse amplitude at the tail evolves as:

$$y_T(t) = A \cdot \cos[Q_0 \omega_0 t - \omega_\xi \hat{\tau}_T \cos(\omega_s t + \phi) + \omega_\xi \hat{\tau}_T \cos(-\omega_s t)] = A \cos[Q_0 \omega_0 t + \omega_\xi \hat{\tau}_T (\cos(-\omega_s t) - 1)] \quad (6.2.8)$$

Measurements are carried out turn by turn, which corresponds to time steps of $t = 2\pi n / \omega_0$, where n is the turn number. Hence the signal at the tail of the bunch for a given turn, n , can be written as:

$$y_T(t) = A \cdot \cos[2\pi n Q_0 + \omega_\xi \hat{\tau}_T (\cos(2\pi n Q_s) - 1)] \quad (6.2.9)$$

being Q_s the synchrotron tune, with $\omega_s = Q_s \omega_0$. A similar expression can also be derived for the head of the bunch: n , can be written as:

$$y_H(t) = A \cdot \cos[2\pi n Q_0 - \omega_\xi \hat{\tau}_H (\cos(2\pi n Q_s) - 1)] \quad (6.2.10)$$

The phase difference between the head and tail as a function of turn number is therefore given by:

$$\Delta\Psi(n) = -\omega_\xi [\hat{\tau}_H + \hat{\tau}_T] [\cos(2\pi n Q_s) - 1] \quad (6.2.11)$$

This equation is a maximum when $nQ_s = 1/2$, i.e. after half a synchrotron period, giving:

$$\Delta\Psi_{MAX} = -2\omega_\xi (\hat{\tau}_H + \hat{\tau}_T) \quad (6.2.12)$$

The *relative chromaticity* can therefore be written as:

$$\xi = \frac{-\eta\Delta\Psi(n)}{Q_0\omega_0\Delta\tau[\cos(2\pi nQ_s)-1]}$$

or

$$\xi = \frac{-\eta\Delta\Psi_{MAX}}{2Q_0\omega_0\Delta\tau} \tag{6.2.13}$$

Since the revolution frequency and the total tune of the machine are known to a high degree of accuracy, and if one considers a machine operating well above transition, the chromaticity will depend only on the maximum phase difference attained between two regions of the same bunch separated longitudinally by a known time.

6.3 MEASUREMENT OF THE HEAD-TAIL DEPHASING

As was pointed out in Section 6.1, the way to calculate the head and tail phase difference is by observing two points within a single bunch during a whole synchrotron period, after the application of a transverse kick. This transverse displacement can be detected with the signals supplied by the two electrodes of a beam position monitor pick-up and that are combined in a Δ/Σ hybrid. The Σ signal gives information about the intensity of the beam while the transverse displacement is indicated by Δ .

6.3.1 Stripline coupler

In the case of the Head-Tail monitor installed in the SPS, a particular type of electromagnetic pick-up was used: a *stripline coupler*.

In a *stripline coupler*, a metal strip is inserted along the chamber. It acts as a transmission line of the image current generated by the beam as it travels through the pipe, and is terminated at both ports by its characteristic impedance [32]. When the beam enters the pick-up, the image current excites the stripline and produces a pulse at the output. The current pulse in the stripline transmission line travels with the beam and, as beam exits the detector, it produces an inverted pulse of equal amplitude which travels in opposite direction. The inverted pulse returns to the input end and produces a negative pulse.

The time domain impulse response of the stripline BPM to a charged particle moving with $v \approx c$ is $h(t) = 1/2[\delta(t) - \delta(t - 2l/c)]$. If we assume that the current of a bunch can be represented by a Gaussian function, then the shape of the pick-up signal will appear as in Figure 6.5 (b).

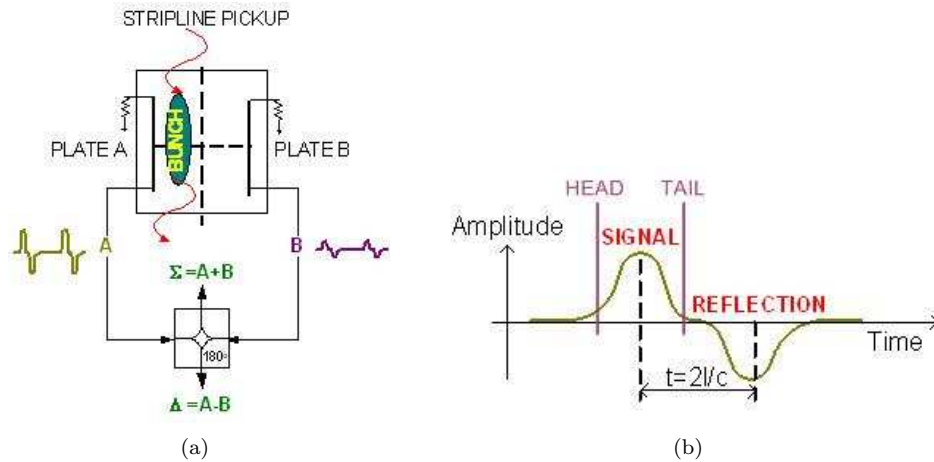


Figure 6.5: (a) Signal supplied by a single strip in a stripline pick-up (b) Sum and Delta signals from a stripline pick-up

If the total bunch length is less than twice the coupler stripline length, then the signal from the bunch and its reflection from the opposite end are well separated in time. If, however, the bunch is longer than twice the stripline length, then the signal and reflection are no longer separated.

The recombination of the signals coming from opposite plates in a Δ/Σ -hybrid allows the Sum and Difference to be obtained and hence information about the intensity of the bunch and its transverse position in the coupler. The shapes of resulting Σ and Δ signals are the same in the case of an offcentered beam, however, when centered, the Δ signal should be equal to zero.

If the coupler is made long enough, then it is possible to separate out the signal and its reflection and allow sampling of the transverse position along the bunch. The main problem with this technique is its sensitivity to the 'static' beam offset, i.e., to the displacement of the beam from the electrical center of the coupler and that reduces the sensitivity to the transverse movement associated to the presence of chromaticity. Figure 6.6 shows the effect of this problem for zero and non-zero chromaticity. In both cases ($\xi = 0$ and $\xi \neq 0$) the resolution of the system is severely reduced in the presence of a static offset. Typically the excitation amplitude has to be of the same

magnitude as the offset for a measurement to be performed. For this reason, it would be desirable to add to the head-tail monitor a 'closed orbit compensation electronics' to improve the sensitivity of the acquisition and allow the measurement to be made with much smaller excitation amplitudes.

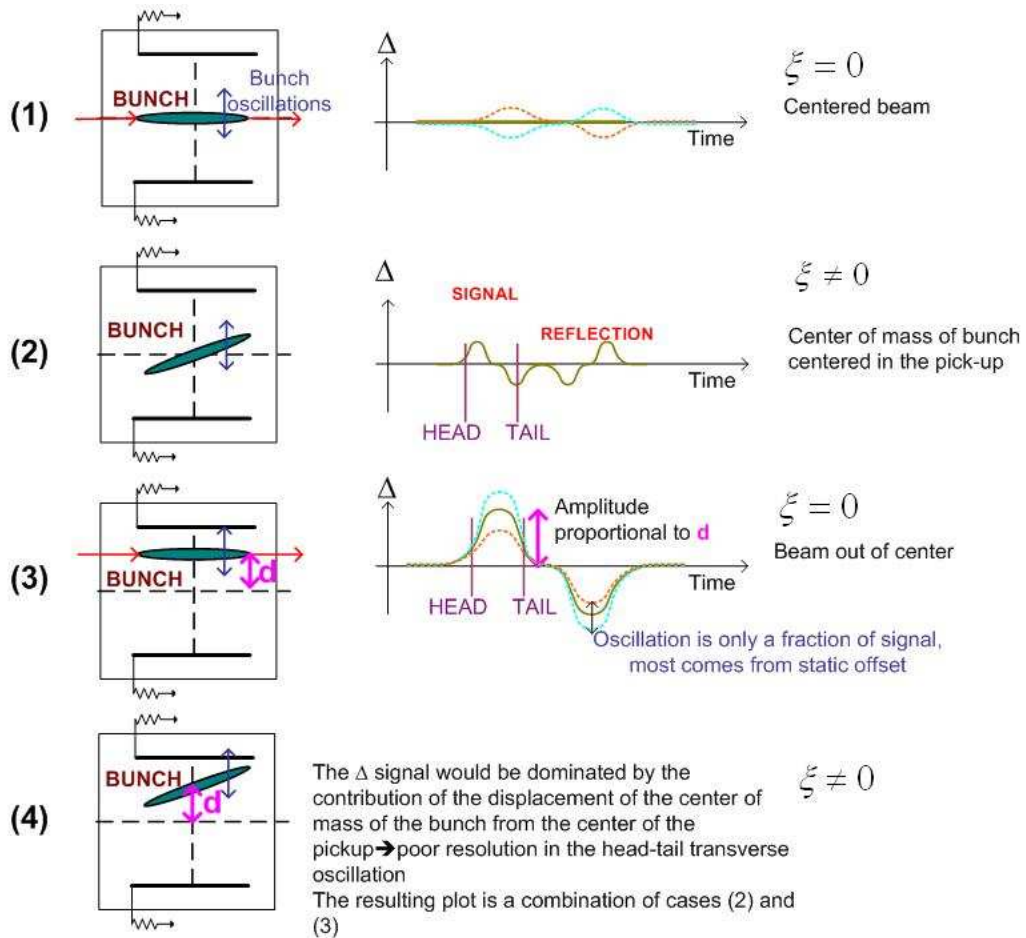


Figure 6.6: Δ signal for different positions and inclinations of a bunch in the stripline pick-up

6.4 DESCRIPTION OF THE CERN HEAD-TAIL MONITOR SYSTEM

A schematic layout of the SPS Head-Tail monitor set-up is shown in Figure 6.7 [33]:

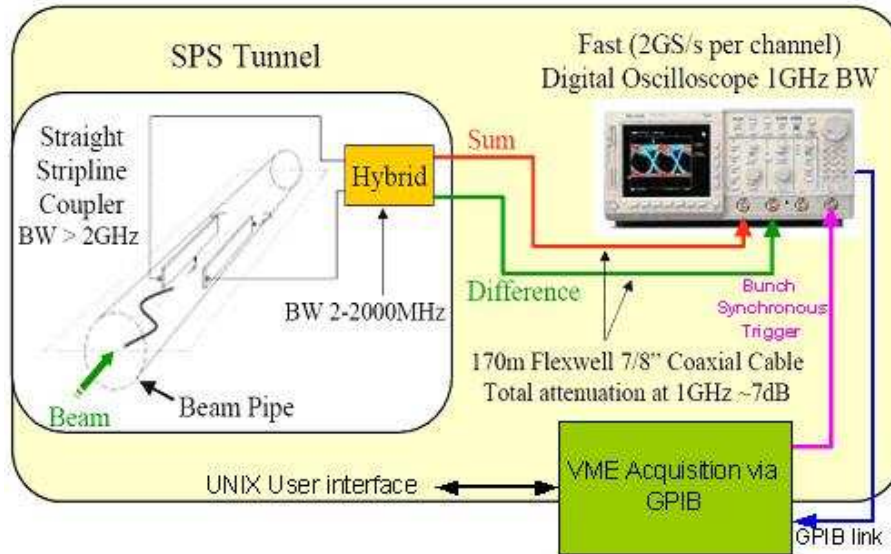


Figure 6.7: Layout of the SPS Head-Tail monitor

The transverse displacement signal of the proton beam is detected with a straight stripline coupler. Signals coming out from the electrodes are combined in a $180^\circ \Delta/\Sigma$ -hybrid to provide the Σ (intensity) and Δ (displacement) signals that are connected to the acquisition system via 170 m of coaxial cable. Both output signals are sampled with a Tektronix TDS7254 digital oscilloscope (1 GHz analog BW, 2 GS/s sampling rate if two channels are used). A VME front-end acquisition crate retrieves the data via a GPIB link. All the oscilloscope and acquisition parameters are accessible from the SPS control room through a UNIX graphical interface.

The oscilloscope is triggered using bunch synchronous timing. The 'fast-frame' capability of the oscilloscope allows 25 ns of data (corresponding to the LHC bunch spacing) to be captured on each SPS revolution. This way the evolution of the signal of a single, specific bunch can be tracked over 372 turns (the memory limit of the oscilloscope).

The pick-up is a straight stripline coupler with 90° electrodes. It has 60cm long electrodes and can therefore fully resolve 4ns long bunches ($2L/c$), provided they are spaced by more than 10ns. This allows head and tail data from the same bunch to be analyzed.

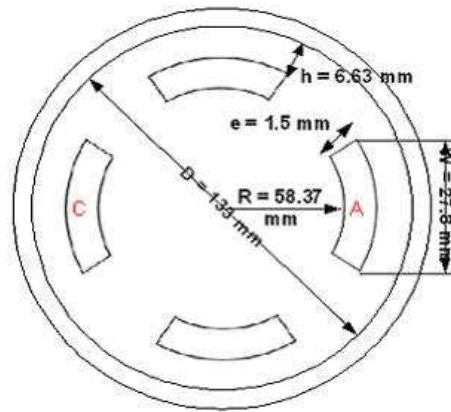


Figure 6.8: Straight stripline coupler used for Head-Tail monitor

For such a pick-up, a $\pm 6dB$ change in signal amplitude on either electrode corresponds roughly to ± 10 mm.

The type of data that is acquired with a 25ns sampling rate digital scope is in figure below:

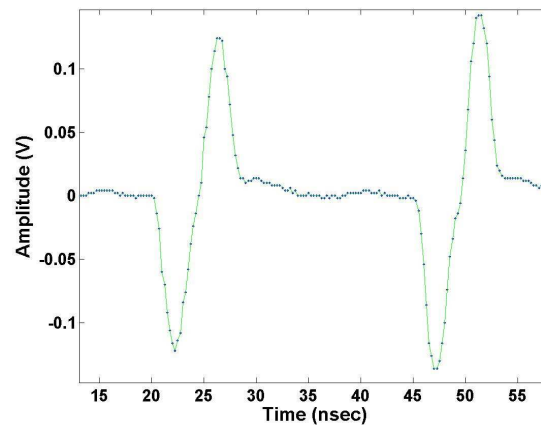


Figure 6.9: Straight stripline coupler used for Head-Tail monitor

Chapter 7

Orbit Compensation

In the method of chromaticity measurement using the head-tail phase shift, a transverse kick to a bunch leads to the generation of betatron oscillations whose frequency can shift as a function of chromaticity. The transverse oscillations are detected using the difference of the signals supplied by the electrodes of a stripline coupler. This Δ signal is the result of the contribution of two components: the static deviation of the bunch from the center of the pick-up and the signal resulting from the betatron oscillations of the particles within the bunch. To optimize the sensitivity of such a method, it is desirable to remove the static component associated with the bunch deviation from the center of the coupler.

This chapter describes the orbit compensation system designed to be included in the Head-Tail monitor already installed in the CERN-SPS and that can be considered as an improvement of a first system designed at DESY (Hamburg).

7.1 DESCRIPTION OF DESY BUILT SYSTEM

Figure 7.1 shows the simple hardware setup used at HERA-p for chromaticity measurement [32]. The transverse displacement signal of the proton beam was detected with the two horizontal 40 cm long stripline electrodes of a beam position pick-up. Their signals were adjusted in time with a variable delay-line and combined in a broadband Δ/Σ -hybrid. Additional fixed and variable attenuators were used to minimize the common mode signal due to the static beam displacement, i.e. the transverse beam orbit.

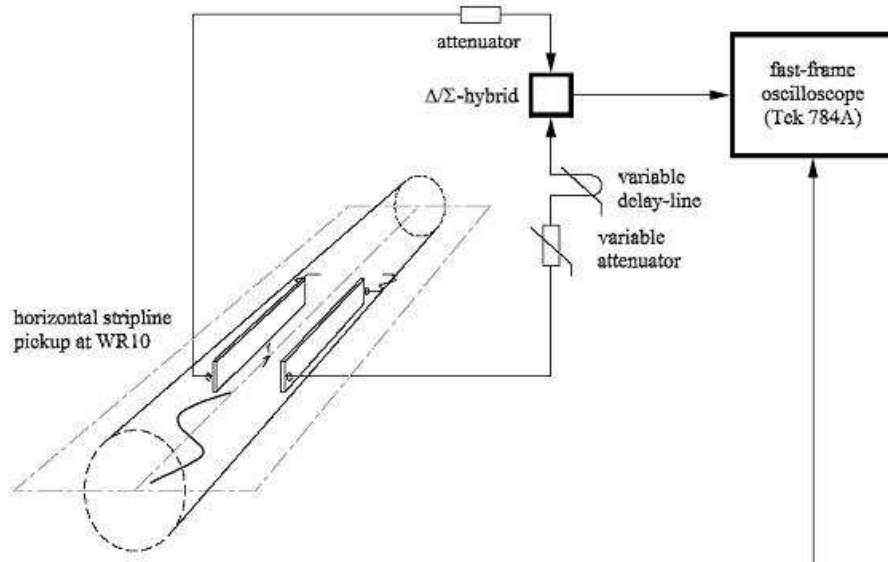


Figure 7.1: Hardware setup for the chromaticity measurements at HERA proton ring

In the case where the beam is perfectly centered in the pick-up, the Δ signal resulting from the difference of signals in opposite electrodes, is equal to zero. In real life, there is often an offset with respect to the electrical center that leads to the production of a non-zero Δ . In the initial HERA system, the correction of the displacement was done via a fixed attenuator connected to the signal path of one electrode and a variable attenuator connected to the other path, whose attenuation had to be changed manually by direct observation of Δ in order to minimize the static offset. This worked fine for static beam, but could not give adequate common mode suppression during acceleration, where the orbit continually moved.

The DESY team therefore built a new orbit compensation system for use in the CERN SPS accelerator. The idea was to automatically correct the orbit using two variable attenuators acting on each electrode with a control voltage calculated as a function of the real deviation of the beam from the electrical center of the pick-up. The 'orbit compensation box' developed for one axis (X or Y) is shown in Figure 7.2.

The principle of operation is as follows: signals coming from opposite pick-up electrodes are fed into 180° Δ/Σ hybrids (H-8-4 M/A-COM 2-2000MHz power dividers) to duplicate them. One of the duplicated signals goes into a commercial beam position monitoring board (Bergoz MX-BPM)

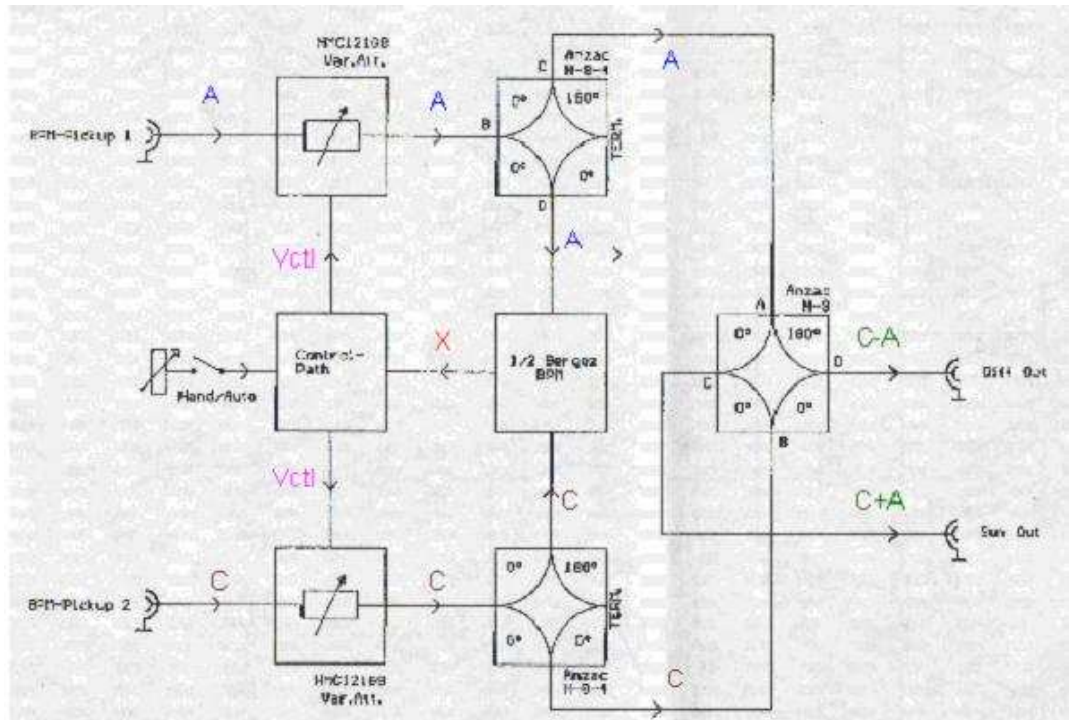


Figure 7.2: Schematic diagram of the orbit compensation system designed at DESY

that calculates the average beam position. The other signal goes to a second hybrid (180° H-9 M/A-COM 2-2000MHz hybrid junction couplers) to get Σ (Sum) and Δ (Delta) signals. Depending on the measured position, a control voltage (V_{ctl}) is applied to the Voltage Controlled Attenuators (Hittite HMC121G8, DC-8GHz) until the average Δ signal is equal to zero, meaning the beam is well centered. The control of the attenuators could be done manually or automatically via a simple analogue feedback circuit. On Figure 7.2, the control path is an analogue circuit composed by a set of operational amplifiers to supply the control voltage.

7.2 PROTOTYPE ORBIT CORRECTION TECHNIQUE FOR CERN HEAD-TAIL MEASUREMENTS

The schematic layout of the prototype orbit correction system tested with the CERN-SPS Head-Tail Monitor set-up is in Figure 7.3.

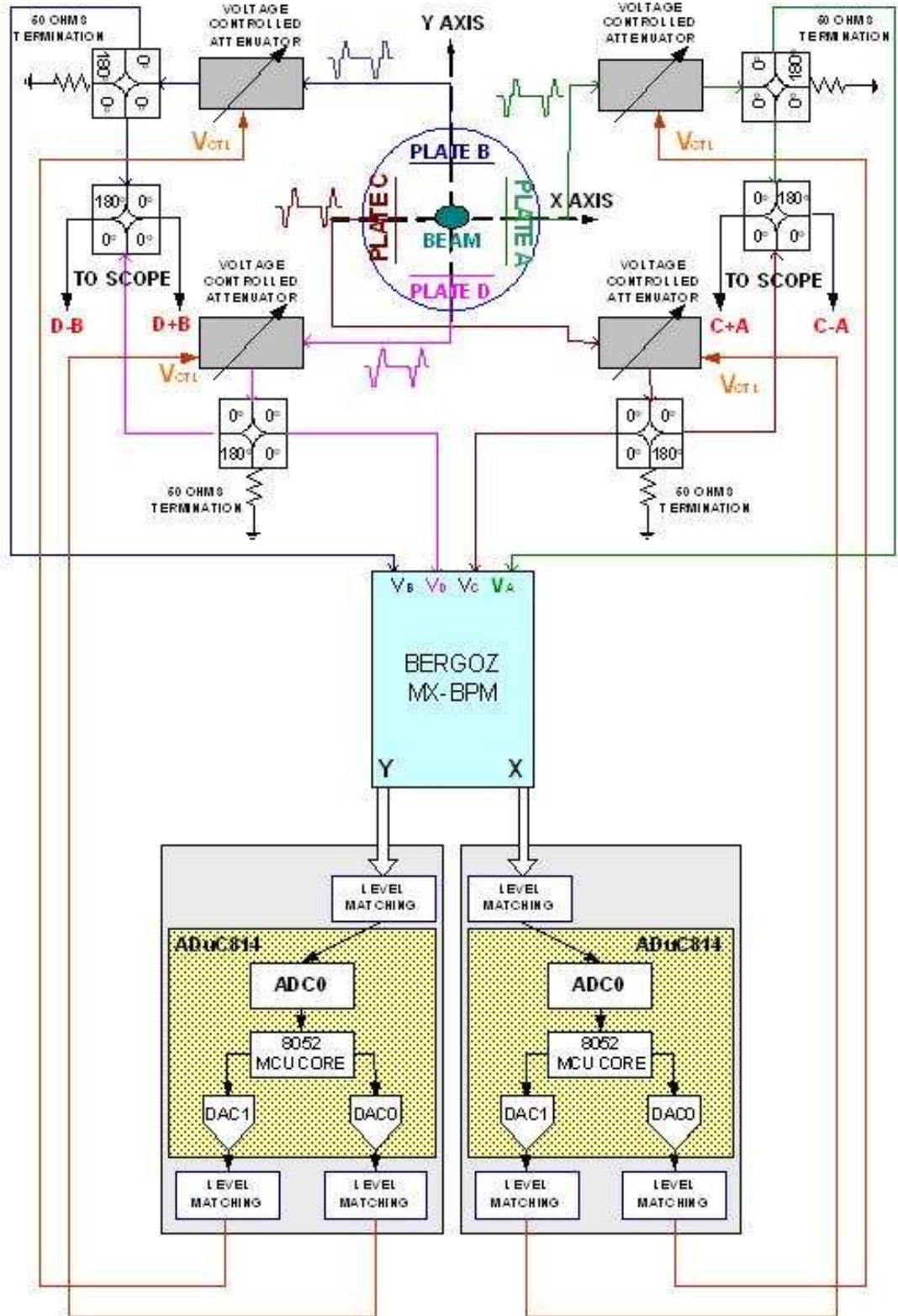


Figure 7.3: Layout of the proposed orbit correction system for SPS Head-Tail Monitor

Here the analogue control circuit developed at DESY is replaced by a *Analog Devices* micro-controller.

The goal is to compensate electronically the deviation of the beam from the geometrical center of the coupler. For that purpose the beam deviation is considered as a displacement from the geometrical center of the pick-up. The pick-up used for tests in SPS has 90° oriented blades with respect to X and Y axis, this means that, for calculating X position only signals from plates A and C would be needed and for calculating Y position we would consider plates B and D (see Figure 7.3). In this case, centered beam means that X and Y values are equal to zero.

In the schematic, for a given axis, Σ and Δ signals are obtained via a 180° Δ/Σ -hybrid. Ideally, if the beam was centered Δ should be equal to zero while Σ value should remain constant independently of the position of the beam with respect to electrical center. In the case that there was a displacement of the beam, Δ would not be zero since one of the electrodes would be delivering to the hybrid a signal higher than the one delivered by the opposite electrode due to the proximity of the beam. A method to get the same amount of signal in hybrid inputs is to attenuate the signal coming from the blade that is closest to the beam. This can be done with Voltage Controlled Attenuators (VCA); however, since the position of beam can vary every revolution period, the control voltage should change according to displacements and track them.

To follow the average displacement of the beam, a feedback system would be useful. This feedback process would take the X and Y signals and, depending on their values, would calculate the optimum control voltage for the attenuators. The orbit compensation should be effective in the same revolution period the X and Y values are being calculated since next turn they could change.

The core of the new system relies in the calculation of the X and Y coordinates of the beam in the pick-up and the control of those values.

The calculation of X and Y is again performed by a Beam Position Monitor (Bergoz MX-BPM) board but the control algorithm relies on a ADuC814 12-bit data acquisition system incorporating ADC's, DAC's and a MCU.

In the next sections, some of the elements integrated into the prototype system for orbit correction are described.

7.3 BERGOZ MULTIPLEXED BEAM POSITION MONITOR (MX-BPM) BOARD

Beam position modules are essential diagnostic instruments in every particle accelerator, and every accelerator project usually includes the development of a specific beam position monitoring system. Conventional beam position pick-ups use 2 or 4 electrodes as position sensors and the position is a function of the amplitude difference of these electrode signals. The fundamental frequencies are specific to each particular machine and the power spectrum may extend to many GHz.

The BPM board used in the orbit correction system of the Head-Tail monitor was developed by 'BERGOZ Precision Beam Instrumentation' [34]. This board is a precision signal processor module for beam position monitors that can easily be adapted to the frequency patterns of different accelerators. It tracks input signals over a limited frequency range (± 200 kHz, extension possible up to ± 1 MHz) and its center frequency is programmable anywhere between 100MHz and 1GHz.

Operating principle

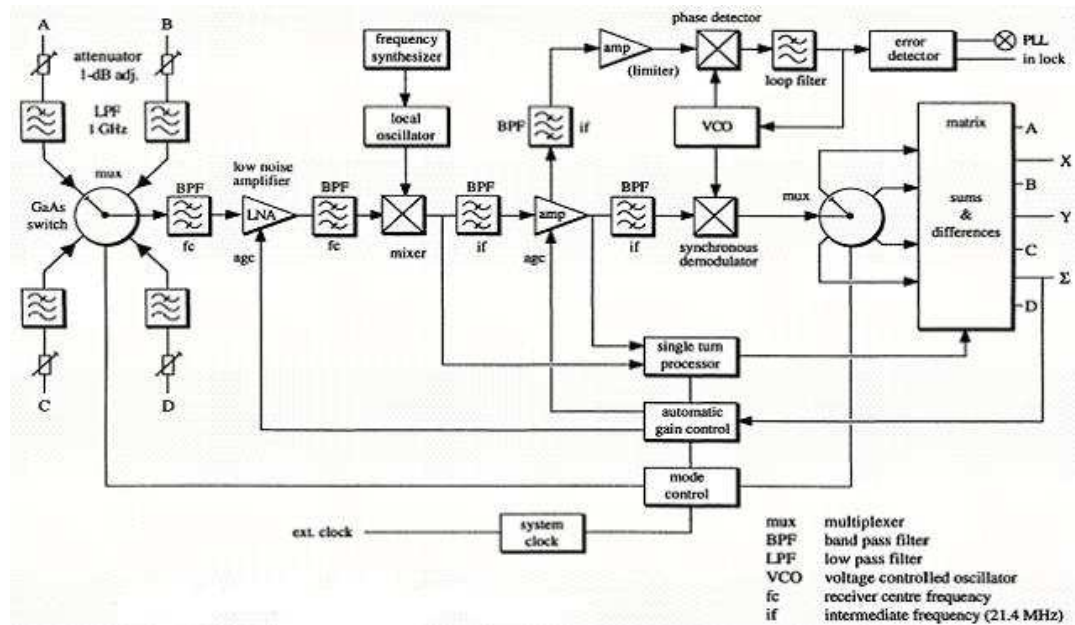


Figure 7.4: BPM signal processor simplified block diagram

The BPM signal processor has 4 parallel input channels for the 4 input signals A to D. The input multiplexer switches sequentially from one input channel to the next. A single receiver measures the signal for each input channel in turn and stores its value in 4 corresponding analog memories. The voltages (V_A to V_D) in each of these memories are therefore proportional to the power levels of the original input signals. To normalize the readings (to make them independent of changing beam current), automatic gain control ('AGC') is used to keep the sum $V_A+V_B+V_C+V_D$ constant.

Algorithm

The X and Y coordinates are calculated with a matrix of sum and difference analog circuits. They use the following equations for a typical position pick-up (with orthogonal electrodes):

$$X = K_X \frac{V_A - V_C}{V_A + V_B + V_C + V_D}$$

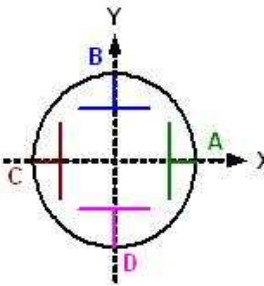
$$Y = K_Y \frac{V_B - V_D}{V_A + V_B + V_C + V_D}$$


Figure 7.5: BPM X and Y algorithm for an orthogonal pick-up

where K_X and K_Y are scaling factors which depend on the geometry of the pick-up.

The board used for our tests was first calibrated in accordance with applicable Bergoz Instruments procedures using an LHC beam pattern. The operating frequency was set to 40 MHz (LHC beam frequency pattern, bunches spaced by 25 ns) and X and Y gains were set to 0.05V/%.

7.3.1 Measurement of the X and Y outputs of the MX-BPM board for different input channel attenuation

According to Bergoz BPM board specifications, X and Y outputs would be equal to zero if beam was centered, that is, if all signals being received from the coupler electrodes were the same. If the beam was non-centered, X and Y DC voltage values would be something other than zero. To characterize

the BPM board to be used in the correction system, one needs to know what the values given by the board are when the beam is offcentered, in order to know the displacement (in mm or dB) and the attenuation to apply to each channel (A, B, C or D).

The objective was to simulate displacements of the beam from the center of the coupler and to measure the outputs X and Y of Bergoz board. To do that, the four inputs of Bergoz board were connected to a fictitious beam that was generated in the laboratory. A variable attenuator was inserted into each MX-BPM input channel to simulate a gradual moving of the beam towards the opposite coupler plate. The experimental setup is shown in Figure 7.6.

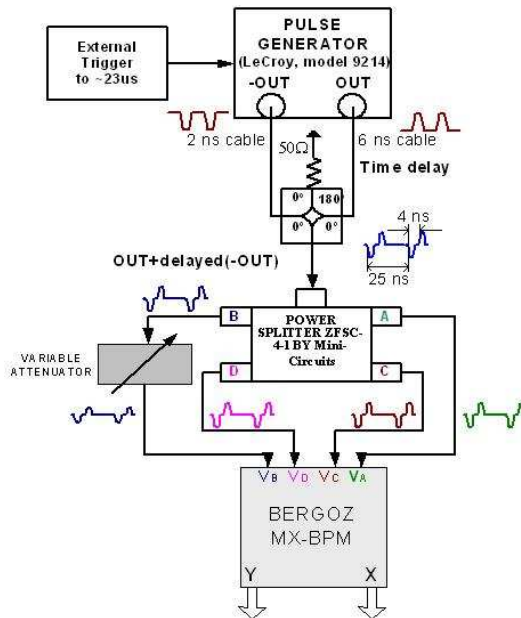


Figure 7.6: Measurements of X and Y outputs in Bergoz board with a variable attenuator

The LHC beam was simulated using a pulse generator and a 180° Δ/Σ -hybrid. The external trigger to the pulse generator was set to the revolution period of the SPS ($23 \mu\text{s}$) and the pulse generator supplied a batch of 72 bunches spaced by 25 ns. The output of the generator was combined with its inverted signal in the hybrid but delayed by 4 ns to get the typical signal measured in a stripline coupler. This simulated beam was splitted into four and that way get the outputs of the four blades of the coupler. The displacement of the beam was simulated with the insertion of a variable attenuator in each of the channels one at a time. Finally the inputs of Bergoz board were

fed with previous four signals. The X and Y values were measured as a function of the attenuation. The results are shown in plots of Figure 7.7.

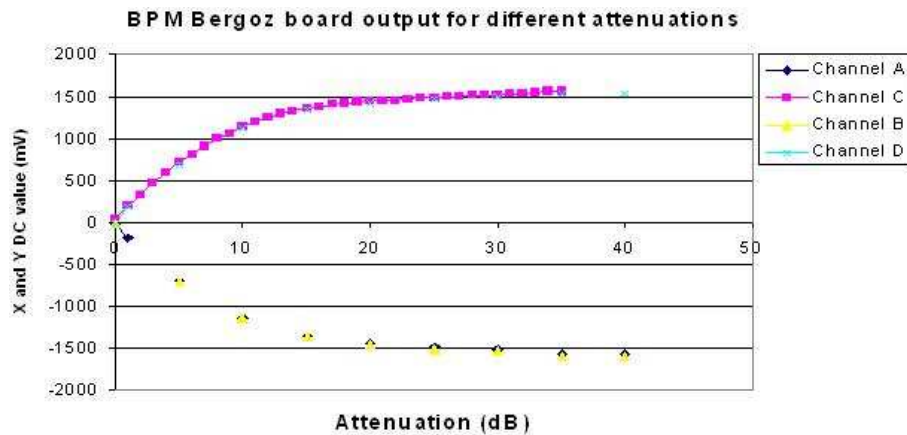


Figure 7.7: X and Y outputs for different attenuations in the four channels

It can be seen that the response is linear up to $\pm 6dB$ and then trends towards a maximum value of 1.5 V.

The maximum excursions of the beam from the center of the pick-up are expected to be around 3 or 4 mm, this means a maximum attenuation to be applied to the pick-up electrodes of $\sim 3dB$. Up to this value, the MX-BPM response is linear.

7.4 ANALOG DEVICES ADuC814 MICROCONVERTER

Next step in the implementation of the orbit compensation system is to process the X and Y values coming from the Bergoz board, to get the right control value to be applied to the voltage controlled attenuators to electronically center the beam. The chosen option was a microcontroller that processes input and calculates output. However, the microcontroller needs as input digital signals and

the attenuators use analog signals for control, this means that X and Y voltages need to be converted to digital and digital signals coming out from microcontroller need to be converted to analog. All these tasks can be accomplished by a single device, an *ADuC814 Analog Devices MicroConverter*.

General description [35]

The ADuC814 is a fully integrated 247 kSps ($T_{\text{sampling}} \approx 4\mu\text{s}$) 12-bit data acquisition system incorporating a high performance multi-channel ADC, an 8-bit Memory Controller Unit (MCU), and program/data Flash/EE memory on a single chip. The block diagram is shown in Figure 7.8 [36].

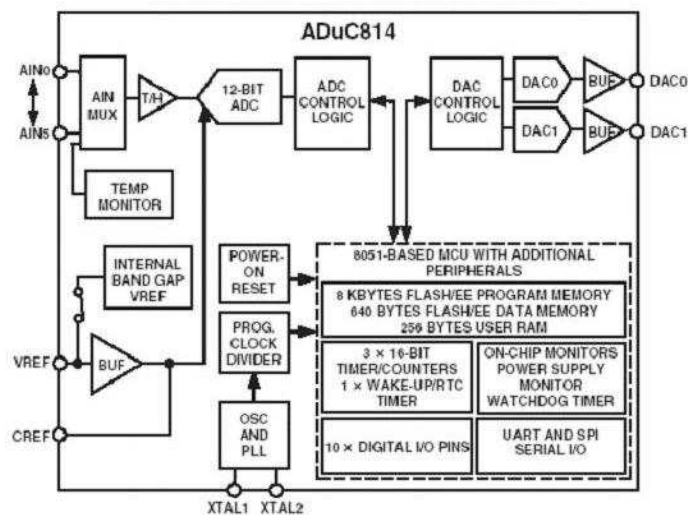


Figure 7.8: ADuC814 functional block diagram

This low power device operates from a 32 kHz crystal with an on-chip PLL generating a high frequency clock of 16.78 KHz. The clock is routed through a programmable clock divider from which the MCU core clock operating frequency is generated.

The microcontroller core is an 8052. 8 Kbytes of non-volatile Flash/EE program memory are provided on-chip. 640 bytes of non-volatile Flash/EE data memory and 256 of RAM are also integrated on-chip.

The ADuC814 incorporates additional analog functionality with 2 dual 12-bit DACs, a power supply monitor, and a band gap reference.

It operates from a single 3 V or 5 V supply. The table in Figure 7.9 shows the specifications for the DAC and ADC channels.

Parameter	V _{DD} = 5V	V _{DD} = 3V	Unit	Test Conditions
ADC channel specifications				
ANALOG INPUT				
Input Voltage Ranges	0 to V _{REF}	0 to V _{REF}	V	
DAC channel specifications				
ANALOG OUTPUTS				
Voltage Range_0	0 to V _{REF}	0 to V _{REF}	V	DAC V _{REF} =2.5V
Voltage Range_1	0 to V _{DD}	0 to V _{DD}	V	DAC V _{REF} =V _{DD}

Figure 7.9: Specifications for DAC and ADC channels.

ADC circuit information

The ADC block incorporates a 4.05 ms, 6-channel, 12-bit resolution, single-supply ADC. The converter accepts an analog input range of 0V to V_{REF} . A precision factory calibrated 2.5V reference is provided on-chip. An external reference may also be used via the external V_{REF} pin. The ADC has six external input channels and two of them are multiplexed with the DAC outputs.

ADC transfer function: The analog input range for the ADC is 0V to V_{REF} (or FS). For this range, the designed code transitions occur midway between successive integer LSB values, i.e., 1/2 LSB, 3/2 LSBs, 5/2 LSBs...FS-3/2 LSBs. The output code is binary with 1 LSB = FS/4096 or 2.5 V/4096 = 0.61 mV when $V_{REF} = 2.5$ V. The ideal input/output transfer characteristic for the 0 V to V_{REF} range is shown in Figure 7.10.

All ADC timing parameters are calculated from the ADCCLK frequency that is a fraction of the maximum core frequency (F_{CORE}), 16.777216 KHz. The total ADC conversion time T_{ADC} is calculated using formula: $T_{ADC} = T_{SYNC} + T_{ACQ} + T_{CONV}$. Where:

- T_{ACQ} is the number of ADCCLK that the ADC input circuitry uses to sample the input signal.

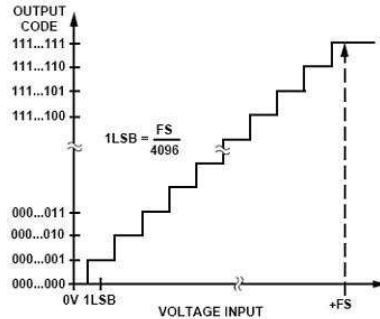


Figure 7.10: ADuC814 ADC Transfer Function

- T_{CONV} is the number of periods needed to convert the acquired signal into its corresponding digital output (it usually takes 15 ADCCLK periods).

- T_{SYNC} is the number of periods needed to synchronize the 'start of conversion' signal to the ADCCLK.

In this case, the ADC conversion was configured with following parameters:

$$F_{ADCCLK} = F_{CORE}/16 = 1 \text{ MHz} \rightarrow T_{ADCCLK} = 1 \mu\text{s} \text{ (configurable via ADCCON1 register)}$$

$$T_{ACQ} = 4 \text{ ADCCLK periods (configurable via ADCCON1 register)}$$

$$T_{CONV} = 15 \text{ ADCCLK periods } T_{SYNC} = 1 \text{ ADCCLK period}$$

This gives a total AD conversion time of:

$$T_{ADC} = (4 + 15 + 1) \times 1 \mu\text{s} = 20 \mu\text{s}$$

For simplicity, reference provided on-chip was used as V_{REF} to give a voltage range of 2.5 V for the input. This implies that the X and Y analog signals coming out from Bergoz board should have a maximum excursion of 2.5 V. However, since the values for the position are between -1.5 V and +1.5 V, the analog values falling into this 3 V interval need to be converted to a 2.5 V range by means of a signal level adaptation stage.

DAC circuit information

The ADuC814 incorporates two 12-bit, voltage output DAC's on-chip. They have two selectable ranges, 0 V to V_{REF} (an external or the internal band gap 2.5 V reference) and 0 V to AV_{DD} , and can operate in 12-bit or 8-bit modes. In this case the internal $V_{REF} = 2.5 \text{ V}$ was used.

Memory organization

Memory space is divided into '*program memory space*' and '*data memory space*'. The device executes code from the internal 8-kByte Flash/EE *program memory* and accesses data in the *data memory address* space that is divided into four blocks: the lower 128 bytes of RAM, the upper 128 bytes of RAM, the 128 bytes of special function register (SFR) area, and a 640-byte Flash/EE data memory. AD and DC conversion control, interruptions enabling, serial communications control and many other tasks can be configured via the SFR's.

7.5 MICROCONVERTER '*QUICKSTART*' DEVELOPMENT SYSTEM

To write, compile, load and execute the control algorithm in the 8052 core of the ADuC814 we need a development tool.

Accutron Aspire [37] is an Integrated Development Environment (IDE) that combines project management and program debug. *Aspire* allows the generation of embedded applications for all ADuC MicroConverter derivatives and allows compilation of C code, assembly of the source files, programming the on chip FLASH, and debugging the target program. It has been specially developed for use with the Analog Devices ADuC range of MicroConverters thus providing an easy-to-use development, debug and test environment which takes full advantage of the programming potential of the MicroConverter family.

This software allows the possibility of configuring *Accutron* or Keil Software assemblers and compilers. The control routine program for this application was done in C code and compiled with the *Accutron C* compiler. The compiler is an entry level ANSI C standard which has been extended to take advantage of hardware facilities found in the ADuC MicroConverter family. All ports and special function registers may be used directly in C using their symbolic names, and additional variables may be defined with explicit addresses in specific memory regions.

The software was used together with the evaluation board QuickStart-PLUS Development System supplied by Analog Devices. The kit consisted of an emulator POD to be connected to the PC via a serial port cable and to the target system (ADuC814) on the prototyping board, as is shown in Figure 7.11.

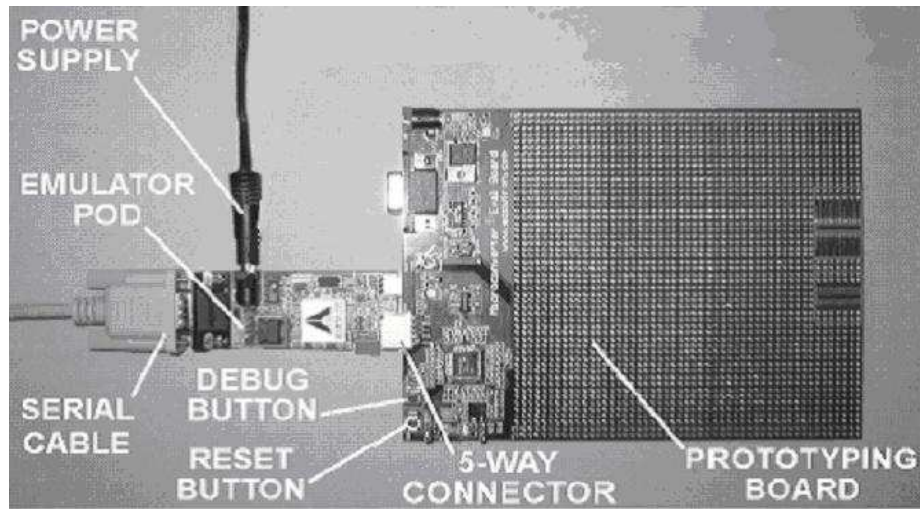


Figure 7.11: Quick Start-Plus assembly

The programming of the on-chip FLASH was done via the RS232 interface. All MicroConverter ports were brought out to holes to ease access on the prototyping board.

7.6 VOLTAGE CONTROLLED ATTENUATORS

The voltage controlled attenuators used were Hittite HMC121G8 type (Hittite Microwave Corporation) [38]. This type of attenuator needs two external control voltages or an additional op-amp plus some circuitry to provide a single voltage control.

Voltage controlled attenuators HMC121G8 features

- For use as a Voltage Variable Attenuation for DC-8 GHz applications.
- 30 dB VVA.
- Typical performance:

The attenuators were controlled with a single line (V1). The remaining control line (V2) was connected to an external op-amp control circuit to maintain impedance match while the attenuation

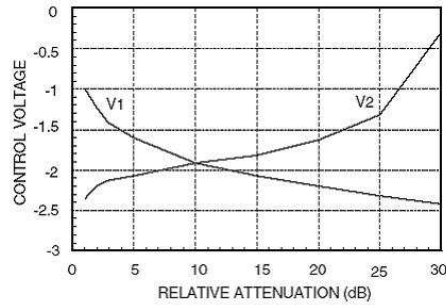


Figure 7.12: Data Sheet, Attenuation vs. Control Voltage in HMC121G8

is varied.

In Section 7.3.1 we concluded that the interval of attenuation will go from 0 to 6dB. A test in the lab with 25ns LHC beam was done to check the response of the attenuators around this value. Results are in Figure 7.13:

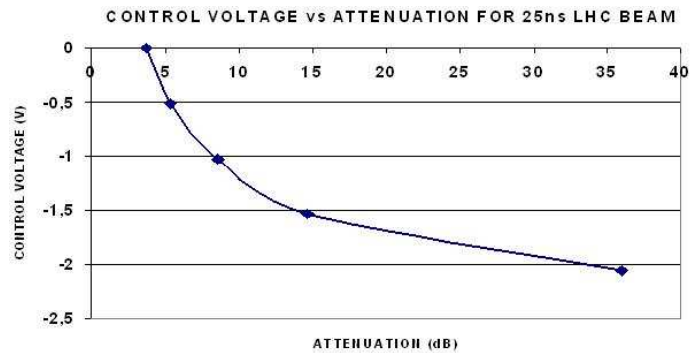


Figure 7.13: Attenuation vs. Control Voltage for LHC beam

For LHC beam there is an attenuation interval of around 34 dB over a control voltage range of 2.5 V (negative). We will work in the linear part up to 6 dB.

7.7 ATTENUATION STRATEGY

Once that all the elements in the orbit compensation system were characterized, and once the idea about how to combine and use them was clear, it was necessary to adapt the signal levels between

devices. The adaptation of signal levels was done using DC level shifting stages with different gains with following circuit:

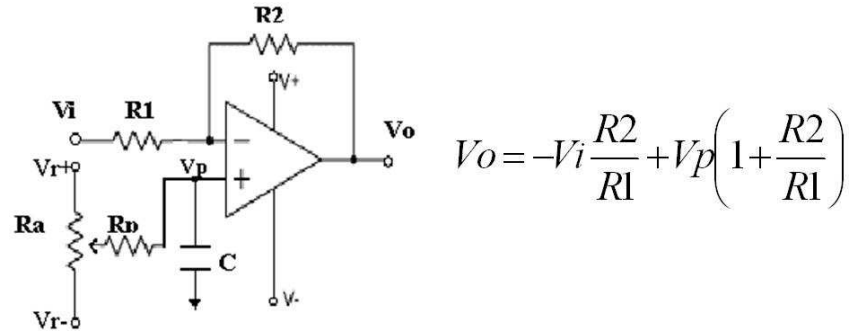


Figure 7.14: DC level shifting for inverting amplifiers

X and Y values given by the Bergoz board will range between -1.5V and +1.5V, with 0V the condition for centered beam. The ADC's in the ADuC814 microconverter accept values from 0V to +2.5V and the level matching stage compresses the 3V interval to 2.5V. This way, the 8052 MCU core processed data from 0x000 to 0xFF and the DACs (DAC0-DAC1) supplies voltages between 0V and +2.5V. Since the HMC121G8 attenuators are controlled with negative voltages going from 0V to -2.5V, only an inverter was needed as level matching stage between the DACs and attenuators.

The condition of centered beam is X and Y equal to zero. After the first level matching stage, the 0V is shifted to +1.25V meaning that in the MCU core the control algorithm will deal with a value 0x7FF for a centered beam.

The adaptation of signal levels and the center beam conditions for corrections in the X axis are indicated in this schematic diagram of Figure 7.15.

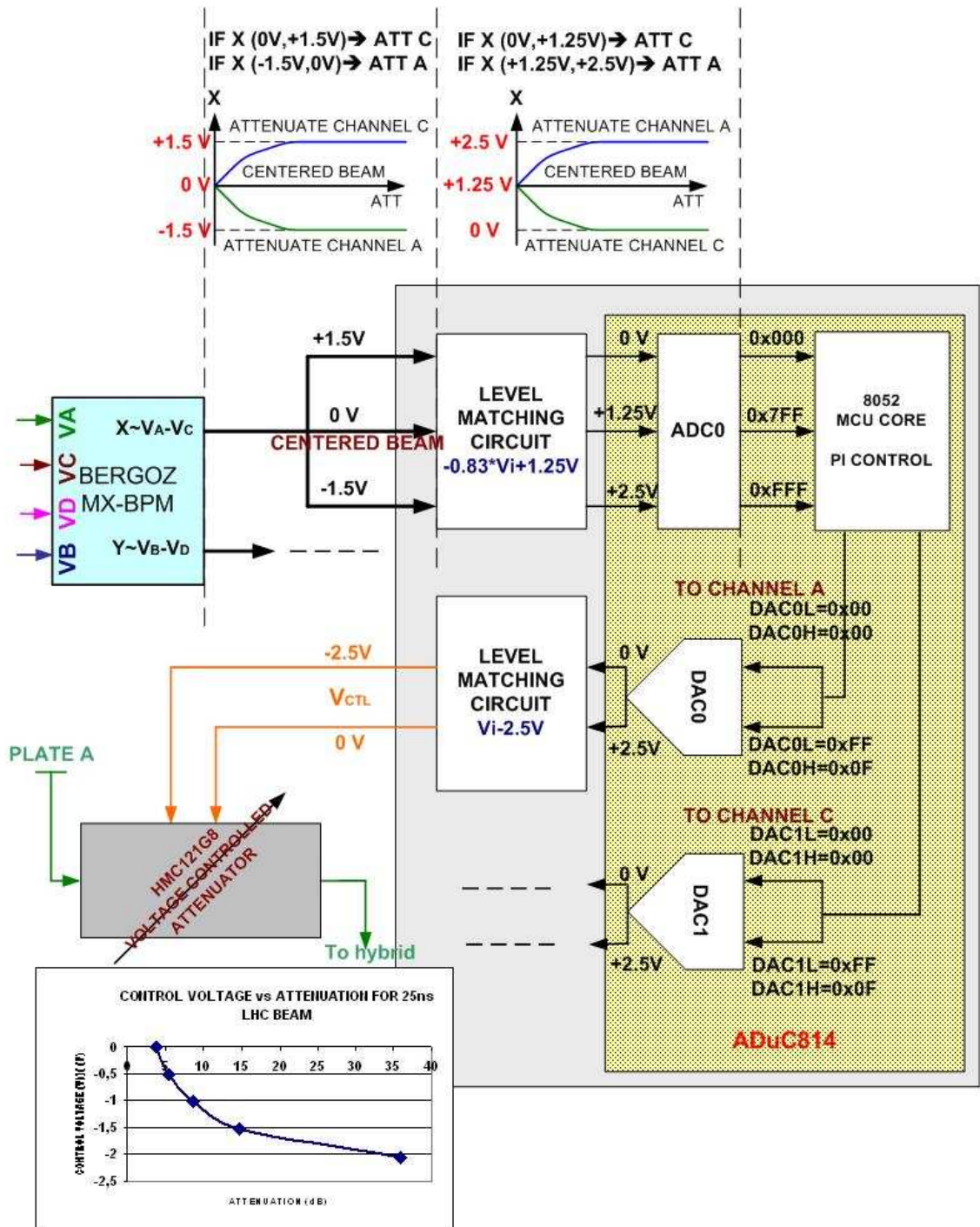


Figure 7.15: General Schematic for signal level adaptation

7.8 INTEGRATION OF THE ORBIT COMPENSATION SYSTEM PROTOTYPE FOR THE SPS IN THE FINAL SYSTEM

Figure 7.16 shows the final orbit compensation system tested in the SPS.

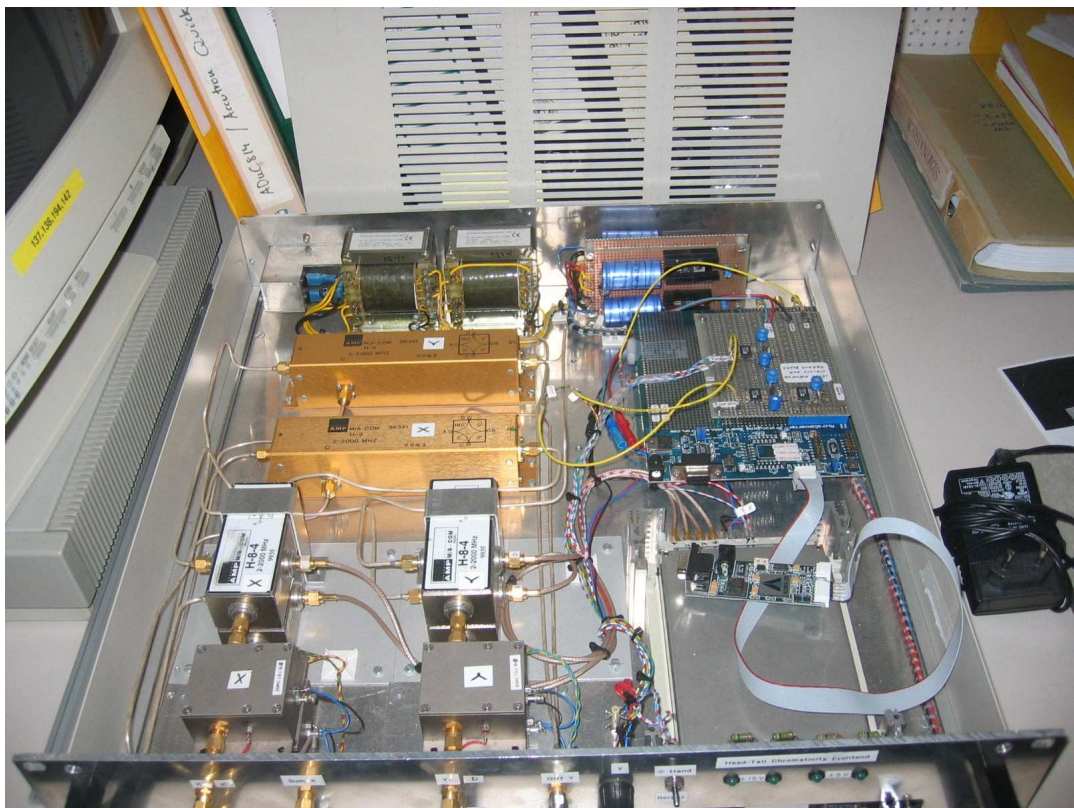


Figure 7.16: Final orbit compensation system to be tested in SPS

In the front panel there are the connectors for the four electrodes of the pick-up, a switch to select between automatic or manual control of the offset of the beam, and outputs for the sum and delta signals, that are an indicator of the intensity of the beam and the beam offset respectively (SumX, DeltaX, SumY and DeltaY).

On the left hand side there are the voltage controlled attenuators followed by splitters to duplicate

the signals that go into the Bergoz board and into a hybrid that generates the sum and delta signals of face-to-face electrodes.

On the right hand side there is the Bergoz board that supplies the X and Y position to the Microconverter QuickStart board. The mezzanine card on top of the Microconverter QuickStart board contains the electronics for the level stage adaptations.

For testing purpose, only the correction in a single plane was done. The X axis was arbitrary chosen.

7.9 CONTROL LAW FOR KEEPING THE BEAM CENTERED IN THE PICK-UP

The system to be controlled is clearly a dynamical system where *control theory* can be applied. In *control theory*, when one or more output variables of a system need to show a certain behavior over time, a controller manipulates the inputs to a system to obtain the desired effect on the output of the system. In this case, the controller is the microprocessor of the ADuC814 that has to be continuously running a control program that will supply the appropriate voltage to the attenuators for the correction of the orbit of the beam.

In addition, the system is a *feedback system* where the position of the beam is fed back to the reference value (X and Y equal to zero) and the controller takes the difference between the reference and the actual position to change the voltages of the attenuators.

Several different control strategies are available the most widely used for simple systems is the *Proportional Integral Differential* (PID) algorithm.

7.9.1 Analog PID, basic algorithm and control parameters

A feedback control loop [39] can be schematically represented in the following way:

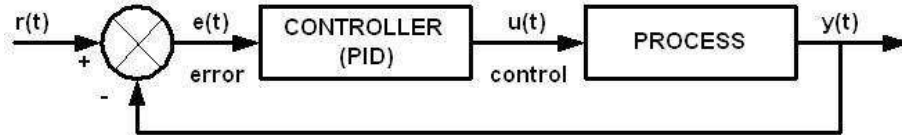


Figure 7.17: A simple feedback control loop with PID controller

where:

- $r(t)$ is the 'reference signal'
- $y(t)$ is the 'output signal'
- $e(t)=r(t)-y(t)$ is the 'error signal' and
- $u(t)$ is the 'control signal'

The controller computes the control signal to be applied to the process as a function of the difference between the reference signal and the output signal. In the case of a linear PID controller, it works following the control algorithm:

$$u(t) = K_p \cdot \left[e(t) + \frac{1}{T_I} \int e(t)dt + T_D \frac{de(t)}{dt} \right] \quad (7.9.1)$$

Applying Laplace Transforms one gets:

$$U(s) = K_p \cdot \left[1 + \frac{1}{T_I s} + T_D s \right] \cdot E(s) = \left[K_p + \frac{K_I}{s} + K_D s \right] \cdot E(s) \quad (7.9.2)$$

This algorithm is considered as the standard PID by the ISA (Instrument Society of America) and defines following basic terms:

- *Proportional control action:* $u_p = e(t)$

Is the action produced by a control signal that is proportional to the deviation of the process output with respect to the reference signal.

- *Integral control action:* $u_i = \int e(t)dt$

Is the action produced by a control signal that is proportional to the time the output of the process has been different from the reference signal.

- *Derivative control action:* $u_d = de(t)dt$

Action produced by a control signal that is proportional to the rate of change of the process with respect to the reference signal.

- *Gains:* Proportional (K_p), Integral ($K_I=K_p/T_I$), Derivative ($K_D=K_p \times T_D$)

A proportional controller will have the effect of reducing the rise time and will reduce, but never eliminate, the steady-state error (difference between input and output of a system when the response has reached the steady state). An integral control will have the effect of eliminating the steady-state error, but it may make the transient response worse. A derivative control will have the effect of increasing the stability of the system, reducing the overshoot and improving the transient response. It is possible to have different control algorithms by the combination of the P, I and D terms, depending on the kind of control we want for the system.

Term	Effect on Control System
Proportional	Typically the main drive in a control loop, K_p reduces a large part of the overall error.
Integral	Reduces the final error in a system. Summing even a small error over time produces a drive signal large enough to move the system towards a smaller error.
Derivative	Counteracts the K_p and K_I terms when the output changes quickly. This helps to reduce the overshoot and ringing. It has no effect on final error.

Figure 7.18: PID terms and their effect on a control system.

Since the PID algorithm is to be implemented digitally, we need to do the conversion of this analog system and the PID equations into the digital world.

7.9.2 Mathematical modeling of digital control systems

The configuration of a digital control system can take many forms, but in this case the configuration is one where the reference signal is a digital signal $r(kT)$ being supplied externally or retrieved from

computer memory, and the sampling is done in the output signal $y(t)$.

Schematically:

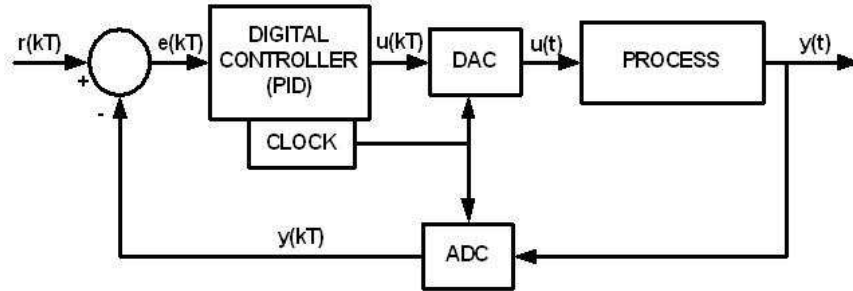


Figure 7.19: Digital control system with output sampling

The complete feedback control system can then be shown as:

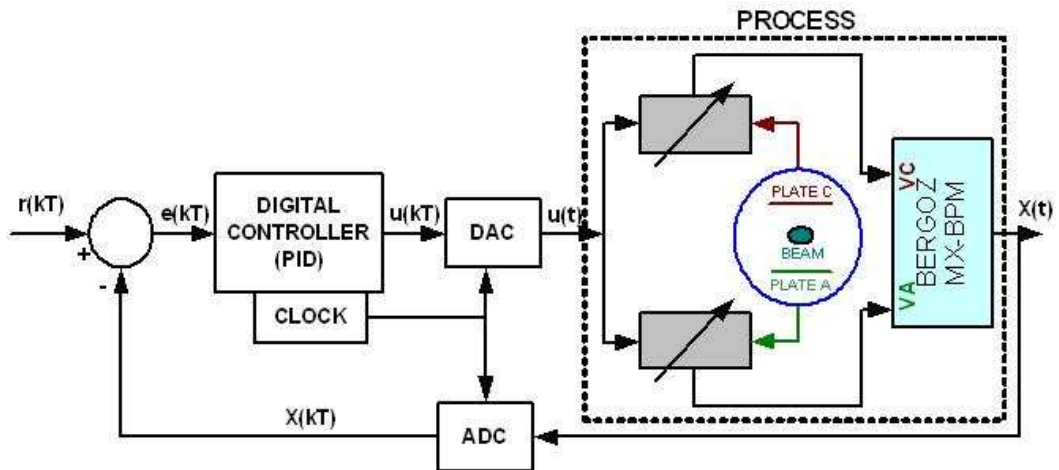


Figure 7.20: Digital control system for attenuation control

where:

- T is the ADC sampling period
- $r(kT)$ is the condition for centered beam, $r(kT) = 0x7FF$
- $X(t)$ is the analog output of Bergoz board for X position

- $X(kT)$ is the digital X position once it has been digitized in the ADC
- $e(kT)$ is the error signal, $e(kT) = r(kT) - X(kT)$
- $u(kT)$ is the digital control signal calculated in the ADuC814
- $u(t)$ is the control voltage once it has been converted into analog in the DAC

The *digital control law* can be extracted from the analog control law using approximations for the different terms:

Proportional term:

$$K_p \cdot e(t) \rightarrow K_p \cdot e(kT) \quad (7.9.3)$$

Derivative term:

$$K_p T_D \frac{de(t)}{dt} = K_D \frac{de(t)}{dt} \rightarrow K_D \frac{e(kT) - e[(k-1)T]}{T} \quad (7.9.4)$$

Integral term:

$$K_I \frac{K_p}{T_I} \int_0^{kT} e(t) dt \rightarrow \frac{K_I T}{2} \sum_{j=1}^k \{e[(j-1)T] + e(jT)\} \quad (7.9.5)$$

The substitution of previous terms in the analog control gives the digital control law:

$$u(k) - u(k-1) = a_0 e(k) + a_1 e(k-1) + a_2 e(k-2) \quad (7.9.6)$$

$$a_0 = K_p + K_I \frac{T}{2} + \frac{K_D}{T} \quad (7.9.7)$$

$$a_1 = -K_p + K_I \frac{T}{2} + -2 \cdot \frac{K_D}{T} \quad (7.9.8)$$

$$a_2 = \frac{K_D}{T} \quad (7.9.9)$$

Different kind of digital controllers can be implemented depending on the terms included in the control law:

- P control
- PD control
- PI control
- PID control

7.9.3 Control algorithm details

Basically, the code running in the 8052 core compares digitized X input value, with the set condition of centered beam (0x7FF) and computes the corrections to apply to both attenuators.

Initially, the attenuators start with a value of 3dB (DAC1=DAC0=0x586) in such a way that there is the same deviation of beam as if the initial attenuation was set to 0 dB. This 0x586 value in the DACs avoids forbidden values to be loaded in the DAC after control algorithm in case the subtraction of value higher than 0x586 is needed for compensation. In other words, the 3dB acts as a safety margin.

A first AD conversion of X value coming out from Bergoz board is needed. If value is higher than 0x7FF this means that the beam is closer to electrode C than to electrode A, hence, channel A needs to be attenuated and DAC0 (the DAC associated to the control of attenuator in channel A) increases its value according to algorithm till reaching desired X value. If digital X is smaller than 0x7FF, channel C needs to be attenuated and DAC1 increases according to algorithm till reaching desired X value.

For code see Appendix A.

Chapter 8

Results with the Orbit Compensation System in the SPS

The *orbit compensation system* was installed in point 4 of the SPS where there was access to the four cables coming out from each of the electrodes of the stripline coupler. The objective of the measurements was to test the head-tail orbit correction system described in the previous chapter under real LHC beam conditions and to compare the results with the ones obtained in the lab with simulated LHC beam.

This chapter describes the tests performed with the system and the final results obtained.

8.1 LHC BEAM TYPE RUNNING IN SPS

Since the chromaticity measurement system described so far is intended to be used in future LHC, all measurements were performed with LHC beam type running in the SPS having following characteristics:

- SPS revolution frequency from 43.35 kHz at injection 26 GeV (RF=200.265MHz), to 43.38 kHz at 450GeV (RF=200.394MHz).
- Beam pattern: 1 batch of 72 bunches spaced by 25 ns (1 bunch → 4 empty buckets → 1 bunch ...)

All the measurements were performed in a 'parasitic' way, that is, no dedicated machine time or specific settings were used for the tests.

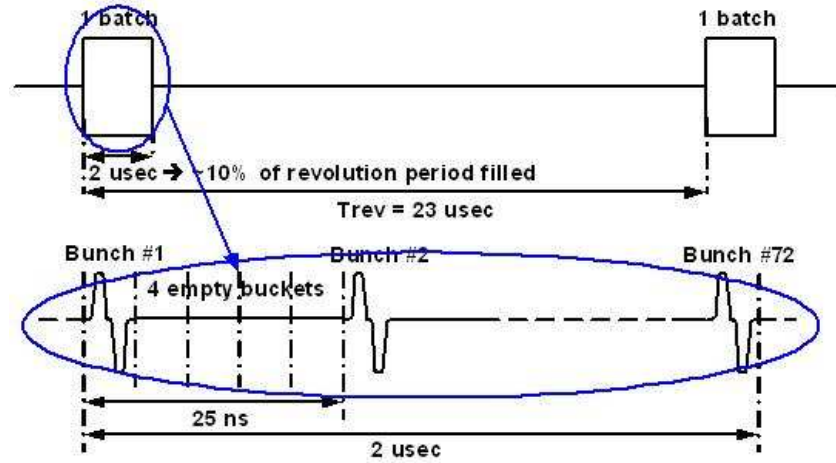


Figure 8.1: 25ns LHC beam in SPS

8.2 EXPERIMENTAL SETTING

In order to be able to calculate the improvement in the correction of the deviation of the beam from the electrical center of the pick-up that was obtained with the new system, an additional stage with two power splitters and a hybrid was inserted right before the 'orbit compensation box' with the purpose of using the extra Σ and Δ obtained this way as reference signals from which it was possible to calculate the degree of improvement.

A schematic diagram of the experimental setting for the X path is shown in Figure 8.2. For a given axis, the difference of the signals of the corresponding electrodes (A and C in the case of X axis) is an indicator of the deviation of the beam from the center of the coupler. For centered beam the expected value for the difference is zero whilst sum signal should be constant for a given kind of beam independently of the degree of deviation, since it is only an indicator of the beam intensity.

8.3 CALIBRATION

From Figure 8.2 it is possible to see that the signals A and C coming out from the electrodes, follow different paths until we finally get Δ/Σ and Δ'/Σ . In order to compare them and to obtain the degree of correction, a calibration of the system is needed, taking into account the

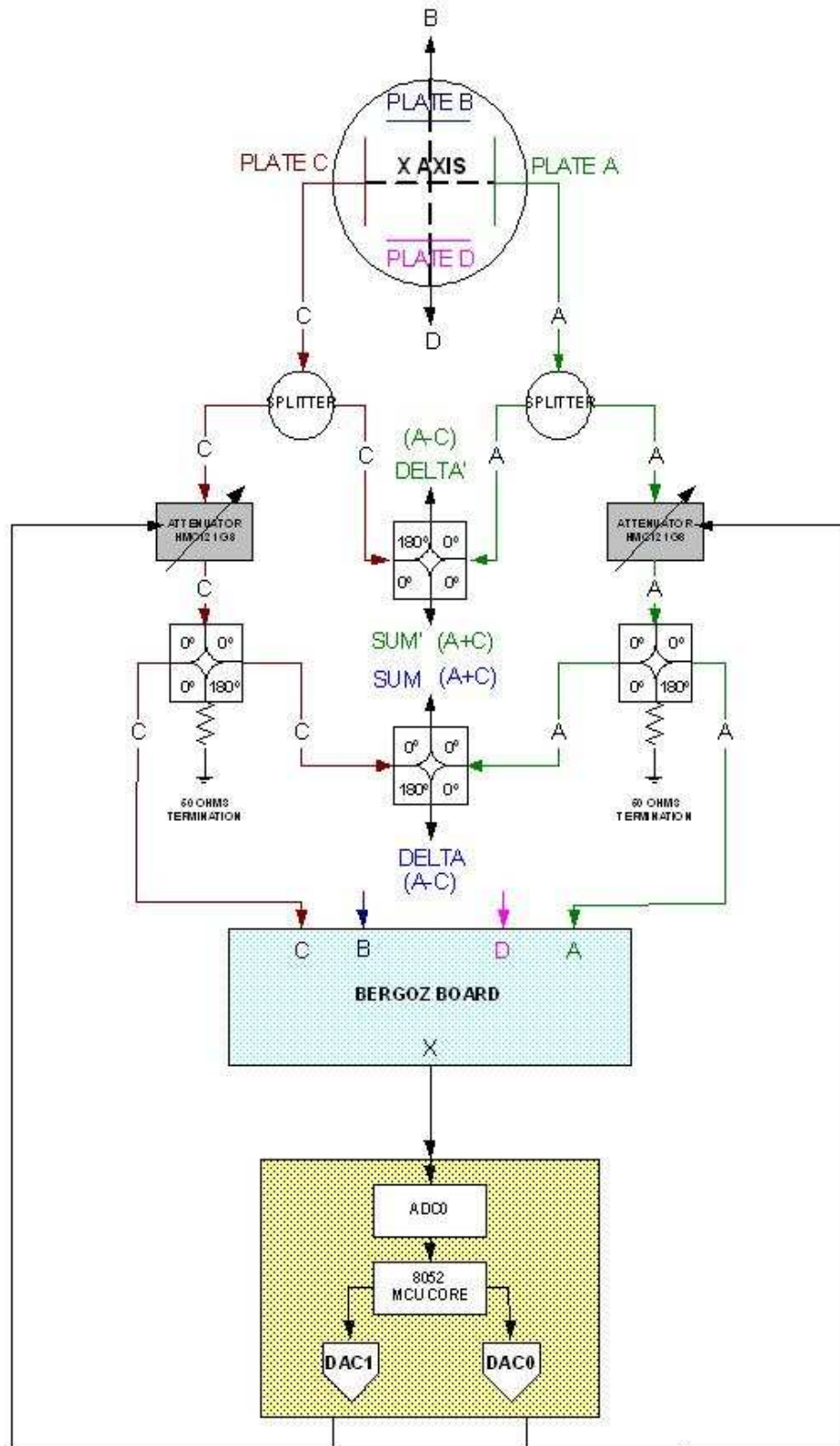


Figure 8.2: Schematic diagram of the experimental setting for the X path

attenuation and the time delays induced by all the devices that the signals pass through.

8.3.1 Signals after a RESET in the Quick Start-Plus card

Following a RESET in the Quick Start-Plus card, DAC0 register in the ADuC814 is set to 0xFF and DAC1 to 0x00, this means that the signal in channel A is being totally attenuated and signal in channel C is not attenuated at all, as a consequence, DELTA and SUM should be exactly equal and with no time delay as Figure 8.3 indicates.

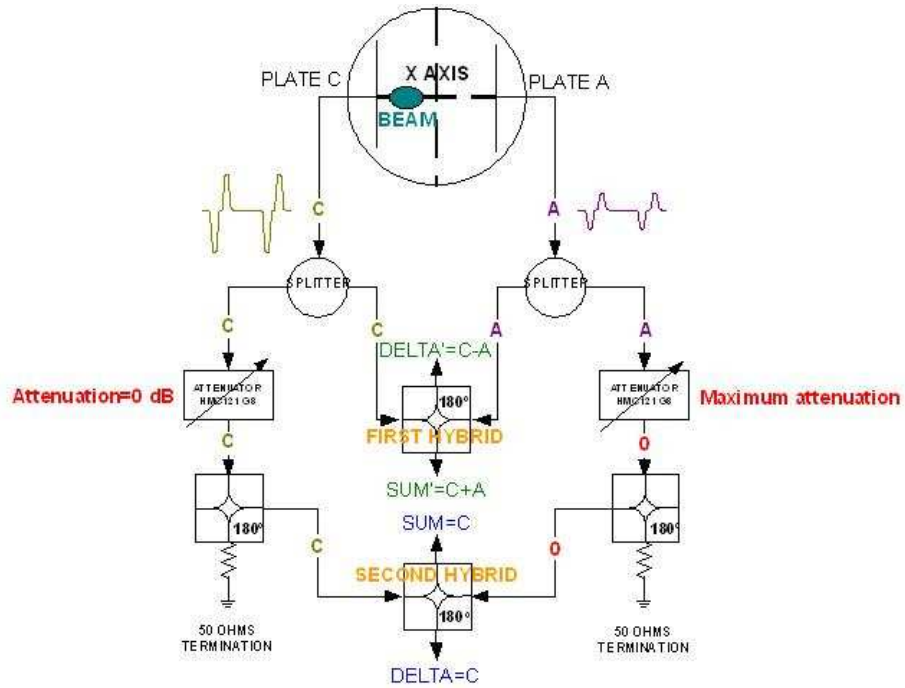


Figure 8.3: Expected Sum and Delta signals after a RESET

To see if this assumption corresponds to real life, some data was taken on 25/10/2004 with 25ns LHC beam and $N_{bunch} = 1.3 \cdot 10^{11}$ p (4 batches). The results are presented in Figure 8.4. The SUM and DELTA are plotted together; the upper plot shows an almost complete overlap of both signals, in amplitude and time. In the lower plot a slight time correction of 0.25 ns was performed by subtraction of the maximum values of the first positive peaks in the signals.

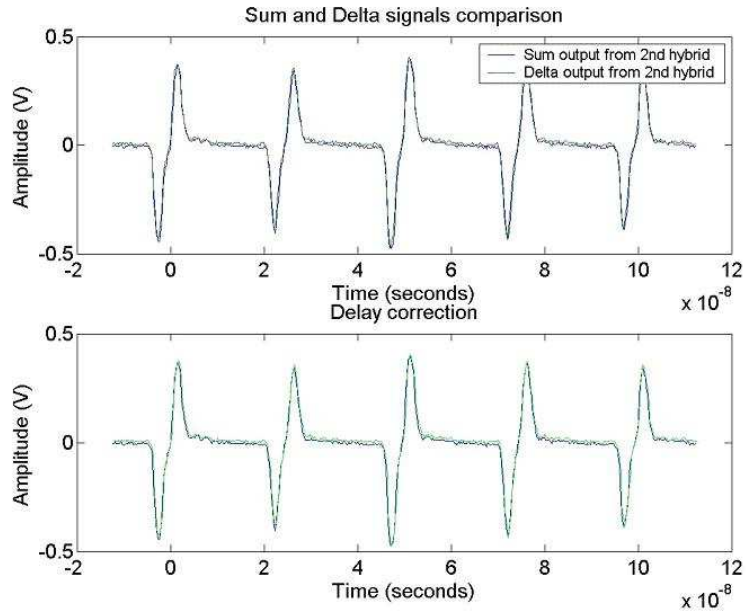


Figure 8.4: SUM and DELTA signals after reset with time delay correction

8.3.2 Method used to calculate the degree of correction

The calculation of the degree of improvement obtained with the orbit correction system will rely on the information extracted from the comparison of the Sum signals: SUM and SUM'. This comparison will let us know the Delta signal we would expect to obtain in the second hybrid if no control was applied and that way it will be possible to compare it with the real Delta signal we measure in the second hybrid with the correction algorithm running. More precisely, the analysis of SUM and SUM' will give us the time delay and the attenuation of signals in the second hybrid with respect to the ones in the first hybrid. Once the attenuation is known, it will be applied to the DELTA' so that we will have the Delta expected to appear in the second hybrid if no correction for orbit displacement was applied. This can then be compared with the real DELTA signal measured in the second hybrid once corrected for the time delay.

As an example of how this method works, the following experiment was performed: we set the DACs that supply the control voltage for the attenuators to a value of DAC0/1=0x586 so that the attenuation is 3dB. Hence, there was no correction applied to the beam and, from the difference

between SUM' and SUM , the value of the attenuation and time delay that the signals experience all along the path until reaching the second hybrid could be extracted. The measurement results are shown in Figure 8.5.

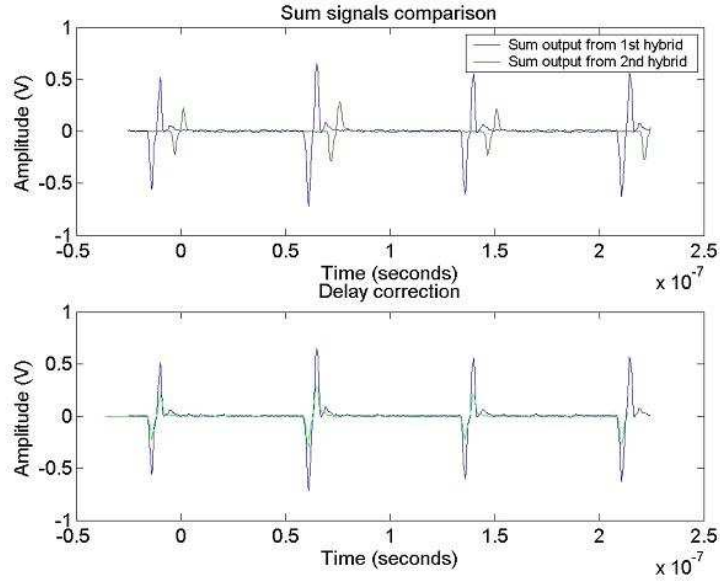


Figure 8.5: Sum signals coming out from hybrids with 3 dB in attenuators

Upper plot shows the measured SUM' and SUM signals, they have different amplitude associated to the attenuation induced by the devices and they are delayed in time. Lower plot shows the overlap of both signals once the delay time correction has been done. The time delay is of 11 ns and the total attenuation is of 7.2 dB.

This leads to the following relation that gives the expected signal in the second hybrid if no orbit correction is applied:

$$\frac{SUM}{SUM'} = \frac{(C + A)/10^{7.2/20}}{C + A} = \frac{1}{10^{7.2/20}} \Rightarrow SUM = \frac{SUM'}{10^{7.2/20}} \quad (8.3.1)$$

The same relation can be applied to $DELTA$ and $DELTA'$:

$$DELTA = \frac{DELTA'}{10^{Attenuation/20}} \quad (8.3.2)$$

where $DELTA'$ is the measured signal in the first hybrid and $Attenuation$ is the total attenuation calculated with the help of the Sum signals.

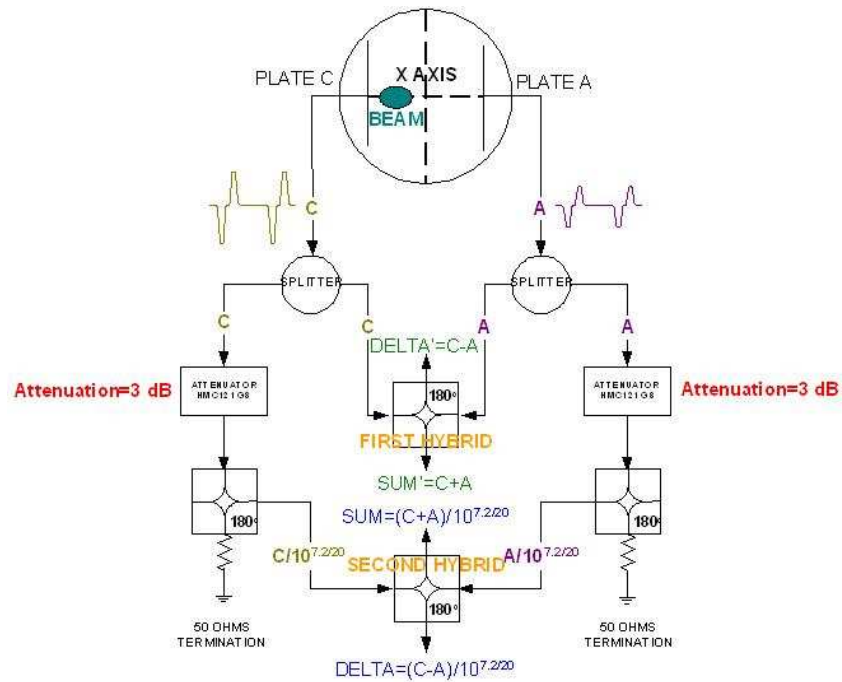


Figure 8.6: Expected Sum and Delta signals after 3 dB attenuation

To check if previous formula works, we consider again Sum signals in Figure 8.5 and apply the formula with the 7.2 dB to the SUM coming out from 1st hybrid. We would expect to obtain the SUM signal in the output of second hybrid and the results are plotted in Figure 8.7. Both signals overlap, so the conclusion is that it is possible to use this technique to measure the reduction in Delta signal once the control for correction is applied.

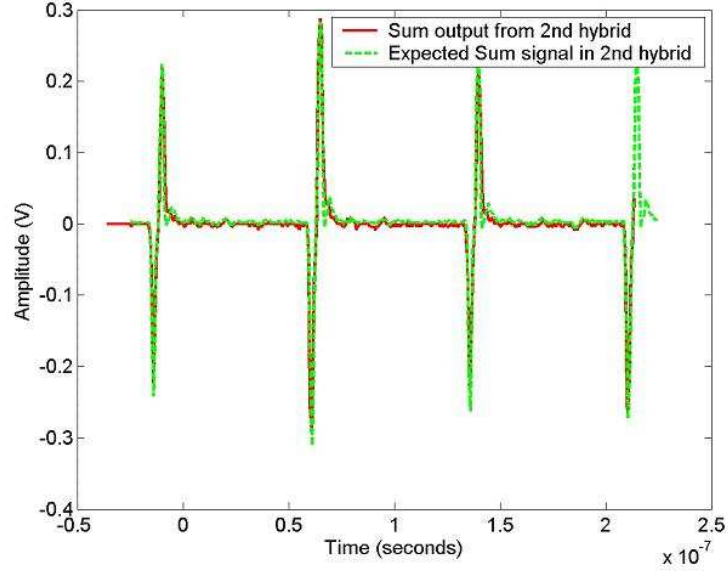


Figure 8.7: 7.2 dB applied to SUM' to get SUM

8.4 EXPERIMENTAL RESULTS

Two programs with different control algorithms running in the ADuC814 were used for tests: one with a P control algorithm and another one with PI control algorithm, with the purpose of comparing the results obtained with both.

8.4.1 P control algorithm

The algorithm obtains the value of the control voltage for attenuation to be loaded in DAC0 or DAC1 as a function of the previous calculated value and the current deviation of the beam from the center of the pick-up.

$$u(k) = u(k-1) + \left[\frac{K_p T}{2} \right] e(k) = u(k-1) + A e(k) \quad (8.4.1)$$

where:

- $u(k)$ is the value to load in DAC0 or DAC1.
- $u(k-1)$ is the previous calculated value.
- $e(k)$ is the difference between the current position of beam and the previous one.

- A is the gain that was determined by trial and error.

Once the program is running, it tries to minimize the deviation from the value that was set in the code as a condition for centered beam (0x7FF) by acting on the attenuators with the values set in the DAC's. In Figure 8.8, we clearly see the way the DAC's respond to the presence of beam by reaching a value that minimizes the Delta signal.

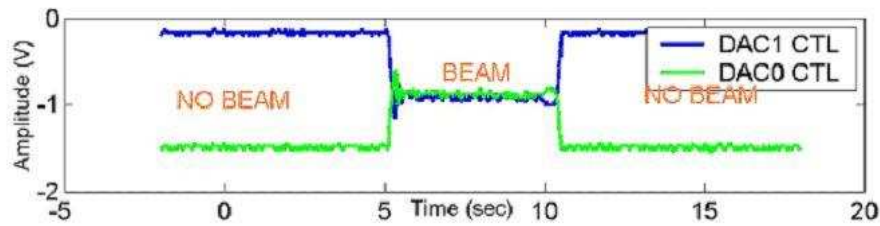


Figure 8.8: Behaviour of the control signals for the attenuators

We let the program run and registered the Sum signals in Figure 8.9 (a).

From them, and applying the procedure described in previous section, we got a correction factor of 6.1 dB and 11.5 ns. By insertion of the 6.1 dB in the formula 8.3.2, the degree of improvement in the correction of the Delta signals can be seen in Figure 8.9 (b). In this Figure, the signal in red is the measured Delta signal in the output of second hybrid and the blue one is the Delta signal one would expect to obtain in the second hybrid if no control algorithm was applied. There is a clear improvement in the reduction of the amplitude of the Delta signal, more precisely and in this case, it was reduced in a 61%.

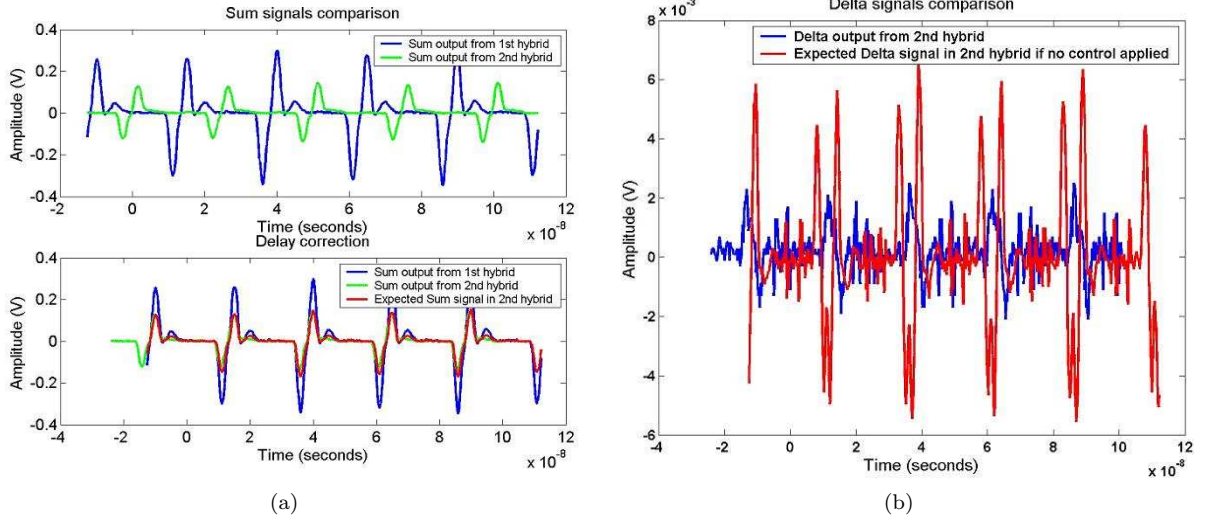


Figure 8.9: (a) P control: calculation of the correction factor from Σ signals (b) Degree of amplitude reduction in Δ signal

8.4.2 PI control algorithm

This algorithm obtains the value of the control voltage for attenuation to be loaded in DAC0 or DAC1 as a function of the previous calculated value, the current deviation of the beam from the center of the pick-up and the previous deviation:

$$u(k) = u(k-1) + \left[\frac{K_p T}{2} \right] e(k) + \left[\frac{K_I T}{2} \right] e(k-1) = u(k-1) + A e(k) + B e(k-1) \quad (8.4.2)$$

where:

- $u(k)$ is the value to load in DAC0 or DAC1.
- $u(k-1)$ is the previous calculated value.
- $e(k)$ is the difference between the current position of beam and the previous one.
- $e(k-1)$ is previous calculated value of the error.
- A is the proportional gain.
- B is the integral gain.

The gains A and B were determined by trial and error ($A=0.9$, $B=0.2$).

Here, again, we let the program run and registered the Sum signals. By measuring SUM and SUM' the correction factor is of 6.1 dB and 11.5 ns.

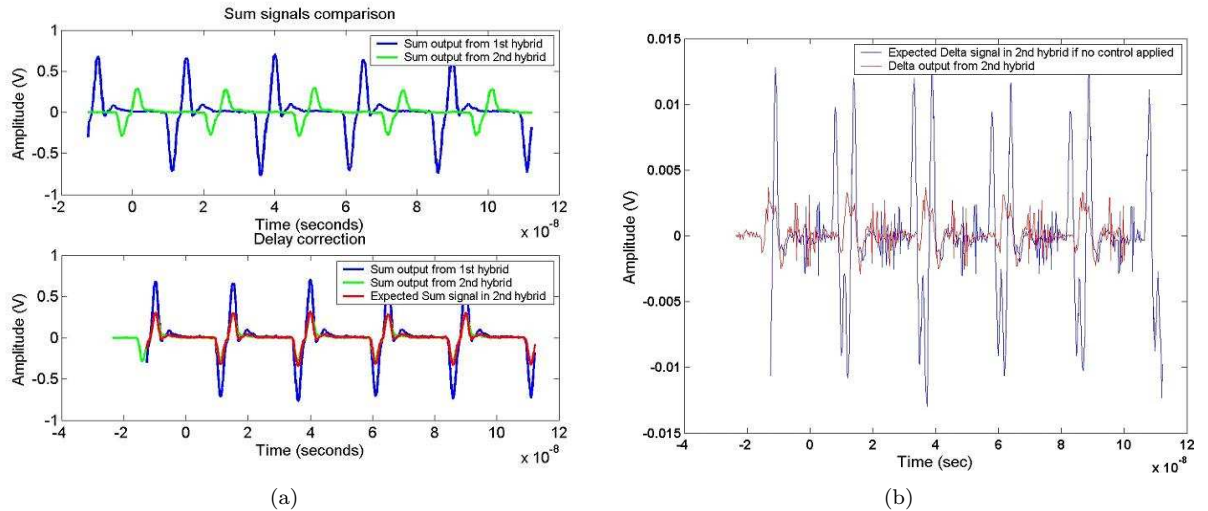


Figure 8.10: (a)PI control: calculation of the correction factor from Σ signals (b)Degree of amplitude reduction in Δ signal

This time, the attenuation is 7.5 dB and the time delay 11 ns and by insertion of the 7.5 dB in the formula 8.3.2, the degree of improvement in the correction of the Delta signals can be seen in Figure 8.10.

There is a clear improvement in the reduction of the amplitude of the Delta signal; in this case, it was reduced in a 72%.

8.4.3 Comparison of P and PI control algorithm responses

This comparison consists in observing the way the voltage controlled attenuators respond to a displacement of the beam from the center of the pickup when one of the two control algorithms is being used. Since the attenuators are controlled by the DAC's we will analyze their response and we will pay attention to the time they spend in reaching the condition of centered beam and the time they spend in settling to that value.

To illustrate this comparison, we took the response the DAC0 shows with P and PI control and overlapped them. The result is shown in Figure 8.11.

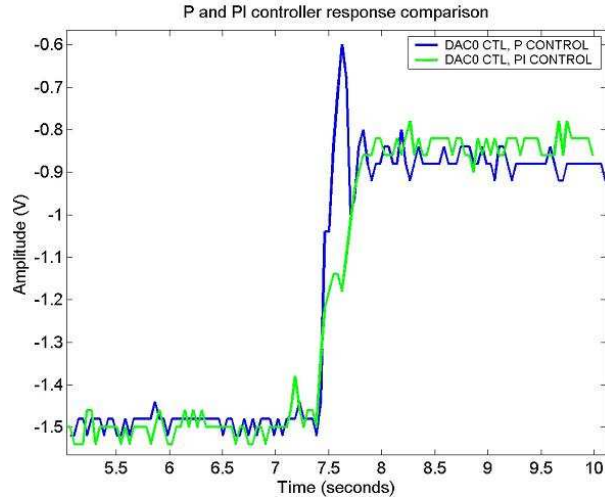


Figure 8.11: Comparison between P and PI control algorithms

With the proportional control (blue line), the response to the presence of beam is fast but there is an initial overshoot and the DAC starts oscillating around the final value before settling to it. In the case of the PI control, the DAC does not respond as fast as the P control but once it reaches the desired output, it stays on it. Globally, the time the DAC reacts to the beam could be considered the same for both algorithms, around 0.6 seconds, if a whole SPS cycle lasts 12 seconds (SC 950) that means a 5% of then time is spent in electronically centering the beam in the case a full correction is needed but usually only small changes have to be corrected.

Since the time to reach the condition of centered beam seems to be the same with both algorithms and since the PI controller has the advantage of eliminating the steady state error, the best option would be to implement the control with a PI controller.

8.5 COMPARISON WITH RESULTS OBTAINED WITHOUT THE ORBIT CORRECTION SYSTEM

Following we show a screen shot of a typical acquisition using the SPS head-tail monitor.

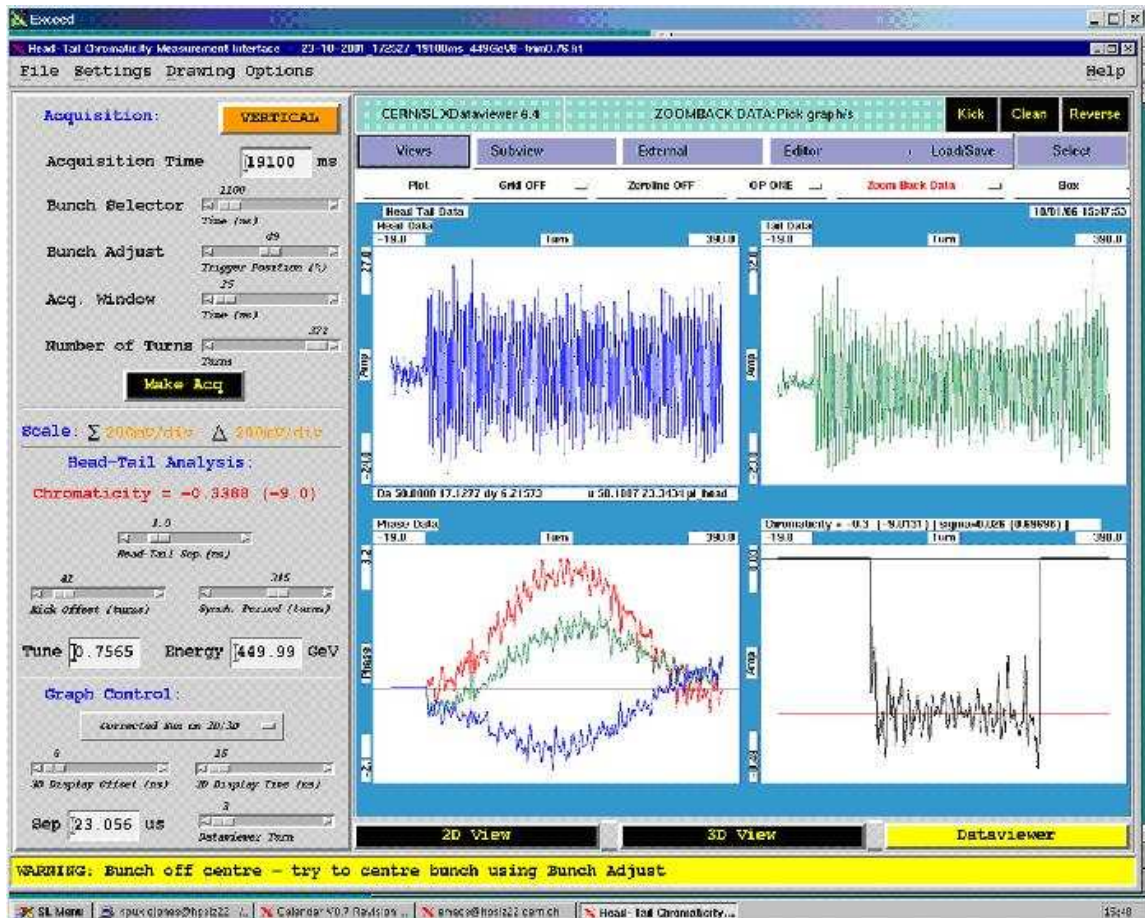


Figure 8.12: SPS head-tail monitor acquisition system

Top plots show in blue the head position data and in green the tail position data taken at 0.5ns either side of the centre of the bunch.

Bottom left shows phase plots for the head and tail together with the phase difference (in red).

Bottom right plot shows chromaticity calculated turn by turn (i.e. using the phase difference calculated in left plot and plugging it into the formula). Useful data is at 1/2 the synchrotron

frequency where dephasing has its maximum. The value of chromaticity is calculated as the average of 20 samples either side of the maximum dephasing point (line in red).

Figure 8.13 shows raw scope data for Σ and Δ signals before and after applying a kick. The difference signal before kicking comes entirely from the closed orbit offset. The difference signal after kicking is the closed orbit offset with the kick added to it. The kick applied is roughly equal to the closed orbit offset, in this case it was 1mm so here we have an offset of 1mm.

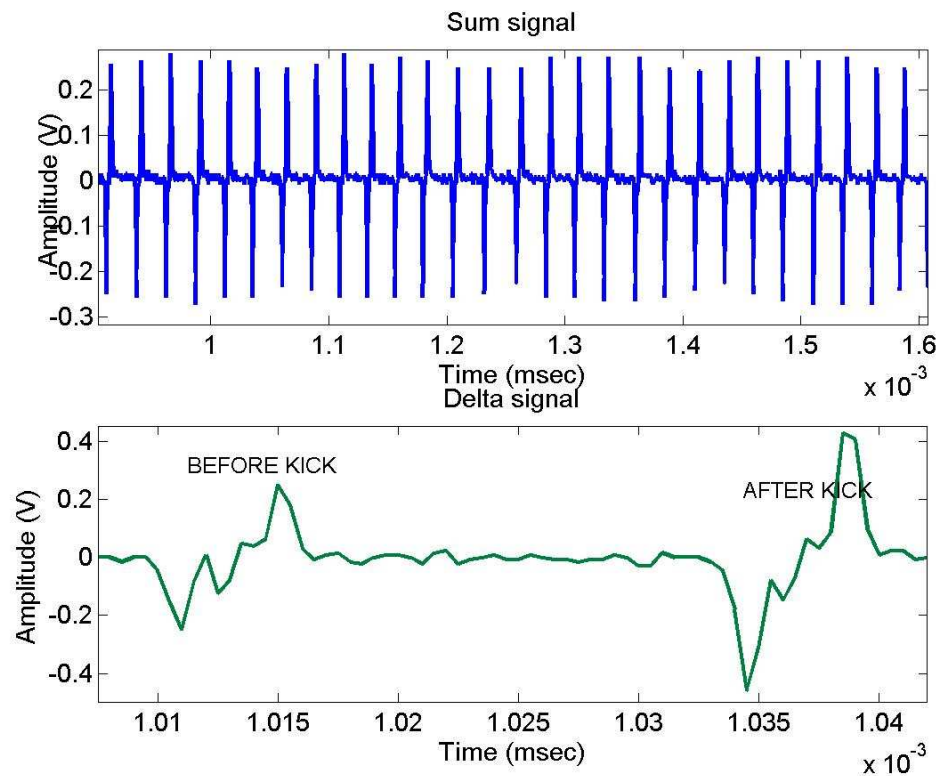


Figure 8.13: Raw scope data for Σ and Δ signals in head-tail monitor

Basically the kick has to, at least, equal the closed orbit offset in order to get good chromaticity measurements. If we can reduce the offset by a factor 3.6 ($\sim 11dB$) using our technique (72% reduction with PI control) then the kick strength can also be a factor 3.6 lower and so we gain a factor of $(3.6)^2$ ($\sim 22dB$) in emittance blow-up.

Chapter 9

Summary and Conclusions

The construction of the unique LHC machine, requires the development of new beam instrumentation that has to be able to cope with the tight requirements for operation of the accelerator in the sense that it has to cause very little beam disturbance but be very sensitive at the same time. A set of new ideas have been developed as methods for determining the parameters of major importance such as tune and chromaticity. This includes the head-tail phase shift monitor for chromaticity measurement and the travelling wave Schottky monitor working at very high frequencies as a general diagnostic tool. It is here where this work sits, with the contribution to the improvement of the sensitivity of the Head-Tail monitor and a study of the use of a traveling wave Schottky monitor in LHC.

Following experiences with Schottky monitors already in use in other accelerators and thanks to a collaboration with FNAL, a travelling wave Schottky pick-up that is similar to the ones already installed in the Recycler and Tevatron rings of Fermilab, was tested in the CERN-SPS with the purpose of studying its possible application as a non-destructive beam diagnostic tool for the LHC. The analysis of the data acquired with LHC beam running in the SPS showed the agreement of the obtained frequency spectra in both transverse and longitudinal planes with what is predicted by Schottky Theory. At the same time, the electronic response of the pick-up was shown to correspond to what was expected according to calculations, and the values obtained for the tune, chromaticity and momentum deviation agreed with the values measured using standard traditional techniques in the SPS when the tests were performed. It can be concluded that a complete transverse diagnostic of the beam in the SPS could be done with this 1.8GHz provided that care was taken to eliminate all the spurious signals that can corrupt the transverse frequency spectrum:

- The strong common-mode lines, that are a consequence of the displacement of the beam from the center of the pick-up and that may hide the incoherent betatron tune sidebands.
- High enough frequency to be above the coherent betatron signal which can modify the appearance of the incoherent lines.
- The noisy frequency lines that originate from elements in the chain of the data acquisition setup.

It has been shown where many of the spurious lines come from and a careful design noting this can effectively eliminate most of these lines . A signal has also been seen for a single LHC pilot bunch, giving rise to the hope that signals due to such low intensity bunches can be monitored in the LHC..

The need of increasing the sensitivity of the Head-Tail monitor under test in the SPS, led to the construction of a prototype system for electronic closed orbit signal suppression. This was aimed at eliminating the transverse signal resulting from a deviation of the beam from the electrical center of the pick-up. The system adopted a feedback loop that has as input the position of the beam and as output the control voltages for attenuators connected to the electrodes of the pick-up and that electronically center the beam. The results obtained for two different control algorithms supplying the control voltages, showed that it was possible to eliminate the undesired transverse signal to a large extent with this method. This led to an overall improvement of the sensitivity by over 11 dB in most cases allowing a similar reduction in excitation level and hence lowering emittance blow-up by 22 dB (i.e. *reduction*²)

Globally the conclusion of this Thesis is that the design of a traveling wave Schottky monitor should be pursued since the SPS results are very promising. In the case of the Head-Tail monitor it has been shown that it is feasible to build an orbit correction system based on a microcontroller acting on variable attenuators. The main limitation is the input level which current attenuators can cope with. In the LHC, with input voltage of several tens of volts, other approaches may need to be investigated to improve the overall sensitivity of the measurement.

Chapter 10

Resumo

DIAGNOSE TRANSVERSAL PARA COLISIONADORES DE HADRÓNS A ALTAS ENERXÍAS

10.1 Introducción

O Gran Colisionador de Hadróns (LHC) é un gran sincrotrón que explorará a Física de partículas a enerxías xamáis alcanzadas co obxectivo de atopar a partícula coñecida como '*o bosón de Higgs*' e coa que se pretende dar explicación ás dúbidas que prantexa o Modelo Estándar. O LHC está sendo construído no CERN (Xenebra, Suiza) e no 2007 estará listo para producir colisións de protóns cunha enerxía de 14 TeV. O emprego de imáns superconductores necesarios para alcanzar altas enerxías, a gran luminosidade requerida para a Física, a limitada apertura dinámica e a gran enerxía almacenada nos feixes de protóns, farán que o control desta inmensa máquina sexa todo un reto, especialmente durante as etapas de inxección de protóns e de aumento de enerxía. Dous problemas particulares deste acelerador serán a alta sensibilidade a perdas do feixe de partículas e unha pobre calidade do campo magnético o que requerirá o uso de elementos de corrección.

A inxección e aceleración dos feixes de protóns no LHC sen perda de partículas e o crecemento do parámetro denominado *emitancia* requerirá dun control preciso dos parámetros que caracterizan ó feixe. O valor do chamado *betatron tune*, é dicir, do número de oscilacións transversais da órbita que realizan as partículas por periodo de revolución, será dunhas 63 unidades e necesitará ser controlado

cunha precisión de 0.003. As *excursións da órbita nominal* deberán de estar limitadas a menos de 0.5 mm. A *cromaticidade* deberá restrinxirse a algunhas unidades...

O control deste acelerador conlevará unha alta dificultade xa que será preciso empregar instrumentos de control e de diagnose que garanticen a estabilidade do feixe de partículas e que eviten ao máximo fenómenos de perturbación que son precisos ás veces para realizar a medida dos parámetros característicos deste tipo de máquinas.

10.2 Obxectivos

A Tese proposta analiza dous prototipos de instrumentos de diagnose creados para a medida dos principais parámetros que caracterizan a un feixe de partículas cando éstas están sendo aceleradas nunha máquina circular, e para os cales o principio de funcionamento debería de ser compatible cos estrictos requerimentos de sensibilidade impostos ao LHC pola súa alta intensidade.

O traballo atópase dividido en dúas partes:

1. As probas levadas a cabo a unha ferramenta de diagnose coñecida como '*monitor Schottky*' e de posible aplicación no LHC
2. e a mellora da sensibilidade da capacidade de medida dun '*monitor Head-Tail*'.

Detrás de ámbolos dous temas existe un obxectivo común e que é a necesidade de dispor de novos métodos de medida e de diagnose dun feixe partículas con carga aceleradas, que sexan de grande precisión e non destructivos, condicións fundamentais para manter as limitadas tolerancias impostas ó acelerador superconductor que é o LHC.

10.3 Contido

O Capítulo 1 explica primeiro que é o CERN e cales son as características e obxectivos do acelerador LHC. A continuación dase unha breve descripción dos sincrotróns e fálase das tendencias futuras destes aceleradores co obxectivo de introducir o contexto no que se desenrolou o traballo desta Tesis. Remátase cunha introducción aos obxectivos do traballo.

O Capítulo 2 argumenta a importancia do *betatron tune* e da *cromaticidade* na diagnose dos parámetros que caracterizan un feixe de partículas nos aceleradores. Explícase o concepto de ámbolos dous parámetros dando unha breve introducción matemática que se extenderá posteriormente nos capítulos adicados a cada un deles. Ademáis, preséntanse as técnicas actuais que se están usando para a medida do *betatrón tune* e da *cromaticidade*. Entre elas están os métodos sobre los que se basa este traballo: o chamado '*ruido Schottky*' e que se usa como ferramenta de medida non destructiva e o desfase creado entre a '*cabeza*' e a '*cola*' dun feixe de partículas tras aplicarlle unha perturbación transversal.

No Capítulo 3 faise un completo desenrolo matemático da *Teoría Schottky* aplicada a un feixe de partículas nun acelerador circular asumindo que este feixe está composto por partículas individuais, cada unha movéndose de forma incoherente en relación ás demais. O resultado deste desenrolo permitirá coñecer o tipo de sinal que se espera observar no dominio da frecuencia. Danse, asimesmo, algúns exemplos de *monitores Schottky* empregados noutros aceleradores.

O Capítulo 4 describe as características do monitor Schottky que se probou no CERN-SPS e que vai ser usado como ferramenta de diagnose transversal no LHC. Este monitor consiste nunha cavidade resonante (*pick-up*) na cal o sinal necesita ser convenientemente adaptado aos dispositivos de adquisición de datos, estes dispositivos foron os seguintes: un analizador de espectros convencional, un analizador FFT (Fast Fourier Transform) e unha tarxeta de son conectada a un ordenador portátil de maior versatilidade e portabilidade que os dous instrumentos anteriores. Aquí tamén se describe detalladamente a montaxe experimental instalada para la adquisición de datos.

No Capítulo 5 preséntanse os resultados obtidos co *pick-up* sintonizado a 1.7 GHz e usado como monitor Schottky no SPS cun tipo de feixe de partículas que ten as mesmas características que o que suministrará o LHC. Pero antes disto, e coñecendo os parámetros característicos do *pick-up*, faise un estudio do tipo de resposta que observariamos cun analizador de espectros, é dicir, a relación Sinal/Ruido (S/N) e o rango de frecuencias do sinal recibido. A continuación amósanse os resultados experimentais: espectros en frecuencia nos planos horizontal e vertical, onde se intenta

observar tódalas características espectrais predicidas pola Teoría de Schottky e así extraer os valores do *betatron tune*, da *cromaticidade* e da desviación do momento lineal con respecto ó nominal. Para rematar, concentrámonos na análise dos datos obtidos co sistema de adquisición máis eficiente: unha tarxeta de son conectado a un ordenador portátil. A maioría dos datos adquiríronse desta forma e a posterior análise trouxo á luz compoñentes en frecuencia adicionais e inesperadas non asociadas a Schottky, por este motivo resulta crucial entender a orixe destas liñas de frecuencia se queremos conseguir un espectro Schottky libre de interferencias e de uso en diagnose. Faise un estudio completo das posibles fontes de ruído nos espectros FFT.

No Capítulo 6 descríbese un efecto particular que ten lugar cando un grupo de partículas con cromaticidade distinta de cero é perturbado transversalmente: na metade dun período sincrotrón as partículas na cabeza do grupo e as que están situadas na cola intercambian as súas posicións. O mostreado de oscilacións transversais en dúas posicións fixas do grupo, unha na cabeza e outra na cola, leva á observación dunha diferenza de fase entre estos dous puntos cun valor máximo na metade do período sincrotrón. Un desenvolvemento matemático completo da dinámica dunha única partícula daranos unha fórmula da cal será posible extraer o valor da cromaticidade relativa a partir do desfase entre a cabeza e a cola. Ademais, como introducción ó que pode considerarse como a segunda parte da Tese, explícase a forma na que se poden medir os desfases e de qué maneira se pode aumentar a sensibilidade ó movemento betatrón.

O Capítulo 7 describe un método para mellorar a sensibilidade do *monitor Head-Tail* instalado no SPS do CERN ó *movemento betatrón head-tail* dun grupo de partículas. Este método é un sistema de compensación do desprazamento da órbita con respecto á nominal e que eliminará do sinal transversal dado por un *'stripline pick-up'* a compoñente asociada ó desprazamento do feixe de partículas do centro eléctrico do pick-up. Desta forma, o único sinal transversal detectado será o asociado ó movemento betatrón da cabeza e da cola do grupo de partículas despois da perturbación. Tamén se presenta neste capítulo o sistema proposto con control automático implementado como un lazo de realimentación onde a entrada é a posición do feixe no pick-up e a saída é unha voltaxe de control aplicada a uns atenuadores conectados ós electrodos do pick-up e que atenuarán o sinal

suministrado por estos electrodos para centralo de forma electrónica. Ademáis describíense os dispositivos incluídos no sistema de corrección.

No Capítulo 8 expóñense os resultados obtidos co sistema de compensación de órbita para un só plano e que foi probado no SPS cun feixe de partículas similar ó que empregará o LHC (grupos de partículas espaciados 25 ns). Descríbense os pasos que se levaron a cabo para calibrar os compoñentes do sistema e a forma na que se realiza a cuantización do grado de mellora na corrección da órbita para diferentes algoritmos.

Finalmente, o Capítulo 9 expón as conclusións dos resultados presentados nos capítulos anteriores.

10.4 Resumo dos resultados

Seguindo experiencias anteriores realizadas cos monitores Schottky que xa están sendo usados noutros aceleradores e gracias á colaboración con FNAL (EEUU), un *pick-up* Schottky, copia dos instalados nos aneis Recycler e Tevatron do Fermilab, foi probado no SPS co propósito de estudar a súa posible aplicación como ferramenta de diagnose do feixe de partículas non destructiva no LHC. A análise dos datos adquiridos no SPS cun feixe de partículas coa mesma estrutura que a que suministrará o LHC, amosou a concordancia dos espectros en frecuencia obtidos nos planos transversal e lonxitudinal cos que predí a Teoría de Schottky. Ó mesmo tempo, a resposta do pick-up correspóndese cos niveis agardados dacordo cos cálculos, e os valores extraídos para o *betatron tune*, a *cromaticidade* e a *variación do momento lineal* son aproximadamente iguais ós existentes no SPS durante a etapa na que se fixo a adquisición de datos.

Poderíase facer unha diagnose transversal completa do feixe de partículas usando este monitor sintonizado a 1.7GHz se fose posible eliminar algúns dos elementos que corrompen os espectros: as liñas de revolución que son consecuencia do desprazamento do feixe de partículas do centro do pick-up e que poden ocultar as bandas do *betatron tune* asociado ó movemento incoherente das partículas, o elemento clave neste método de diagnóstico; os sinais coherentes do betatron tune que solapan as incoherentes e nos cales a amplitude e o ancho pódense ver afectados por outros

efectos distintos da variación do momento e da cromaticidade, parámetros que se poden obter a partir do espectro Schottky; e finalmente, as compoñentes en frecuencia asociadas ó ruído orixinado polos elementos que compoñen a cadea de adquisición de datos. Poderían facerse probas adicionais con '*pilot beam*' para ver a sensibilidade do monitor a un único grupo de partículas presente no feixe.

A necesidade de aumentar a sensibilidade a oscilacións transversais da cabeza e da cola do grupo de partículas no *monitor Head-Tail* instalado no SPS, levou á construción do prototipo dun sistema de corrección de órbita do feixe de partículas cando pasa por un 'stripline coupler'. Con isto, limítase o sinal transversal resultante da desviación do feixe do centro eléctrico do pick-up e que só da información acerca do grado de desprazamento. Eliminar esta compoñente de desprazamento implicaría a diminución da perturbación aplicada ó feixe de partículas e que é necesaria para a aparición das oscilacións da cabeza e da cola do grupo de partículas. O sistema consiste nun lazo de realimentación que ten como entrada a posición do feixe e como saída as tensións que controlan a atenuación a aplicar nos electrodos do pick-up e que centran de forma electrónica o feixe. Os resultados obtidos cos dous algoritmos de control distintos (P e PI) amosou que é posible eliminar o sinal transversal non desexado nun 70%. Deberíase poñer máis énfase nos algoritmos de control: intentar determinar de forma precisa o estado para o cal o feixe de partículas se atopa centrado no pick-up e integrar a variable máis axeitada no algoritmo e intentar construír un algoritmo do tipo PID para seguir cambios rápidos na posición do feixe.

10.5 Conclusións

Globalmente pódese concluir que, cos resultados obtidos co presente traballo, sentamos as bases para continuar investigando a posible aplicación do *monitor Schottky* no LHC xa que os resultados preliminares son bastante prometedores. No caso do monitor Head-Tail, podería ser factible construír un sistema de compensación completo incluíndo a corrección da órbita nos dous planos, X e Y. Co novo prototipo, sería de grande interese facer medidas de cromaticidade co monitor e comparalas con aquelas obtidas sen a compensación da desviación da órbita.

Bibliography

- [1] <http://public.web.cern.ch/Public/Content/Chapters/AboutCERN/AboutCERN-en.html>
- [2] <http://lhc.web.cern.ch/lhc/>
- [3] <http://lhc-machine-outreach.web.cern.ch/lhc-machine-outreach/lhc-vital-statistics.htm>
- [4] <http://greybook.cern.ch/>
- [5] <http://ab-div.web.cern.ch/ab-div/Publications/LHC-DesignReport.html>
- [6] P. J. Bryant. '*A Brief History and Review of Accelerators*'. In Proc. CAS, v.1, 1994.
- [7] S. Tazzari, M. Ferrario. '*Trends in High Energy Particle Accelerators*'. Reports on Progress in Physics. 21 May 2003.
- [8] H. Koziol. '*Beam Diagnostics for Accelerators*'. In Proc. CAS, v.2, 1994.
- [9] E. J. N. Wilson. '*Transverse Beam Dynamics*'. In Proc. CAS, v.1, 1994.
- [10] M. Gasior, R. Jones. '*High Sensitivity Tune Measurement by Direct Diode Detection*'. CERN-AB-2005-060 BDI, October, 2005.
- [11] L. Bojtar. '*Application programs for the AD machine tune, chromaticity and dispersion measurements*'. PS/OP Note 2002-014, 19 December 2001.
- [12] H. Schmickler. '*Diagnostics and Control of the Time Evolution of Beam Parameters*'. (CERN/SL/97/68), presented at the 3rd European Workshop on Beam Accelerators (DIPAC 97), Frascati, Italy, October 1997.
- [13] G. Minty, F. Zimmermann. '*Beam Techniques-Beam Control and Manipulation*'. US Particle Accelerator School, June 14-25, 1999.

-
- [14] S. Guiducci. '*Chromaticity*'. In Proc. CAS, v.1, 1994.
- [15] O.S. Brunigh et al. . '*Chromaticity Measurements via RF Phase Modulation and Continuous Tune Tracking*'. 8th European Particle Accelerator Conference, 3-7 June 2002, Paris.
- [16] D. Boussard. '*Schottky Noise and Beam Transfer Diagnostics*'.
- [17] T. Linnekar. '*Schottky Beam Instrumentation*'. CERN-PE-ED 001-92.
- [18] P. J. Chou et al.. '*A Transverse Tune Monitor for the Fermilab Main Ring*'.
- [19] T. Linnekar. '*The High Frequency Longitudinal and Transverse Pick-ups Used in the SPS*'. CERN-SPS/ARF/78-17.
- [20] S. van der Meer. '*Stochastic cooling and the accumulation of antiprotons*'. Nobel lecture, 8 December 1984, CERN.
- [21] R. J. Pasquinelli et al.. '*A 1.7 GHz waveguide Schottky detector*'. Proceedings of the 2003 Particle Accelerator Conference.
- [22] T. Kroyer. '*Incoherent High-frequency Schottky Signals in LHC*'. AB-Note-2006-000 RF, Geneva, 20th August 2006.
- [23] D. McGinnis. '*Slotted Waveguide Slow-Wave Stochastic Cooling Arrays*'. Proceedings of the 1999 Particle Accelerator Conference, New York, 1999.
- [24] P. Baudrenghien et al.. '*Nominal Longitudinal Parameters for the LHC Beam in the CERN SPS*'. Proceedings of the 2003 Particle Accelerator Conference.
- [25] A. Ferrari et al.. '*Design of a Bunch Phase Monitor for the CTF3 Preliminary Phase*'. CTF3 Note 046 (Tech.), PS/AE/Note 2002-061, Geneva, Switzerland, 2002.
- [26] A. Frank D'Souza. '*Design of Control Systems*'. Prentice-Hall, 1988.
- [27] P. Derwent. '*Accumulator 4-8 GHz Cooling Pickups Impedance Measurements*'. Pbar Note 624, November 1999 .
- [28] LHC Design Report Volume III. Part 2. The SPS as LHC injector.
- [29] R. Jones. '*The Determination of Chromaticity by the Measurement of a Head-Tail Phase Shift*'. SL Seminar December 1997.
- [30] R.P. Walker. '*Radiation Damping*'. In Proc. CAS, v.1, 1994.

-
- [31] D. Cocq et al. . '*The measurement of Chromaticity via a Head-Tail Phase Shift*'. 8th Beam Instrumentation Workshop BIW'98, Stanford, CA, USA, 4-7 May 1998.
- [32] A. Boudsko, et al. . '*Chromaticity Measurements at Hera-p Using the Head-Tail Technique with Chirp Excitation*'. Presented at DIPAC'99, Chester, UK, May 1999.
- [33] R. Jones et al. . '*The Measurement of Q' and Q'' in the CERN-SPS by Head-Tail Phase Shift Analysis*'. Proceedings of the Particle Accelerator Conference, 2001, Chicago.
- [34] Klaus B. Unser. '*New Generation Electronics Applied to Beam Position Monitors*'. Preprint of a contribution to the 1996 Beam Instrumentation Workshop, Argonne, Illinois, 1996.
- [35] http://www.analog.com/UploadedFiles/Data_Sheets/37181751606559ADuC814a.pdf
- [36] http://www.analog.com/UploadedFiles/Technical_Documentation/474914614814qref0.pdf
- [37] <http://www.accutron.com/products>
- [38] <http://www.datasheetarchive.com/datasheet/pdf/8847.html>
- [39] A. Frank D'Souza. '*Design of Control Systems*'. Prentice-Hall, 1988.

Appendix A

CODE FOR P AND PI CONTROL ALGORITHMS